

**Molecular Squares, Coordination Polymers and Mononuclear
Complexes Supported by 2,4-Dipyrazolyl-6H-1,3,5-triazine and
4,6-Dipyrazolylpyrimidine Ligands**

Izar Capel Berdiell, Sarah E. Farmiloe, Rafal Kulmaczewski
and Malcolm A. Halcrow*

**School of Chemistry, University of Leeds, Woodhouse Lane, Leeds LS2 9JT,
United Kingdom.
E-mail: m.a.halcrow@leeds.ac.uk*

Supporting Information

| | Page |
|--|------|
| Experimental details | S4 |
| Scheme S1 Synthesis of L^1 - L^4 . | S4 |
| Table S1 Experimental data for the organic ligand crystal structure determinations. | S7 |
| Table S2 Experimental data for the metal complex crystal structure determinations. | S8 |
| Figure S1 ^1H and ^{13}C NMR spectra of L^2 . | S11 |
| Figure S2 ^1H and ^{13}C NMR spectra of L^3 . | S12 |
| Figure S3 ^1H and ^{13}C NMR spectra of L^4 . | S13 |
| Figure S4 View of the asymmetric unit of $L^2 \cdot \text{MeCN}$. | S14 |
| Figure S5 Packing diagram of $L^2 \cdot \text{MeCN}$. | S14 |
| Figure S6 View of the asymmetric unit of $L^4 \cdot 2\text{CHCl}_3$. | S15 |
| Figure S7 Packing diagram of $L^4 \cdot 2\text{CHCl}_3$. | S15 |
| Table S3 C–H...N hydrogen bond parameters in the crystal structures of $L^2 \cdot \text{MeCN}$ and $L^4 \cdot 2\text{CHCl}_3$. | S16 |
| Figure S8 View of the molecule in the asymmetric unit of α - L^7 . | S16 |
| Table S4 Hydrogen bond parameters in the crystal structure of α - L^7 . | S16 |
| Figure S9 Packing diagrams of α - L^7 . | S17 |
| Figure S10 Packing diagrams of β - L^7 . | S18 |
| Definitions of the structural parameters discussed in the paper | S19 |
| Scheme S2 The Ψ parameter. | S19 |
| Scheme S3 Angles used in the definitions of the coordination distortion parameters Σ and Θ . | S19 |
| Figure S11 The $\{[\text{BF}_4 \leftarrow \text{Fe}_4(L^1)_4(\mu-L^1)_4] \cdot 0.5(\text{C}_3\text{H}_4\text{N}_2\text{BF}_3)\}^{7+}$ assembly in $[\{\text{Fe}(L^1)\}_4(\mu-L^1)_4][\text{BF}_4]_{8 \cdot \frac{1}{2}} \text{PzBF}_3 \cdot n\text{MeCN}$ | S20 |
| Table S5 Selected bond lengths and angles for $[\{\text{Fe}(L^1)\}_4(\mu-L^1)_4][\text{BF}_4]_{8 \cdot \frac{1}{2}} \text{PzBF}_3 \cdot n\text{MeCN}$ | S21 |
| Table S6 Intermolecular dipole...dipole interactions in $[\{\text{Fe}(L^1)\}_4(\mu-L^1)_4][\text{BF}_4]_{8 \cdot \frac{1}{2}} \text{PzBF}_3 \cdot n\text{MeCN}$ | S22 |
| Table S7 Intermolecular $\pi \dots \pi$ interactions in $[\{\text{Fe}(L^1)\}_4(\mu-L^1)_4][\text{BF}_4]_{8 \cdot \frac{1}{2}} \text{PzBF}_3 \cdot n\text{MeCN}$ | S22 |
| Figure S12 Space filling views of the assembly in $[\{\text{Fe}(L^1)\}_4(\mu-L^1)_4][\text{BF}_4]_{8 \cdot \frac{1}{2}} \text{PzBF}_3 \cdot n\text{MeCN}$ | S23 |
| Figure S13 Intermolecular $\pi \dots \pi$ interactions in $[\{\text{Fe}(L^1)\}_4(\mu-L^1)_4][\text{BF}_4]_{8 \cdot \frac{1}{2}} \text{PzBF}_3 \cdot n\text{MeCN}$. | S24 |
| Figure S14 Electrospray mass spectrum of $[\{\text{Fe}(L^1)\}_4(\mu-L^1)_4][\text{BF}_4]_{8 \cdot \frac{1}{2}} \text{PzBF}_3$. | S25 |
| Figure S15 ^1H NMR spectrum of $[\{\text{Fe}(L^1)\}_4(\mu-L^1)_4][\text{BF}_4]_{8 \cdot \frac{1}{2}} \text{PzBF}_3$. | S25 |
| Figure S16 Solid state and solution magnetic data for $[\{\text{Fe}(L^1)\}_4(\mu-L^1)_4][\text{BF}_4]_{8 \cdot \frac{1}{2}} \text{PzBF}_3$. | S26 |
| Figure S17 View of a polymer chain in $[\text{Ag}(\mu-L^2)]\text{ClO}_4$. | S27 |
| Figure S18 View of a polymer chain in $[\text{Ag}(\text{NCMe})(\mu-L^2)]\text{ClO}_4$. | S28 |
| Table S8 Selected bond lengths and angles for $[\text{Ag}(\mu-L^2)]\text{ClO}_4$ and $[\text{Ag}(\text{NCMe})(\mu-L^2)]\text{ClO}_4$. | S29 |
| Table S9 Anion... π contacts in $[\text{Ag}(\mu-L^2)]\text{ClO}_4$ and $[\text{Ag}(\text{NCMe})(\mu-L^2)]\text{ClO}_4$. | S29 |
| Figure S19 Packing diagram of $[\text{Ag}(\mu-L^2)]\text{ClO}_4$, showing the intermolecular anion... π interactions. | S30 |
| Figure S20 Packing diagram of $[\text{Ag}(\text{NCMe})(\mu-L^2)]\text{ClO}_4$, showing its intra-chain anion... π contacts. | S31 |
| Figure S21 The molecular assembly in $[\text{Ag}_4(\mu-L^3)_4][\text{ClO}_4]_4$ | S32 |
| Table S10 Selected bond lengths and angles for $[\text{Ag}_4(\mu-L^3)_4][\text{ClO}_4]_4$. | S33 |
| Table S11 Intermolecular dipole...dipole interactions in $[\text{Ag}_4(\mu-L^3)_4][\text{ClO}_4]_4$. | S33 |

| | | |
|-------------------|---|-----|
| Figure S22 | The molecular assembly in $[\text{Ag}_4(\mu\text{-}L^3)_4][\text{ClO}_4]_4 \cdot 3.2\text{MeNO}_2 \cdot 1.2\text{H}_2\text{O}$. | S34 |
| Table S12 | Selected bond lengths and angles for $[\text{Ag}_4(\mu\text{-}L^3)_4][\text{ClO}_4]_4 \cdot 3.2\text{MeNO}_2 \cdot 1.2\text{H}_2\text{O}$. | S35 |
| Table S13 | Intermolecular dipole...dipole interactions in $[\text{Ag}_4(\mu\text{-}L^3)_4][\text{ClO}_4]_4 \cdot 3.2\text{MeNO}_2 \cdot 1.2\text{H}_2\text{O}$. | S35 |
| Figure S23 | The molecular assembly in $[\text{Ag}_4(\mu\text{-}L^3)_4][\text{SbF}_6]_4 \cdot \text{MeNO}_2$ | S36 |
| Table S14 | Selected bond lengths and angles for $[\text{Ag}_4(\mu\text{-}L^3)_4][\text{SbF}_6]_4 \cdot \text{MeNO}_2$. | S37 |
| Table S15 | Intermolecular dipole...dipole interactions in $[\text{Ag}_4(\mu\text{-}L^3)_4][\text{SbF}_6]_4 \cdot \text{MeNO}_2$. | S37 |
| Figure S24 | The molecular assembly in $[\text{Ag}_4(\mu\text{-}L^4)_4][\text{ClO}_4]_4 \cdot \text{MeNO}_2$. | S38 |
| Table S16 | Selected bond lengths and angles for $[\text{Ag}_4(\mu\text{-}L^4)_4][\text{ClO}_4]_4 \cdot \text{MeNO}_2$. | S39 |
| Table S17 | Intermolecular dipole...dipole interactions in $[\text{Ag}_4(\mu\text{-}L^4)_4][\text{ClO}_4]_4 \cdot \text{MeNO}_2$. | S39 |
| Figure S25 | Intermolecular interactions in solvated and unsolvated $[\text{Ag}_4(\mu\text{-}L^3)_4][\text{ClO}_4]_4$. | S40 |
| Figure S26 | Intermolecular interactions in $[\text{Ag}_4(\mu\text{-}L^3)_4][\text{SbF}_6]_4 \cdot \text{MeNO}_2$ and $[\text{Ag}_4(\mu\text{-}L^4)_4][\text{ClO}_4]_4 \cdot \text{MeNO}_2$. | S41 |
| Figure S27 | Space-filling views of the supramolecular assembly in $[\text{Ag}_4(\mu\text{-}L^3)_4][\text{ClO}_4]_4$. | S42 |
| Figure S28 | Space-filling views of the assembly in $[\text{Ag}_4(\mu\text{-}L^3)_4][\text{ClO}_4]_4 \cdot 3.2\text{MeNO}_2 \cdot 1.2\text{H}_2\text{O}$ | S43 |
| Figure S29 | Space-filling views of the supramolecular assembly in $[\text{Ag}_4(\mu\text{-}L^3)_4][\text{SbF}_6]_4 \cdot \text{MeNO}_2$. | S44 |
| Figure S30 | Space-filling views of the supramolecular assembly in $[\text{Ag}_4(\mu\text{-}L^4)_4][\text{ClO}_4]_4 \cdot \text{MeNO}_2$. | S45 |
| Figure S31 | Packing diagram of $[\text{Ag}_4(\mu\text{-}L^3)_4][\text{ClO}_4]_4$. | S46 |
| Figure S32 | Packing diagram of $[\text{Ag}_4(\mu\text{-}L^3)_4][\text{ClO}_4]_4 \cdot 3.2\text{MeNO}_2 \cdot 1.2\text{H}_2\text{O}$. | S47 |
| Figure S33 | Packing diagram of $[\text{Ag}_4(\mu\text{-}L^3)_4][\text{SbF}_6]_4 \cdot \text{MeNO}_2$. | S48 |
| Figure S34 | Packing diagram of $[\text{Ag}_4(\mu\text{-}L^4)_4][\text{ClO}_4]_4 \cdot \text{MeNO}_2$. | S49 |
| Figure S35 | The asymmetric unit of $[\text{Ag}(\text{NCMe})(L^3)]\text{ClO}_4$. | S50 |
| Table S18 | Selected bond lengths and angles for $[\text{Ag}(\text{NCMe})(L^3)]\text{ClO}_4$. | S50 |
| Figure S36 | The asymmetric units of $[\text{Fe}(\text{NCS})_2(L^5)_2]$, $[\text{Fe}(\text{NCS})_2(L^5)_2] \cdot \text{MeOH}$ and $[\text{Fe}(\text{NCSe})_2(L^5)_2] \cdot \text{MeOH}$ | S51 |
| Figure S37 | The asymmetric units of $[\text{Fe}(\text{NCSe})_2(L^5)_2] \cdot \frac{1}{2}\text{EtOH}$ and $[\text{Fe}(\text{NCSe})_2(L^5)_2] \cdot \frac{1}{2}\text{Me}_2\text{CO}$ | S52 |
| Table S19 | Selected bond lengths and angles for mononuclear $[\text{Fe}(\text{NCE})_2(L^5)_2]$ (E = S, Se). | S53 |
| Table S20 | Hydrogen bond parameters for mononuclear $[\text{Fe}(\text{NCE})_2(L^5)_2]$ (E = S, Se). | S54 |
| Figure S38 | The asymmetric unit of $[\text{Fe}(\text{NCSe})_2(L^6)_2]$. | S55 |
| Table S21 | Selected bond lengths and angles for mononuclear $[\text{Fe}(\text{NCSe})_2(L^6)_2]$. | S55 |
| Figure S39 | Packing diagram of $[\text{Fe}(\text{NCS})_2(L^5)_2]$, showing the intermolecular $\pi \dots \pi$ interactions | S56 |
| Figure S40 | Packing diagram of $[\text{Fe}(\text{NCS})_2(L^5)_2] \cdot \text{MeOH}$, showing the intermolecular $\pi \dots \pi$ interactions | S57 |
| Table S22 | Intermolecular $\pi \dots \pi$ interactions in $[\text{Fe}(\text{NCS})_2(L^5)_2]$ and $[\text{Fe}(\text{NCSe})_2(L^6)_2]$. | S58 |
| Table S23 | Intermolecular $\pi \dots \pi$ interactions in the $[\text{Fe}(\text{NCSe})_2(L^5)_2] \cdot \text{solv}$ crystals. | S58 |
| Figure S41 | The asymmetric units of $[\text{Fe}(\text{NCS})_2(\mu\text{-}L^6)]$, $[\text{Fe}(\text{NCS})_2(\mu\text{-}L^7)]$ and $[\text{Fe}(\text{NCSe})_2(\mu\text{-}L^7)]$. | S59 |
| Table S24 | Selected bond lengths and angles for $[\text{Fe}(\text{NCS})_2(\mu\text{-}L^6)]$, $[\text{Fe}(\text{NCS})_2(\mu\text{-}L^7)]$ and $[\text{Fe}(\text{NCSe})_2(\mu\text{-}L^7)]$. | S60 |
| Table S25 | Hydrogen bond parameters for $[\text{Fe}(\text{NCE})_2(L^7)_2]$ (E = S, Se). | S60 |
| Figure S42 | A polymer chain in $[\text{Fe}(\text{NCS})_2(\mu\text{-}L^6)]$ surrounded by its nearest neighbours in the lattice. | S61 |
| Figure S43 | Packing diagram of $[\text{Fe}(\text{NCS})_2(\mu\text{-}L^6)]$ showing the interdigitation of the polymer chains. | S62 |

| | | |
|-------------------|--|-----|
| Figure S44 | Magnetic data for $[\text{Fe}(\text{NCS})_2(L^5)_2]$, $[\text{Fe}(\text{NCS})_2(L^5)_2] \cdot \text{MeOH}$ and $[\text{Fe}(\text{NCSe})_2(L^5)_2] \cdot \text{Me}_2\text{CO}$. | S63 |
| Figure S45 | Magnetic data for $[\text{Fe}(\text{NCS})_2(\mu-L^6)]$, $[\text{Fe}(\text{NCS})_2(\mu-L^7)]$ and $[\text{Fe}(\text{NCSe})_2(\mu-L^7)]$. | S63 |
| Figure S46 | Magnetic data showing the reproducible annealing behaviour of $[\text{Fe}(\text{NCSe})_2(L^5)_2] \cdot \text{solv}$. | S64 |
| Figure S47 | X-ray powder diffraction data for $[\text{Fe}(\text{NCSe})_2(L^5)_2] \cdot \text{MeOH}$, before and after annealing. | S65 |
| Figure S48 | X-ray powder diffraction data for the other iron complexes of L^5-L^7 . | S66 |
| Figure S49 | The asymmetric unit of $[\text{Fe}(\text{OH}_2)_2(\mu-L^5)][\text{ClO}_4]_2$. | S68 |
| Table S26 | Selected bond lengths and angles for $[\text{Fe}(\text{OH}_2)_2(\mu-L^5)][\text{ClO}_4]_2$. | S69 |
| Table S27 | Hydrogen bond parameters for $[\text{Fe}(\text{OH}_2)_2(\mu-L^5)][\text{ClO}_4]_2$. | S69 |
| Figure S50 | Packing diagram of $[\text{Fe}(\text{OH}_2)_2(\mu-L^5)][\text{ClO}_4]_2$, showing the hydrogen bonding between the polymer chains. | S70 |
| Figure S51 | Packing diagram of $[\text{Fe}(\text{OH}_2)_2(\mu-L^5)][\text{ClO}_4]_2$, showing the hydrogen-bonded layers in the lattice. | S71 |
| Figure S52 | X-ray powder diffraction data for $[\text{Fe}(\text{OH}_2)_2(\mu-L^5)][\text{ClO}_4]_2$. | S71 |
| References | | S72 |

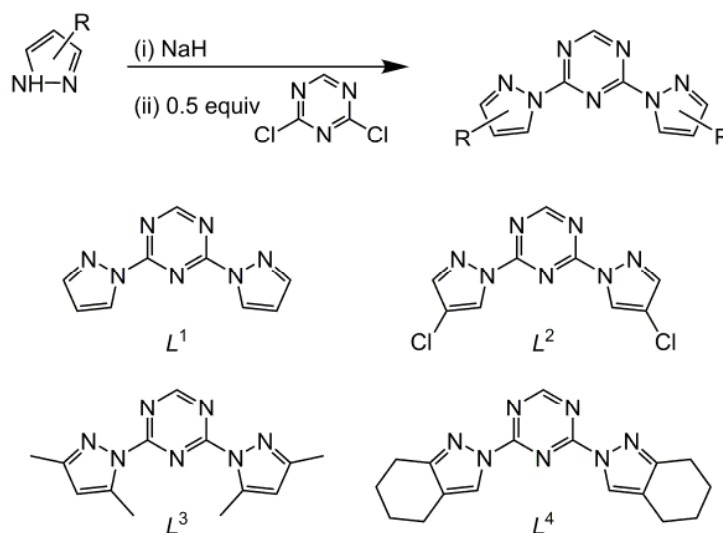
Experimental

Synthetic procedures and characterisation data for the metal complexes, and descriptions of other experimental procedures, are given in the Experimental section of the main article. Synthetic procedures and characterisation data for the previously unreported ligands L^2 - L^4 are given below (Scheme S1).

Synthesis of 2,4-di(4-chloropyrazol-1-yl)-6H-1,3,5-triazine (L^2). 4-Chloro-1H-pyrazole (1.00 g, 9.8 mmol) and NaH (60 wt % suspension in mineral oil; 0.41 g, 10.2 mmol) were dissolved in tetrahydrofuran (50 cm³) under an N₂ atmosphere, and stirred until the solution turned clear. Solid 2,4-dichloro-1,3,5-triazine (0.73 g, 4.9 mmol) was then added, and the reaction was stirred at room temperature for 16 hrs. The solvent was removed by rotary evaporation and the residue was redissolved in the minimum amount of chloroform. The product solution was washed with water (3 x 40 cm³), then dried over MgSO₄. The chloroform was then removed to give the product as white powder, which was analysed without further purification. Yield 0.85 g, 62 %. ES⁺-MS m/z 282.0009 (calcd for [HL⁵]⁺ 282.0056). ¹H NMR (CDCl₃) δ 7.85 (s, 2H, Pz H^3), 8.66 (s, 2H, Pz H^5), 9.08 (s, 1H, Trz H^6). ¹³C NMR (CDCl₃) δ 116.1 (2C, Pz C^4), 127.6 (2C, Pz C^5), 144.9 (2C, Pz C^3), 162.0 (1C, Trz C^6), 169.8 (2C, Trz $C^{2/4}$).

Synthesis of 2,4-di(3,5-dimethylpyrazol-1-yl)-6H-1,3,5-triazine (L^3). Method as for L^2 , using 3,5-dimethyl-1H-pyrazole (0.94 g, 9.8 mmol). The product required purification by flash silica chromatography in ethyl acetate eluent. Yield 0.73 g, 56 %. ES⁺-MS m/z 270.1476 (calcd for [HL⁶]⁺ 270.1462), 292.1288 (calcd for [NaL⁶]⁺ 292.1281), 561.2674 (calcd for [Na(L⁶)₂]⁺ 561.2670). ¹H NMR (CDCl₃) δ 2.33 and 2.75 (both s, 6H, CH³), 6.09 (s, 2H, Pz H^4), 9.01 (s, 1H, Trz H^6). ¹³C NMR (CDCl₃) δ 13.0, 15.8 (both 2C, CH₃), 112.2 (2C, Pz C^4), 144.6 (2C, Pz C^5), 153.7 (2C, Pz C^3), 163.4 (1C, Trz C^6), 168.5 (2C, Trz $C^{2/4}$).

Synthesis of 2,4-di(4,5,6,7-tetrahydroindazol-2-yl)-6H-1,3,5-triazine (L^4). Method as for L^2 , using 4,5,6,7-tetrahydro-1H-indazole (1.20 g, 9.8 mmol). The product was purified by flash silica chromatography in ethyl acetate eluent. Yield 0.64 g, 41 %. ES⁺-MS m/z 322.1784 (calcd for [HL⁷]⁺ 322.1775), 344.1601 (calcd for [NaL⁷]⁺ 344.1594), 665.3299 (calcd for [Na(L⁷)₂]⁺ 665.3296). ¹H NMR (CDCl₃) δ 1.83 (m, 4H, Ind CH₂⁵ and CH₂⁶), 2.64 (t, 4H, 5.9 Hz) and 2.83 (t, 4H, 6.2 Hz; Ind CH₂⁴ and CH₂⁷), 8.33 (s, 2H, Ind H^3), 8.93 (s, 1H, Trz H^6). ¹³C NMR (CDCl₃) δ 20.7, 22.9, 23.0, 24.0 (all 2C, Ind C^{4-7}), 121.6 (2C, Ind C^{3a}), 126.4 (2C, Ind C^3), 157.2 (2C, Ind C^{7a}), 161.8 (1C, Trz C^6), 169.2 (2C, Trz $C^{2/4}$).



Scheme S1 Synthesis of L^1 - L^4 . Conditions: thf, 298 K, 16 hrs.

Single Crystal Structure Analyses

Diffraction data for $[\text{Fe}(\text{NCS})_2(\mu\text{-}L^7)]$ were recorded at station I19 of the Diamond synchrotron ($\lambda = 0.6889 \text{ \AA}$). All other crystallographic data were measured with an Agilent Supernova dual-source diffractometer using monochromated $\text{Cu-K}\alpha$ ($\lambda = 1.5418 \text{ \AA}$) or $\text{Mo-K}\alpha$ ($\lambda = 0.7107 \text{ \AA}$) radiation. The diffractometer was fitted with an Oxford Cryostream low-temperature device. Experimental details of the structure determinations in this study are given in Table S1. All the structures were solved by direct methods (*SHELXS97*), and developed by full least-squares refinement on F^2 (*SHELXL97*). Crystallographic figures were prepared using *XSEED*,² and octahedral coordination volumes (V_{Oh}) were calculated with *Olex2*.³

Unless otherwise stated, all crystallographically ordered non-H atoms in each structure were refined anisotropically, and H atoms were placed in calculated positions and refined using a riding model.

Structure refinements of $L^2\text{-MeCN}$, $[\text{Ag}(\mu\text{-}L^2)]\text{ClO}_4$, $[\text{Ag}(\mu\text{-}L^2)(\text{NCMe})]\text{ClO}_4$, $[\text{Ag}(\text{NCMe})L^3]\text{ClO}_4$, $[\text{Fe}(\text{NCS})_2(L^5)_2]$, $[\text{Fe}(\text{NCS})_2(\mu\text{-}L^6)]$ and $[\text{Fe}(\text{NCSe})_2(L^6)_2]$. No disorder is present in these structures and no restraints were applied to their refinements.

Structure refinement of $L^4\text{-}2\text{CHCl}_3$. The asymmetric unit contains two molecules of L^4 and four chloroform solvent molecules. Two of the solvent molecules are disordered over two sites, whose occupancies refined to 0.61:0.39 and 0.64:0.36. These were treated with the fixed restraints $\text{C}\text{--}\text{Cl} = 1.72(2)$ and $\text{Cl}\dots\text{Cl} = 2.81(2) \text{ \AA}$. All non-H atoms except the minor disorder sites were refined anisotropically.

Structure refinements of $\alpha\text{-}L^7$. No disorder is present in these structures and no restraints were applied to the refinements. H atoms were located in the Fourier map and refined, with U_{iso} constrained to $1.2x U_{\text{eq}}\{\text{C}\}$ for the aromatic C–H groups, or $1.5x U_{\text{eq}}\{\text{N}\}$ for the amino group.

Structure refinement of $[\text{Fe}_4(L^1)_4(\mu\text{-}L^1)_4][\text{BF}_4]_8\cdot\frac{1}{2}\text{PzBF}_3\cdot n\text{MeCN}$ ($n \approx 5.9$). One uncoordinated pyrazole substituent is disordered over two sites, with a refined occupancy ratio of 0.67:0.33. The major orientation was refined without restraints, but the C–C and C–N bond lengths in the minor orientation were restrained to a common value of $1.38(2) \text{ \AA}$ to ensure a reasonable geometry. This disorder is coupled to the presence or absence of a half-occupied a half-occupied pyrazole-derived fragment, positioned to hydrogen bond to the major ligand disorder site. That moiety was modelled as the *1H*-pyrazole $\rightarrow\text{BF}_3$ adduct, which refined acceptably without restraints.

Three of the BF_4^- ions are also disordered over two equally occupied orientations, using the refined restraints $\text{B}\text{--}\text{F} = 1.39(2)$ and $\text{F}\dots\text{F} = 2.27(2) \text{ \AA}$. Nine acetonitrile molecules were located in the Fourier map, whose occupancies ranged from 0.2 to 1.0. The two lowest-occupancy MeCN sites were modelled with fixed restraints $\text{C}\text{--}\text{C} = 1.45(2)$, $\text{C}\text{--}\text{N} = 1.15(2)$ and $1,3\text{-C}\dots\text{N} = 2.63(2) \text{ \AA}$; the 0.2-occupied MeCN site is co-localized with the half-occupied *1H*-pyrazole $\rightarrow\text{BF}_3$ adduct. All non-H atoms with occupancy >0.5 were refined anisotropically, while H atoms were placed in calculated positions and refined using a riding model. The highest residual Fourier peak of $+1.2 e\text{\AA}^{-3}$ is associated with the pyrazole $\rightarrow\text{BF}_3$ half-molecule, and may imply additional, weakly occupied solvent in this region of the lattice.

Structure refinement of $[\text{Ag}_4(\mu\text{-}L^3)_4][\text{ClO}_4]_4$. The asymmetric unit contains one-quarter of a formula unit, with a quarter of the cyclic tetramer encircling the $\bar{4}$ site $\frac{1}{2}, \frac{1}{2}, \frac{1}{2}$ and two complete ClO_4^- half-anions spanning C_2 axes $\frac{1}{2}, 0, z$ and $\frac{1}{2}, \frac{1}{2}, z$. No restraints were applied to the model in the final least squares cycles. All fully occupied non-H atoms plus the Cl half-atoms were refined anisotropically.

Structure refinement of $[\text{Ag}_4(\mu\text{-}L^3)_4][\text{ClO}_4]_4\cdot 3.2\text{MeNO}_2\cdot 1.2\text{H}_2\text{O}$. The asymmetric unit contains half a cyclic tetrameric complex, spanning the crystallographic C_2 axis $\frac{1}{2}, y, \frac{3}{4}$; two half anions, also on crystallographic C_2 axes; another whole perchlorate ion on a general crystallographic position; and three partially occupied or disordered solvent sites, one of which is also close to a crystallographic C_2 axis. While all the perchlorate ions are ordered, all the partial nitromethane molecules required fixed restraints to refine to reasonable geometries. These were $\text{C}\text{--}\text{N} = 1.45(2)$, $\text{N}\text{--}\text{O} = 1.22(2)$, $\text{O}\dots\text{O} = 2.09(2)$ and $\text{C}\dots\text{O} = 2.30(2) \text{ \AA}$. An antibumping restraint involving a disordered solvent site was also included, to address a CheckCif alert.

H atoms associated with the partially occupied water molecule are not included in the model, but are accounted for in the molecular weight and density calculations. The highest residual Fourier peak of $+2.4 e\text{\AA}^{-3}$ is 0.9 \AA from Cl(44), and may represent a small amount of unmodelled disorder in that half-anion. Attempts to include this peak in the model as part of a 10 % disorder site were unsuccessful, however.

Structure refinement of $[\text{Ag}_4(\mu\text{-L}^3)_4][\text{SbF}_6]_4\cdot\text{MeNO}_2$. There is no internal crystallographic symmetry in this assembly, which lies on a general crystallographic site. No disorder is present in the model, and no restraints were applied to its refinement. The highest residual Fourier peak and trough of $+1.7$ and $-1.7 e\text{\AA}^{-3}$ lie 0.9\AA from Ag(2) and Sb(99), respectively.

Structure refinement of $[\text{Ag}_4(\mu\text{-L}^4)_4][\text{ClO}_4]_4\cdot\text{MeNO}_2$. These crystals diffracted more weakly than the other silver compounds, possibly because of their needle morphology, and data were only obtained to 84 % completeness to $2\theta = 144^\circ$.

The asymmetric unit of this crystal contains half a formula unit, that is: half a tetrameric complex molecule surrounding the crystallographic C_2 axis $\frac{1}{2}, y, \frac{3}{4}$; four ClO_4^- half-anions, either ordered or disordered about C_2 axes; and one nitromethane half-molecule, also spanning a C_2 axis. One half-anion is further disordered over two orientations, whose occupancy ratio refined to 0.33:0.17. The disordered half-anion was refined using the fixed restraints $\text{Cl-O} = 1.43(2)$ and $\text{O}\cdots\text{O} = 2.34(2) \text{\AA}$, while the solvent half-molecule also required the following fixed restraints to achieve a sensible geometry: $\text{C-N} = 1.45(2)$, $\text{N-O} = 1.22(2)$, $\text{O}\cdots\text{O} = 2.09(2)$ and $\text{C}\cdots\text{O} = 2.30(2) \text{\AA}$. All crystallographically ordered non-H atoms, plus disordered half-occupied Cl atoms, were refined anisotropically. The highest residual Fourier peak of $+1.3 e\text{\AA}^{-3}$ lies on the C_2 axis within the disordered half-anion.

Structure refinements of $[\text{Fe}(\text{NCS})_2(\text{L}^5)_2]\cdot\text{MeOH}$ and $[\text{Fe}(\text{NCSe})_2(\text{L}^5)_2]\cdot\text{MeOH}$. No disorder is present in these structures and no restraints were applied to the refinements. The methanol hydroxyl H atom was located in the Fourier map and refined, subject to the restraint $\text{O-H} = 0.90(2) \text{\AA}$ and the constraint $U_{\text{iso}}\{\text{H}\} = 1.5x U_{\text{eq}}\{\text{O}\}$.

Structure refinements of $[\text{Fe}(\text{NCSe})_2(\text{L}^5)_2]\cdot\frac{1}{2}\text{EtOH}$ and $[\text{Fe}(\text{NCSe})_2(\text{L}^5)_2]\cdot\frac{1}{2}\text{Me}_2\text{CO}$. The asymmetric unit of these crystals contains one molecule of the complex, and half a molecule of solvent near the crystallographic inversion centre. One Se atom in both these structures is disordered over two positions, which were refined without restraints with refined occupancies close to 0.5:0.5. The solvent half-molecules are in turn disordered over two orientations whose occupancies sum to 0.5. These were treated with fixed C-C , C-O , $1,3\text{-C}\cdots\text{C}$ and/or $1,3\text{-C}\cdots\text{O}$ distance restraints; the acetone solvent disorder sites also required SIMU displacement ellipsoid restraints to refine reasonably. All crystallographically ordered non-H atoms, plus the disordered Se atoms, were refined anisotropically.

Structure refinement of $[\text{Fe}(\text{OH}_2)_2(\mu\text{-L}^5)][\text{ClO}_4]_2$. The asymmetric unit contains two iron half-atoms lying on special positions: Fe(1), lying on the crystallographic C_2 axis $\frac{1}{2}, y, \frac{1}{4}$; and Fe(2), on the inversion centre $\frac{1}{2}, 1, \frac{1}{2}$. There is also one whole organic bridging ligand, one aqua ligand per iron atom, and two disordered perchlorate anions which were modelled over two orientations with the refined restraints $\text{Cl-O} = 1.43(2) \text{\AA}$ and $\text{O}\cdots\text{O} = 2.34(2) \text{\AA}$. Fully occupied non-H atoms plus the partial Cl atoms were refined anisotropically, and C-bound H atoms were placed in calculated positions and refined using a riding model.

Three of the four H atoms on the two aqua ligands were located in the Fourier map and refined positionally, with the fixed restraints $\text{O-H} = 0.90(2)$ and $\text{H}\cdots\text{H} = 1.37(2) \text{\AA}$ and the constraint $U_{\text{iso}}\{\text{H}\} = 1.5x U_{\text{eq}}\{\text{O}\}$. The fourth H atom H(20B), bound to O20, was not located but is accounted for in the molecular weight and density calculations. Potential H-bond acceptors for this H atom are disordered anion $\text{O}(28\text{A}^{\text{xxxi}})/\text{O}(29\text{B}^{\text{xxxi}})$ or $\text{O}(27\text{A}^{\text{xxxii}})$ (Figure S49; symmetry codes: (xxxi) $x, 2-y, \frac{1}{2}+z$; (xxxii) $1-x, 1+y, \frac{1}{2}-z$).

Structure refinements of $[\text{Fe}(\text{NCS})_2(\mu\text{-L}^7)]$ and $[\text{Fe}(\text{NCSe})_2(\mu\text{-L}^7)]$. Crystals of $[\text{Fe}(\text{NCS})_2(\mu\text{-L}^7)]$ were small and weakly diffracting, and were analysed at the Diamond synchrotron. Despite the use of synchrotron radiation the dataset is only 85.5 % complete, and only 50 % of those data are observed. Hence, although the residuals are good, the precision of this refinement is lower than for the other complexes in this study.

No disorder is present in either of these structures and no restraints were applied to the refinements. The amino group H atoms were located in the Fourier map and refined positionally, subject to the distance restraint $\text{N-H} = 0.90(2) \text{\AA}$ and the constraint $U_{\text{iso}}\{\text{H}\} = 1.5x U_{\text{eq}}\{\text{N}\}$.

CCDC-1550948 and 1957573-1957592 contain the supplementary crystallographic data for this paper (Tables S1 and S2). These data can be obtained free of charge from The Cambridge Crystallographic Data Centre via www.ccdc.cam.ac.uk/data_request/cif.

Table S1 Experimental data for the organic ligand crystal structure determinations. Data are included for a second polymorph of L^7 , whose unit cell was determined but which diffracted too weakly for a full structure refinement.

| | L^2 -MeCN | L^4 -2CHCl ₃ | α - L^7 | β - L^7 |
|--|---|--|---|---|
| molecular formula | C ₁₁ H ₈ Cl ₂ N ₈ | C ₁₉ H ₂₁ Cl ₆ N ₇ | C ₁₀ H ₉ N ₇ | C ₁₀ H ₉ N ₇ |
| M_r | 323.15 | 560.13 | 227.24 | 227.24 |
| crystal class | orthorhombic | triclinic | monoclinic | orthorhombic |
| space group | $P2_12_12_1$ | $P\bar{1}$ | $C2/c$ | $P2_12_12_1$ |
| $a / \text{\AA}$ | 3.9058(4) | 9.3073(3) | 17.0960(11) | 3.8429(1) |
| $b / \text{\AA}$ | 16.7955(15) | 11.3030(3) | 10.5273(4) | 14.8655(6) |
| $c / \text{\AA}$ | 20.5409(9) | 23.5856(8) | 13.4500(6) | 18.0160(10) |
| $\alpha / ^\circ$ | – | 88.648(2) | – | – |
| $\beta / ^\circ$ | – | 86.046(3) | 121.235(4) | – |
| $\gamma / ^\circ$ | – | 87.961(2) | – | – |
| $V / \text{\AA}^3$ | 1347.48(19) | 2473.19(13) | 2069.78(18) | 1029.19(8) |
| Z | 4 | 4 | 8 | 4 |
| T / K | 120(2) | 120(2) | 120(2) | 120(2) |
| μ / mm^{-1} | 4.411 ^c | 6.530 ^c | 0.100 ^d | 0.822 ^c |
| D_c / gcm^{-3} | 1.593 | 1.504 | 1.458 | 1.467 |
| measured reflections | 3249 | 19525 | 5264 | – |
| independent reflections | 2346 | 9320 | 2471 | – |
| R_{int} | 0.026 | 0.052 | 0.019 | – |
| parameters | 192 | 609 | 181 | – |
| restraints | 0 | 24 | 0 | – |
| $R_1 [F_0 > 4\sigma(F_0)]^a$ | 0.033 | 0.077 | 0.040 | – |
| wR_2 , all data ^b | 0.088 | 0.220 | 0.106 | – |
| goodness of fit | 1.065 | 1.819 | 1.099 | – |
| $\Delta\rho_{\text{min/max}} / e\text{\AA}^{-3}$ | –0.29/+0.25 | –0.83/+1.08 | –0.22/+0.31 | – |
| Flack parameter | 0.346(19) ^e | – | – | – |
| CCDC | 1957574 | 1957573 | 1957575 | – |

$$^a R = \sum [|F_o| - |F_c|] / \sum |F_o|$$

$$^b wR = [\sum w(F_o^2 - F_c^2) / \sum wF_o^4]^{1/2}$$

^cCollected with Cu- K_α radiation.

^dCollected with Mo- K_α radiation.

^eThis crystal was refined as a racemic twin.

Table S2 Experimental data for the metal complex crystal structures in this work.

| | $[\{\text{Fe}(L^1)\}_4(\mu-L^1)_4][\text{BF}_4]_8 \cdot \frac{1}{2}\text{PzBF}_3 \cdot n\text{MeCN}$ ($n \approx 5.9$) | $[\text{Ag}(\mu-L^2)]\text{ClO}_4$ | $[\text{Ag}(\text{NCMe})(\mu-L^2)]\text{ClO}_4$ | $[\text{Ag}_4(\mu-L^3)_4][\text{ClO}_4]_4$ | $[\text{Ag}_4(\mu-L^3)_4][\text{ClO}_4]_4 \cdot 3.2\text{MeNO}_2 \cdot 1.2\text{H}_2\text{O}$ |
|--|--|---|--|--|---|
| molecular formula | $\text{C}_{85.3}\text{H}_{75.7}\text{B}_{8.5}\text{F}_{33.5}\text{Fe}_4\text{N}_{62.9}$ | $\text{C}_9\text{H}_5\text{AgCl}_3\text{N}_7\text{O}_4$ | $\text{C}_{11}\text{H}_8\text{AgCl}_3\text{N}_8\text{O}_4$ | $\text{C}_{52}\text{H}_{60}\text{Ag}_4\text{Cl}_4\text{N}_{28}\text{O}_{16}$ | $\text{C}_{55.2}\text{H}_{72}\text{Ag}_4\text{Cl}_4\text{N}_{31.2}\text{O}_{23.6}$ |
| M_r | 2933.77 | 489.42 | 530.47 | 1906.56 | 2123.52 |
| crystal class | triclinic | monoclinic | monoclinic | tetragonal | monoclinic |
| space group | $P\bar{1}$ | $P2_1/n$ | $P2_1/n$ | $P42_1c$ | $C2/c$ |
| $a / \text{\AA}$ | 16.1862(6) | 8.0112(2) | 13.5601(2) | 13.9144(2) | 20.8911(9) |
| $b / \text{\AA}$ | 17.2352(5) | 10.5868(3) | 8.2545(1) | – | 27.7398(10) |
| $c / \text{\AA}$ | 23.7427(7) | 16.9917(3) | 15.4017(3) | 17.8688(3) | 15.8143(7) |
| $\alpha / ^\circ$ | 97.839(2) | – | – | – | – |
| $\beta / ^\circ$ | 91.234(3) | 95.332(2) | 95.121(1) | – | 107.315(5) |
| $\gamma / ^\circ$ | 105.400(3) | – | – | – | – |
| $V / \text{\AA}^3$ | 6314.5(4) | 1434.88(6) | 1717.06(5) | 3459.59(9) | 8749.3(6) |
| Z | 2 | 4 | 4 | 2 | 4 |
| T / K | 120(2) | 120(2) | 120(2) | 120(2) | 120(2) |
| μ / mm^{-1} | 4.676 ^c | 16.771 ^c | 14.097 ^c | 11.110 ^c | 1.089 ^d |
| D_c / gcm^{-3} | 1.543 | 2.266 | 2.052 | 1.830 | 1.612 |
| measured reflections | 54575 | 6035 | 6561 | 6825 | 31510 |
| independent reflections | 23884 | 2729 | 3338 | 3221 | 10539 |
| R_{int} | 0.033 | 0.029 | 0.026 | 0.028 | 0.061 |
| parameters | 1754 | 217 | 245 | 241 | 578 |
| restraints | 72 | 0 | 0 | 0 | 37 |
| $R_1 [F_0 > 4\sigma(F_0)]^a$ | 0.078 | 0.030 | 0.028 | 0.036 | 0.074 |
| wR_2 , all data ^b | 0.235 | 0.080 | 0.077 | 0.092 | 0.211 |
| goodness of fit | 1.029 | 1.051 | 1.024 | 1.051 | 1.039 |
| $\Delta\rho_{\text{min/max}} / e\text{\AA}^{-3}$ | –0.71/1.21 | –0.82/1.10 | –0.56/0.57 | –0.93/1.17 | –1.16/2.37 |
| Flack parameter | – | – | – | 0.170(10) ^f | – |
| CCDC | 1550948 | 1957577 | 1957576 | 1957578 | 1957579 |

^a $R = \Sigma[|F_o| - |F_c|] / \Sigma|F_o|$

^b $wR = [\Sigma w(F_o^2 - F_c^2) / \Sigma wF_o^4]^{1/2}$

^cCollected with Cu- K_α radiation.^dCollected with synchrotron radiation.^eCollected with Mo- K_α radiation.^fThis crystal was refined as a racemic twin.

Table S2 continued.

| | [Ag ₄ (μ-L ³) ₄][SbF ₆] ₄ - ·MeNO ₂ | [Ag ₄ (μ-L ⁴) ₄][ClO ₄] ₄ - ·MeNO ₂ | [Ag(NCMe)L ³] ₃ ClO ₄ | [Fe(NCS) ₂ (L ⁵) ₂] | [Fe(NCS) ₂ (L ⁵) ₂]- ·MeOH | [Fe(NCSe) ₂ (L ⁵) ₂]- ·MeOH |
|---|--|---|---|--|---|---|
| molecular formula | C ₅₃ H ₆₃ Ag ₄ F ₂₄ N ₂₉ O ₂ Sb ₄ | C ₆₉ H ₇₉ Ag ₄ Cl ₄ N ₂₉ O ₁₈ | C ₁₅ H ₁₈ AgClN ₈ O ₄ | C ₂₂ H ₁₆ FeN ₁₄ S ₂ | C ₂₃ H ₂₀ FeN ₁₄ OS ₂ | C ₂₃ H ₂₀ FeN ₁₄ OSe |
| <i>M_r</i> | 2512.80 | 2175.89 | 517.69 | 596.46 | 628.50 | 722.30 |
| crystal class | monoclinic | monoclinic | triclinic | triclinic | monoclinic | monoclinic |
| space group | <i>P</i> 2 ₁ / <i>n</i> | <i>C</i> 2/ <i>c</i> | <i>P</i> $\bar{1}$ | <i>P</i> $\bar{1}$ | <i>P</i> 2 ₁ / <i>n</i> | <i>P</i> 2 ₁ / <i>n</i> |
| <i>a</i> / Å | 22.9855(3) | 20.7165(11) | 7.7857(3) | 8.1002(4) | 13.1916(3) | 12.9026(2) |
| <i>b</i> / Å | 14.9629(3) | 33.8226(13) | 11.0383(5) | 11.5650(6) | 14.3276(3) | 14.5475(2) |
| <i>c</i> / Å | 23.3614(3) | 15.6449(6) | 12.5260(5) | 14.0754(7) | 15.8098(4) | 16.1511(2) |
| <i>α</i> / ° | – | – | 74.006(4) | 101.393(4) | – | – |
| <i>β</i> / ° | 95.028(1) | 131.404(3) | 71.927(4) | 93.048(4) | 110.841(2) | 109.427(2) |
| <i>γ</i> / ° | – | – | 71.187(4) | 91.065(4) | – | – |
| <i>V</i> / Å ³ | 8003.8(2) | 8222.3(6) | 950.11(7) | 1290.19(11) | 2792.61(11) | 2858.97(7) |
| <i>Z</i> | 4 | 4 | 2 | 2 | 4 | 4 |
| <i>T</i> / K | 120(2) | 120(2) | 120(2) | 120(2) | 120(2) | 120(2) |
| <i>μ</i> / mm ⁻¹ | 19.250 ^c | 9.462 ^c | 10.188 ^c | 6.565 ^c | 6.123 ^c | 7.528 ^c |
| <i>D_c</i> / gcm ⁻³ | 2.085 | 1.758 | 1.810 | 1.535 | 1.495 | 1.678 |
| measured reflections | 33503 | 10874 | 7034 | 9319 | 11284 | 14817 |
| independent reflections | 15778 | 6881 | 3554 | 4858 | 5480 | 5531 |
| <i>R</i> _{int} | 0.046 | 0.055 | 0.026 | 0.026 | 0.027 | 0.025 |
| parameters | 1062 | 578 | 267 | 352 | 374 | 383 |
| restraints | 0 | 26 | 0 | 0 | 1 | 1 |
| <i>R</i> ₁ [<i>F</i> ₀ > 4σ(<i>F</i> ₀)] ^a | 0.044 | 0.064 | 0.031 | 0.030 | 0.038 | 0.030 |
| <i>wR</i> ₂ , all data ^b | 0.120 | 0.168 | 0.079 | 0.075 | 0.101 | 0.079 |
| goodness of fit | 1.044 | 1.062 | 1.101 | 1.018 | 1.029 | 1.051 |
| Δρ _{min/max} / eÅ ⁻³ | -1.70/1.70 | -0.88/1.29 | -0.81/0.91 | -0.30/0.26 | -0.48/0.66 | -0.42/0.59 |
| CCDC | 1957580 | 1957581 | 1957582 | 1957583 | 1957584 | 1957585 |

^a $R = \Sigma[|F_o| - |F_c|] / \Sigma|F_o|$

^b $wR = [\Sigma w(F_o^2 - F_c^2) / \Sigma wF_o^4]^{1/2}$

^cCollected with Cu-*K*_α radiation.

^dCollected with Mo-*K*_α radiation.

^eCollected with synchrotron radiation.

^fThis crystal was refined as a racemic twin.

Table S2 continued.

| | [Fe(NCSe) ₂ (L ⁵) ₂]- ·½EtOH | [Fe(NCSe) ₂ (L ⁵) ₂]- ·½Me ₂ CO | [Fe(NCS) ₂ (μ-L ⁶)] | [Fe(NCSe) ₂ (L ⁶) ₂] | [Fe(NCS) ₂ (μ-L ⁷)] | [Fe(NCSe) ₂ (μ-L ⁷)] | [Fe(OH) ₂ (μ-L ⁵)]- [ClO ₄] ₂ |
|---|--|--|---|---|--|---|--|
| molecular formula | C ₂₃ H ₁₉ FeN ₁₄ O _{0.5} Se ₂ | C _{23.5} H ₁₉ FeN ₁₄ O _{0.5} Se ₂ | C ₁₃ H ₁₀ FeN ₈ S ₂ | C ₂₄ H ₂₀ FeN ₁₄ Se ₂ | C ₁₂ H ₉ FeN ₉ S ₂ | C ₁₂ H ₉ FeN ₉ Se ₂ | C ₁₀ H ₁₂ C ₁₂ FeN ₆ O ₁₀ |
| <i>M_r</i> | 713.29 | 719.30 | 398.26 | 718.31 | 399.25 | 493.05 | 503.01 |
| crystal class | monoclinic | monoclinic | tetragonal | triclinic | tetragonal | tetragonal | monoclinic |
| space group | <i>P</i> 2 ₁ / <i>n</i> | <i>P</i> 2 ₁ / <i>n</i> | <i>I</i> 4 ₁ / <i>a</i> | <i>P</i> $\bar{1}$ | <i>I</i> 4 ₁ / <i>a</i> | <i>I</i> 4 ₁ / <i>a</i> | <i>C</i> 2/ <i>c</i> |
| <i>a</i> / Å | 12.6992(7) | 12.7269(5) | 16.1912(6) | 8.1773(4) | 16.0404(2) | 16.4591(3) | 20.888(2) |
| <i>b</i> / Å | 14.4699(6) | 14.6440(6) | – | 12.1684(6) | – | – | 9.323(2) |
| <i>c</i> / Å | 16.2226(9) | 16.1908(7) | 25.146(3) | 14.1965(8) | 25.1086(3) | 25.0804(6) | 19.916(2) |
| <i>α</i> / ° | – | – | – | 77.437(4) | – | – | – |
| <i>β</i> / ° | 108.645(6) | 109.447(4) | – | 83.062(4) | – | – | 113.519(13) |
| <i>γ</i> / ° | – | – | – | 89.966(4) | – | – | – |
| <i>V</i> / Å ³ | 2824.6(3) | 2845.4(2) | 6592.1(8) | 1368.22(12) | 6460.30(14) | 6794.3(2) | 3556.3(10) |
| <i>Z</i> | 4 | 4 | 16 | 2 | 16 | 16 | 8 |
| <i>T</i> / K | 120(2) | 120(2) | 120(2) | 120(2) | 100(2) | 120(2) | 125(2) |
| <i>μ</i> / mm ⁻¹ | 7.598 ^c | 7.549 ^c | 9.830 ^c | 7.834 ^c | 1.114 ^e | 12.161 ^e | 10.228 ^c |
| <i>D_c</i> / gcm ⁻³ | 1.677 | 1.679 | 1.605 | 1.744 | 1.642 | 1.928 | 1.879 |
| measured reflections | 11028 | 10897 | 7784 | 10627 | 13505 | 7393 | 6362 |
| independent reflections | 5540 | 5537 | 3232 | 5148 | 2629 | 3326 | 3454 |
| <i>R</i> _{int} | 0.026 | 0.032 | 0.022 | 0.034 | 0.068 | 0.031 | 0.039 |
| parameters | 387 | 393 | 218 | 372 | 223 | 223 | 284 |
| restraints | 6 | 18 | 0 | 0 | 2 | 2 | 44 |
| <i>R</i> ₁ [<i>F</i> ₀ > 4σ(<i>F</i> ₀)] ^a | 0.032 | 0.049 | 0.056 | 0.042 | 0.056 | 0.046 | 0.088 |
| <i>wR</i> ₂ , all data ^b | 0.077 | 0.136 | 0.157 | 0.117 | 0.175 | 0.128 | 0.250 |
| goodness of fit | 1.031 | 1.041 | 1.076 | 1.032 | 0.904 | 1.011 | 1.038 |
| Δρ _{min/max} / eÅ ⁻³ | -0.38/0.36 | -0.63/0.64 | -0.40/0.64 | -0.68/1.25 | -0.41/0.33 | -0.86/0.84 | -0.94/0.67 |
| CCDC | 1957586 | 1957587 | 1957588 | 1957589 | 1957590 | 1957591 | 1957592 |

^a $R = \sum [|F_o| - |F_c|] / \sum |F_o|$
^b $wR = [\sum w(F_o^2 - F_c^2) / \sum wF_o^4]^{1/2}$
^cCollected with Cu-*K*_α radiation.

^dCollected with Mo-*K*_α radiation.

^eCollected with synchrotron radiation.

^fThis crystal was refined as a racemic twin.

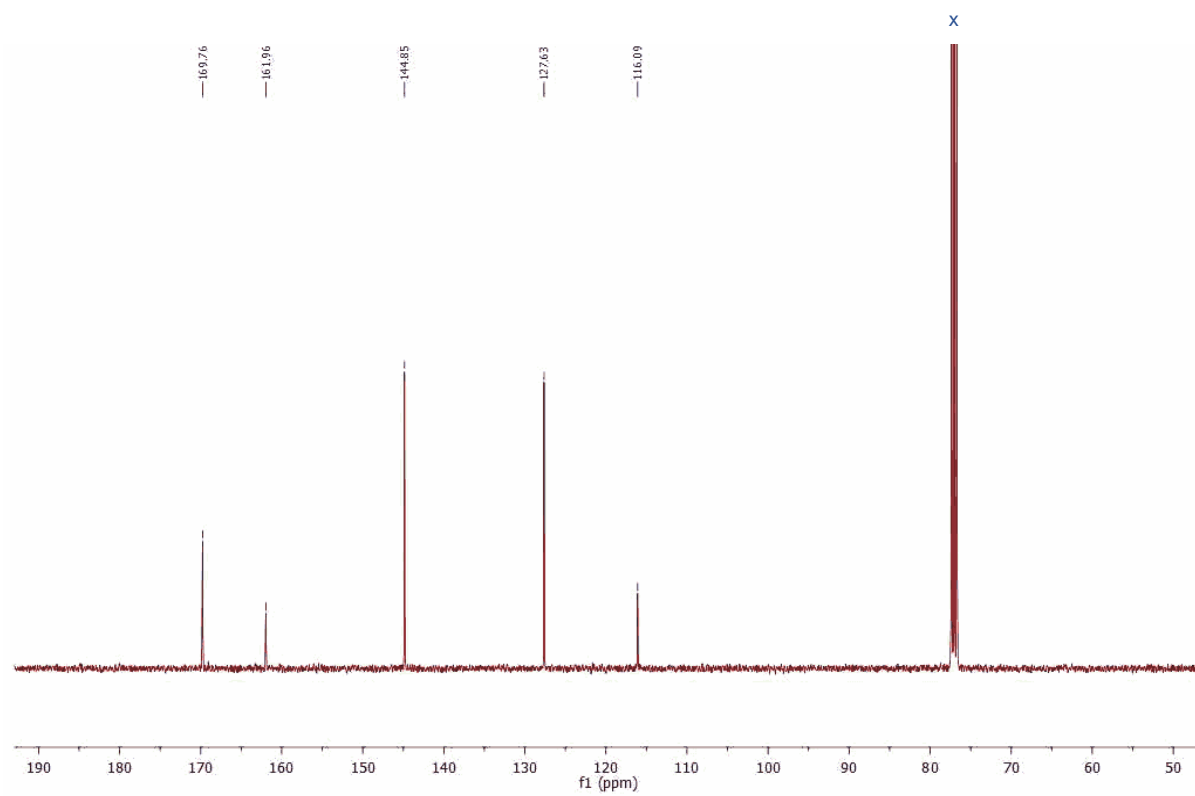
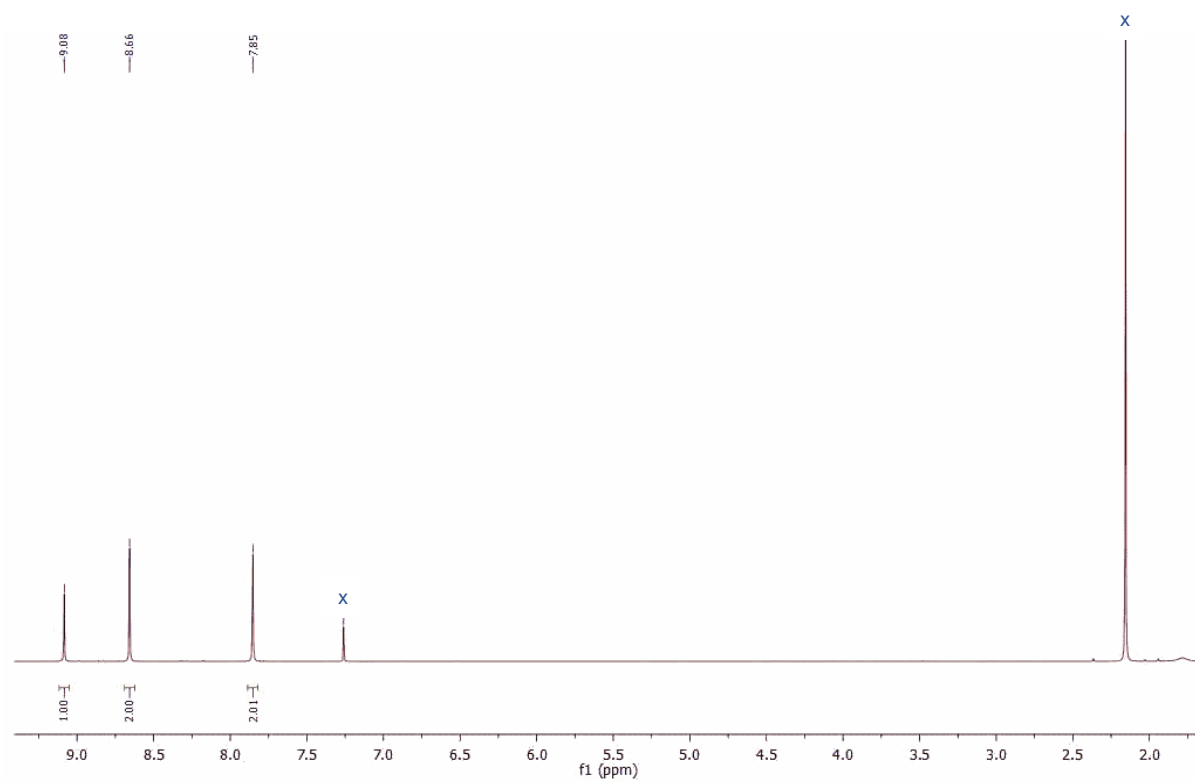


Figure S1 ^1H (top) and ^{13}C (bottom) NMR spectra of the new ligand L^2 (CDCl_3).

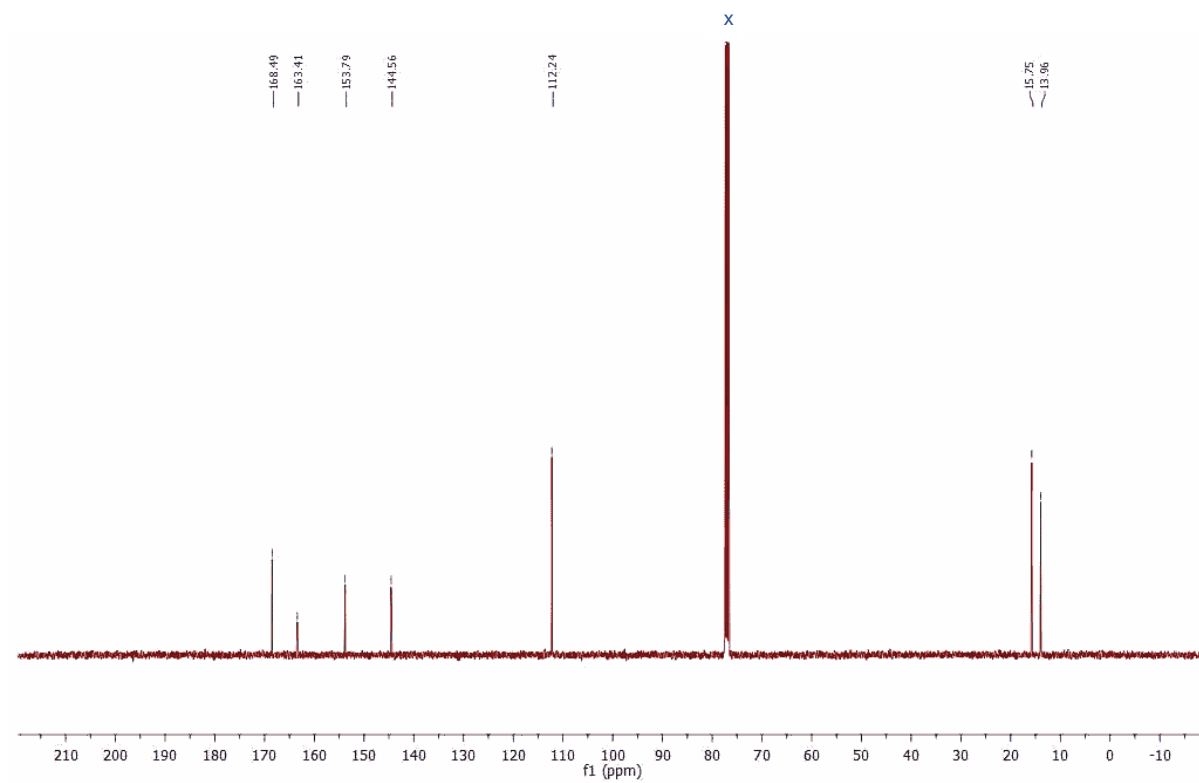
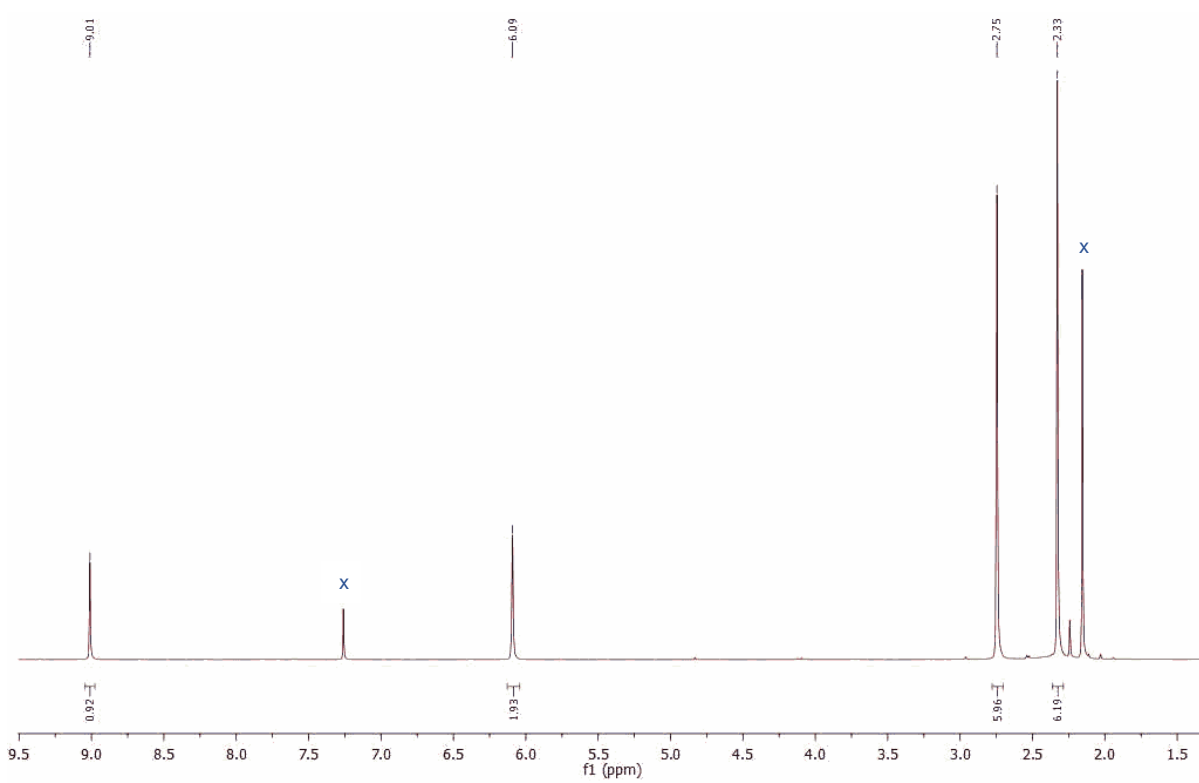


Figure S2 ^1H (top) and ^{13}C (bottom) NMR spectra of the new ligand L^3 (CDCl_3).

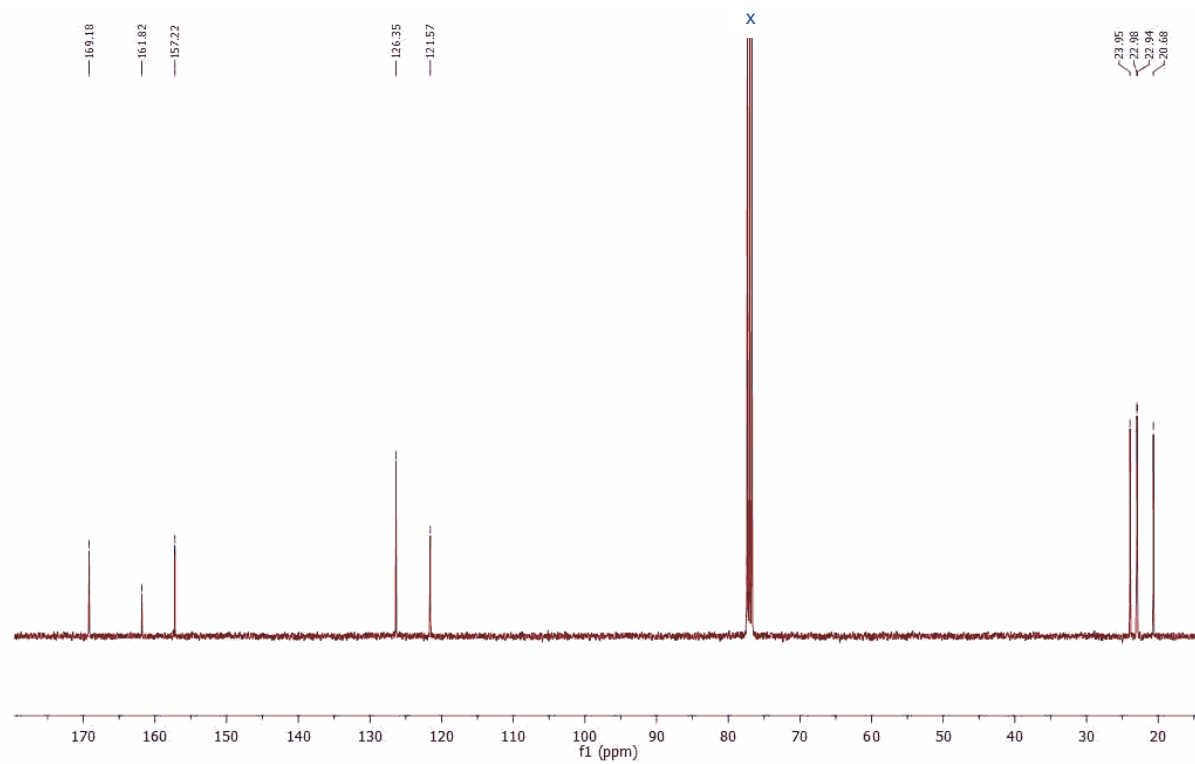
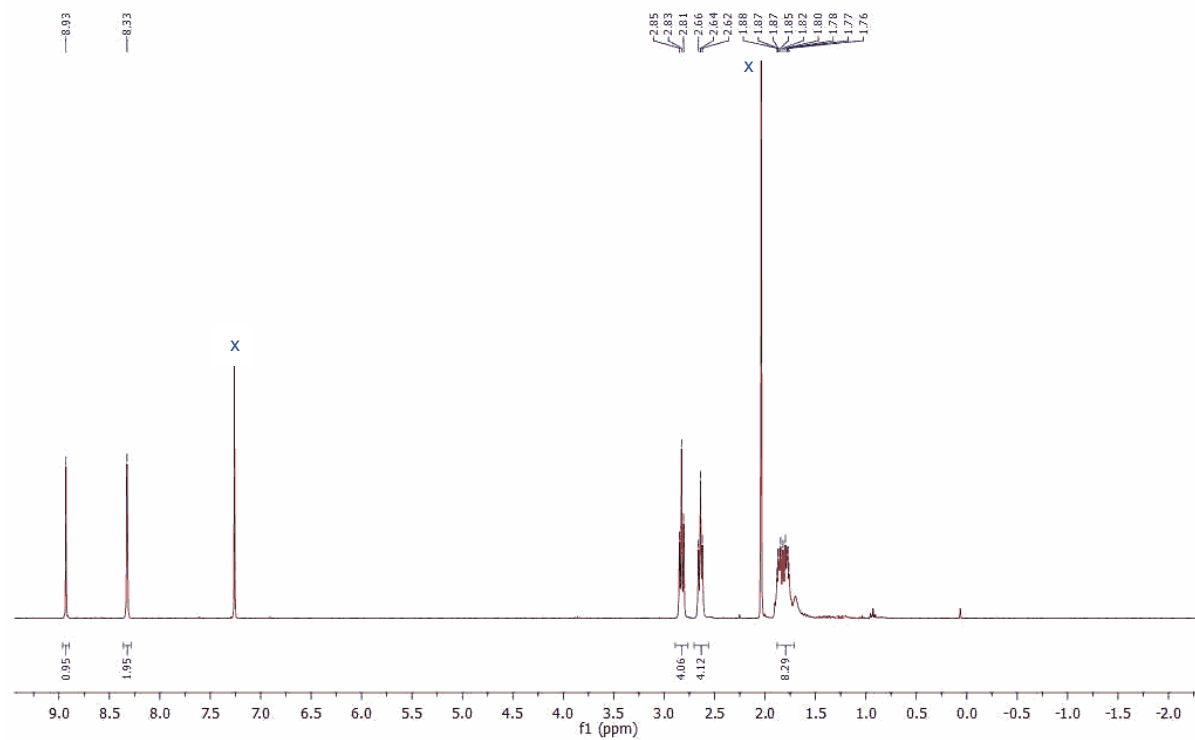


Figure S3 ^1H (top) and ^{13}C (bottom) NMR spectra of the new ligand L^4 (CDCl_3).

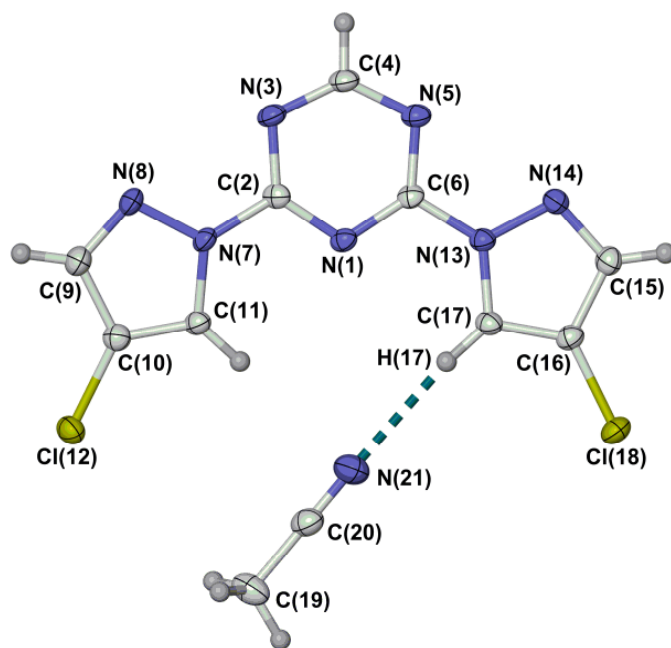


Figure S4 View of the asymmetric unit of L^2 -MeCN. Displacement ellipsoids are at the 50 % probability level, except for H atoms which have arbitrary radii. Colour code C, white; H, grey; Cl, yellow; N, blue.

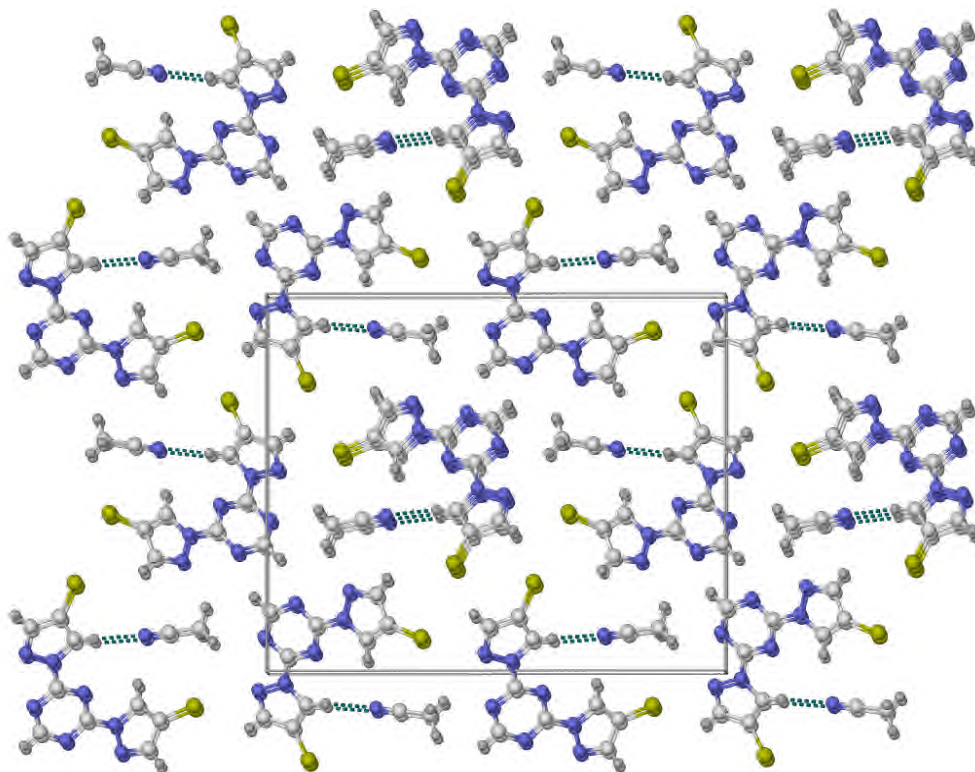


Figure S5 Packing diagram of L^2 -MeCN, viewed approximately parallel to the (100) crystal vector with the unit cell c axis horizontal. Colour code C, white; H, grey; Cl, yellow; N, blue.

The $\{L^2\text{-MeCN}\}$ assemblies form canted stacks along the crystallographic a direction. Adjacent molecules in the stacks are related by translation along a , are coplanar by symmetry and separated by 3.270(5) Å.

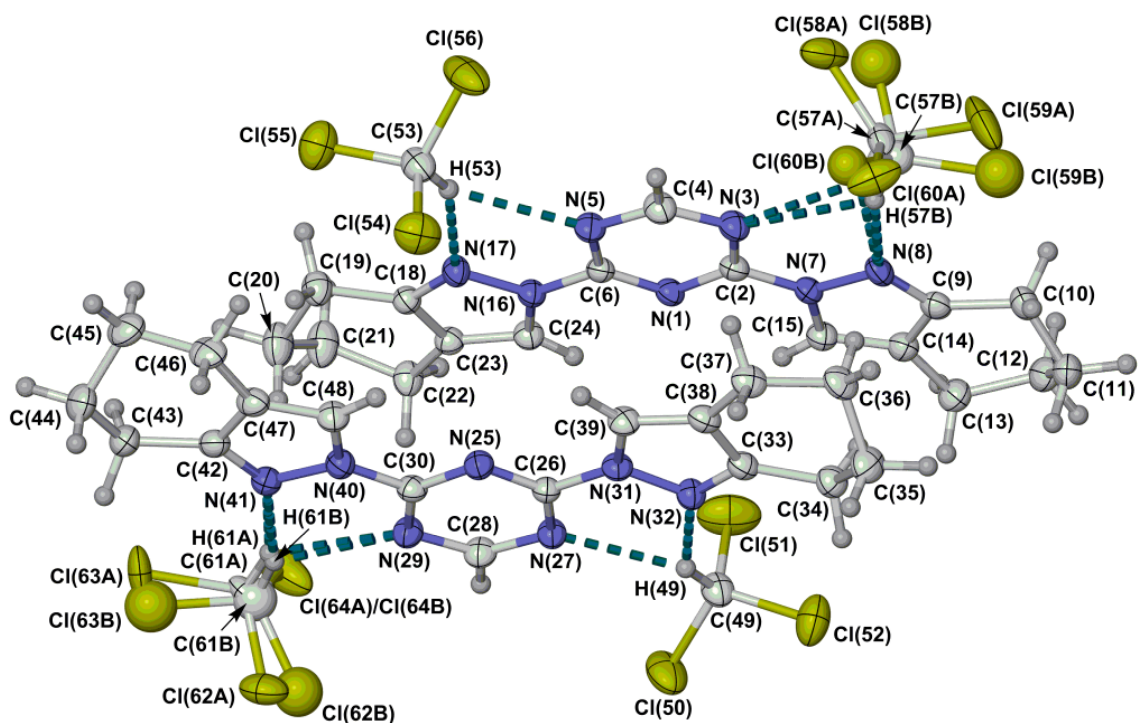


Figure S6 View of the asymmetric unit of $L^4 \cdot 2\text{CHCl}_3$. Displacement ellipsoids are at the 50 % probability level, except for H atoms which have arbitrary radii. H(57A) is hidden from view behind Cl(60A).

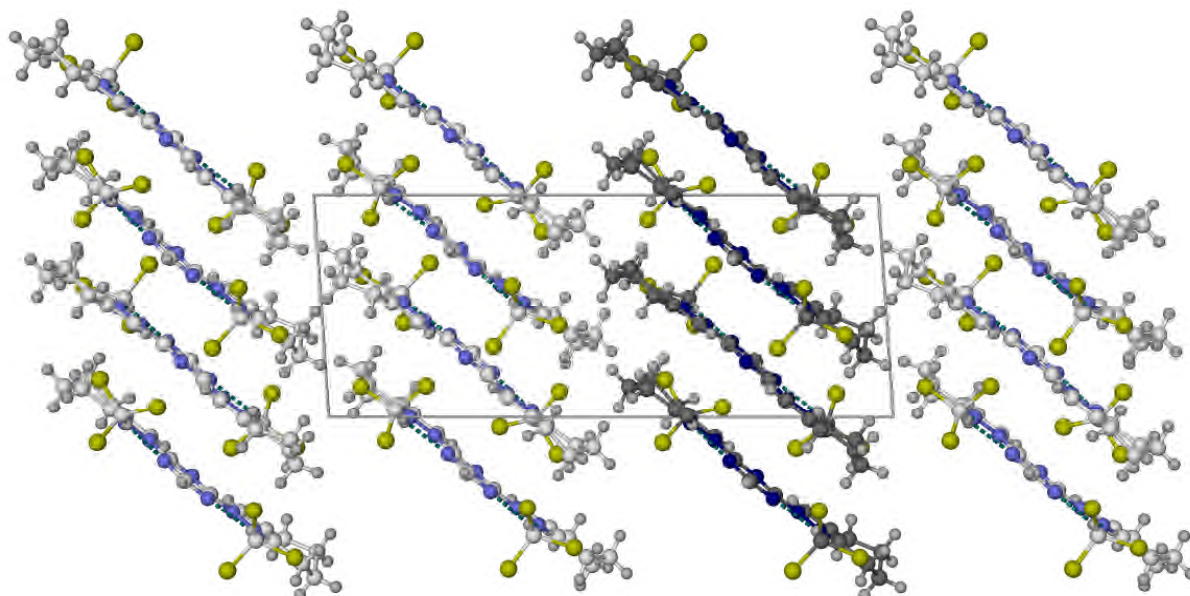


Figure S7 Packing diagram of $L^4 \cdot 2\text{CHCl}_3$, viewed parallel to the (010) crystal vector with the unit cell c axis horizontal. Colour code C, white or dark grey; H, pale grey; Cl, yellow; N, pale or dark blue.

The $\{L^4 \cdot 2\text{CHCl}_3\}$ assemblies associate into canted stacks along the crystallographic a direction (one stack is highlighted with dark colouration). Adjacent molecules in the stacks have a dihedral angle of $1.30(10)^\circ$ between their heterocyclic cores, and are separated by $3.36(3)$ or $3.39(3)$ Å.

Table S3 Metric parameters for the C–H...N hydrogen bonds in the crystal structure of L^2 ·MeCN and L^4 ·2CHCl₃ (Å, °). See Figures S4 and S6 for the atom numbering schemes.

| | D–H | H...A | D...A | D–H...A |
|-------------------------------------|------|-----------|--------------------|-------------|
| L^2 ·MeCN | | | | |
| C(17)–H(17)...N(21) | 0.95 | 2.38 | 3.322(4) | 173.4 |
| L^4 ·2CHCl ₃ | | | | |
| C(49)–H(49)...N(27) | 1.00 | 2.38 | 3.220(9) | 141.7 |
| C(49)–H(49)...N(32) | 1.00 | 2.30 | 3.170(9) | 145.2 |
| C(53)–H(53)...N(5) | 1.00 | 2.46 | 3.258(10) | 135.9 |
| C(53)–H(53)...N(17) | 1.00 | 2.28 | 3.194(9) | 151.6 |
| C(57A)–H(57A)/C(57B)–H(57B)...N(3) | 1.00 | 2.34/2.48 | 3.165(16)/ 3.23(3) | 138.8/130.8 |
| C(57A)–H(57A)/C(57B)–H(57B)...N(8) | 1.00 | 2.38/2.14 | 3.277(18)/ 3.05(3) | 149.5/152.0 |
| C(61A)–H(61A)/C(61B)–H(61B)...N(29) | 1.00 | 2.45/2.41 | 3.230(17)/3.16(5) | 134.1/131.0 |
| C(61A)–H(61A)/C(61B)–H(61B)...N(41) | 1.00 | 2.29/2.38 | 3.200(19)/3.32(5) | 151.0/157.0 |

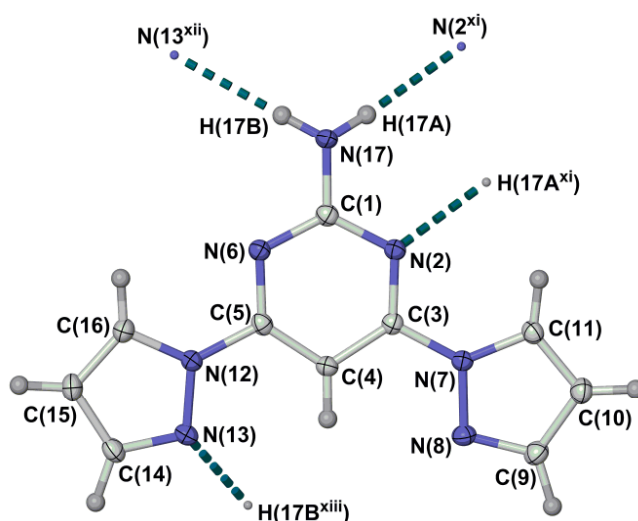


Figure S8 View of the molecule in the crystal structure of α - L^7 . Displacement ellipsoids are at the 50 % probability level, except for H atoms which have arbitrary radii. Symmetry codes:

(xi) $-x, y, 1/2-z$; (xii) $x, 1-y, -1/2+z$; (xiii) $x, 1-y, 1/2-z$.

Colour code C, white; H, grey; N, blue.

Table S4 Hydrogen bond parameters for the crystal structure of α - L^7 (Å, °). See Figure S8 for the atom numbering scheme. Symmetry codes: (xi) $-x, y, 1/2-z$; (xii) $x, 1-y, -1/2+z$.

| | D–H | H...A | D...A | D–H...A |
|---------------------------------------|-----------|-----------|------------|-----------|
| N(17)–H(17A)...N(2 ^{xi}) | 0.872(18) | 2.231(19) | 3.0986(15) | 173.2(17) |
| N(17)–H(17B)...N(13 ^{xiii}) | 0.901(19) | 2.210(19) | 3.1088(16) | 175.1(16) |

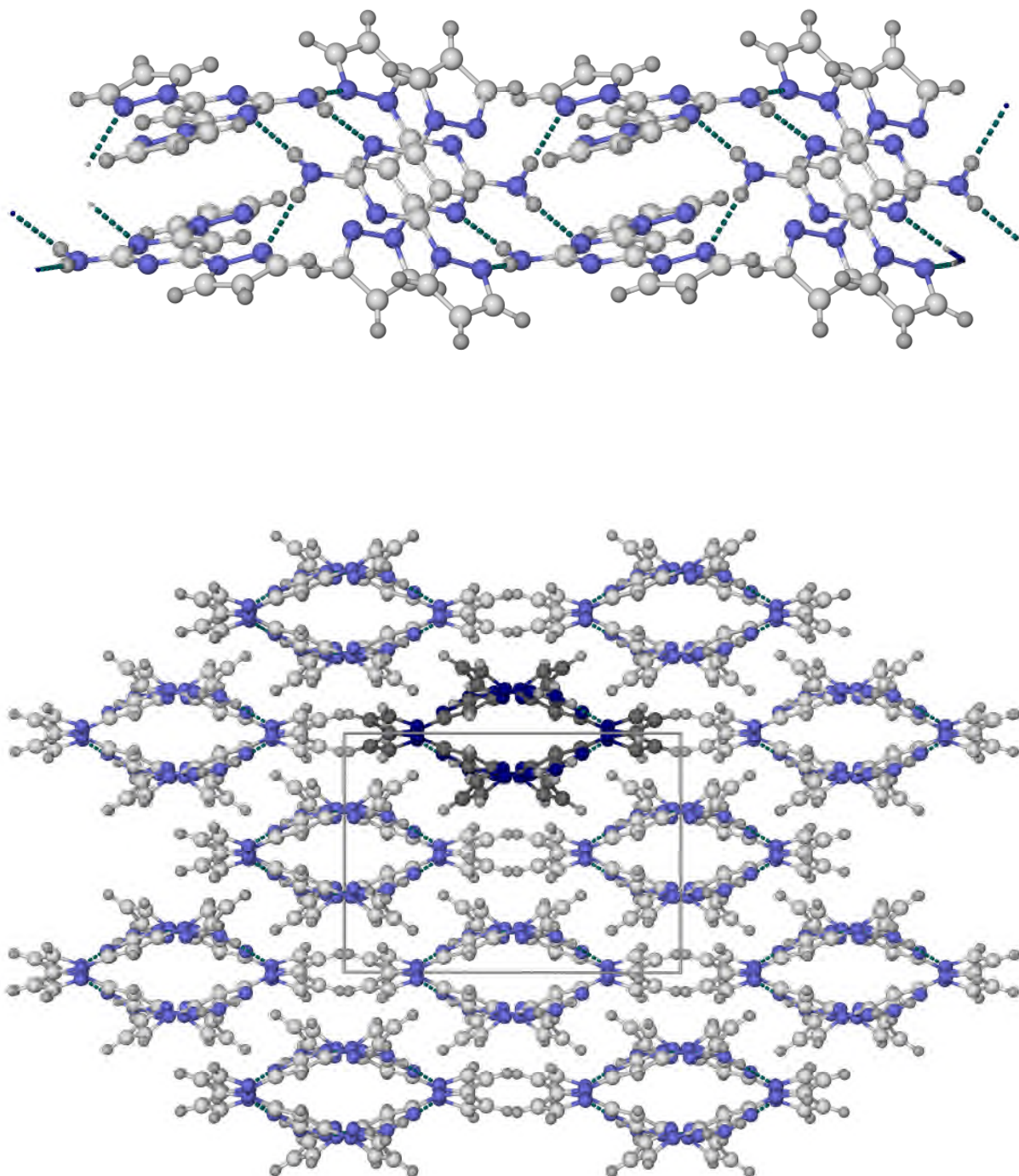


Figure S9 Packing diagrams of α - L^7 . Top: a hydrogen bonded chain of molecules. Bottom, the packing of those chains in the lattice, viewed parallel to the (001) crystal vector, with the unit cell a axis horizontal. One hydrogen-bonded chain in the bottom view is highlighted with dark colouration.

Colour code C, white or dark grey; H, grey; N, pale or dark blue.

Stacked molecules within the chains are related by a crystallographic inversion centre, are coplanar by symmetry and separated by 3.481(1) Å.

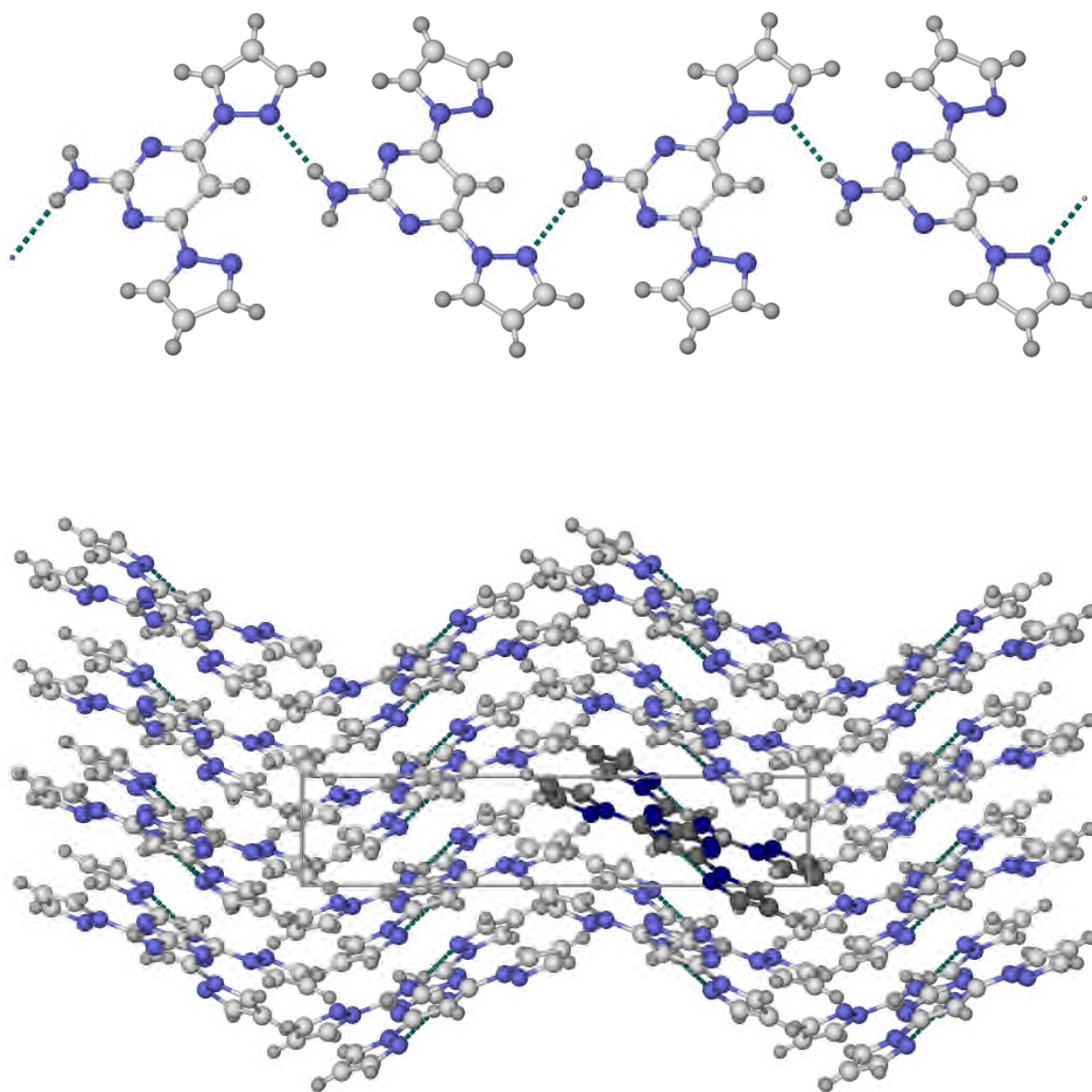


Figure S10 Packing diagrams of β - L^7 . Top: a hydrogen bonded chain of molecules. Bottom, the packing of those chains in the lattice, viewed parallel to the (010) crystal vector, with the unit cell c axis horizontal. One hydrogen-bonded chain in the bottom view is highlighted with dark colouration.

Colour code C, white or dark grey; H, grey; N, pale or dark blue.

These diagrams are generated from a preliminary, isotropic refinement of this polymorph. The structure has not been deposited with the CCDC.

There is no acceptor group within hydrogen-bonding distance of the free N–H group in this structure. The hydrogen-bonded chains form canted π ... π stacks along the crystallographic a direction.

Definitions of the structural parameters discussed in the paper

Ψ is the dihedral angle between the least squares planes of two bidentate heterocyclic ligands ('L') in a $[\text{ML}_2\text{X}_2]$ -type complex (Scheme S2). Ψ is usually close to 90° in low-spin iron(II) complexes, but can deviate significantly from ideality in their high-spin forms.⁴

In this study Ψ is calculated using only the two heterocyclic rings that are coordinated to the metal ion in question, rather than the entire ligand molecule, to allow for bending of the heterocycle conformations in some of these structures. Ψ is also used to describe the $[\text{Fe}(\text{NCE})_2(\mu\text{-L})]$ and $[\text{Ag}(\mu\text{-L})]\text{X}$ coordination polymers, and the $[\{\text{Fe}(\text{L})\}_4(\mu\text{-L})_4]\text{X}_8$ and $[\text{Ag}_4(\mu\text{-L})_4]\text{X}_4$ molecular squares, as shown in the Scheme.

V_{Oh} is the volume (in \AA^3) of the FeN_6 coordination octahedron in the complex molecule, which is typically $<10 \text{\AA}^3$ in low-spin iron(II) compounds and $\geq 12 \text{\AA}^3$ in their high-spin form.⁵

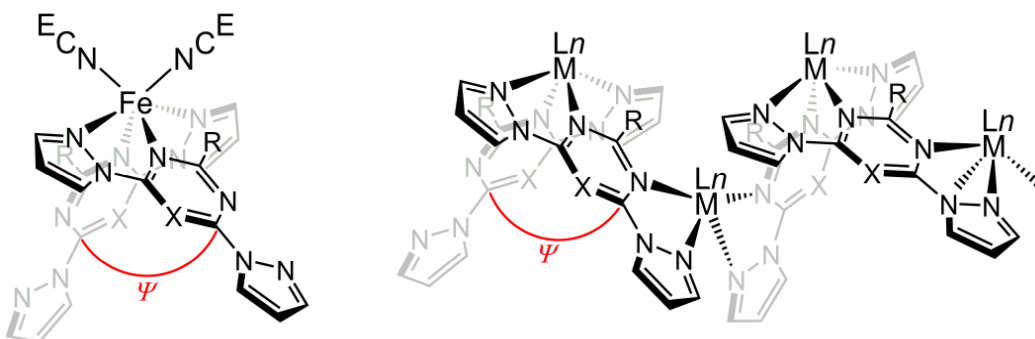
Σ and Θ are defined as follows:

$$\Sigma = \sum_{i=1}^{12} |90 - \beta_i| \qquad \Theta = \sum_{j=1}^{24} |60 - \gamma_j|$$

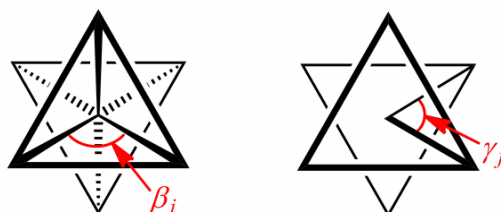
where β_i are the twelve *cis*-N–Fe–N angles about the iron atom and γ_j are the 24 unique N–Fe–N angles measured on the projection of two triangular faces of the octahedron along their common pseudo-threefold axis (Scheme S3). Σ is a general measure of the deviation of a metal ion from an ideal octahedral geometry, while Θ more specifically indicates its distortion towards a trigonal prismatic structure. A perfectly octahedral complex gives $\Sigma = \Theta = 0$.

Σ and Θ were originally introduced to quantify small differences in the coordination geometries of high-spin iron(II) complexes of polydentate ligands.⁶ More recently, they were popularized by Guionneau *et al.* as a way of confirming the spin state of a metal ion in a crystal structure; and to quantify the magnitude of the structural changes taking place during spin-crossover.⁵ Typical values for these parameters for $[\text{Fe}(\text{NCE})_2\text{L}_2]$ -type complexes are tabulated in ref. 5.

V_{Oh} , Σ and Θ are only quoted for the iron complexes in this study.



Scheme S2 The Ψ parameter.⁸



Scheme S3 Angles used in the definitions of the coordination distortion parameters Σ and Θ .⁹

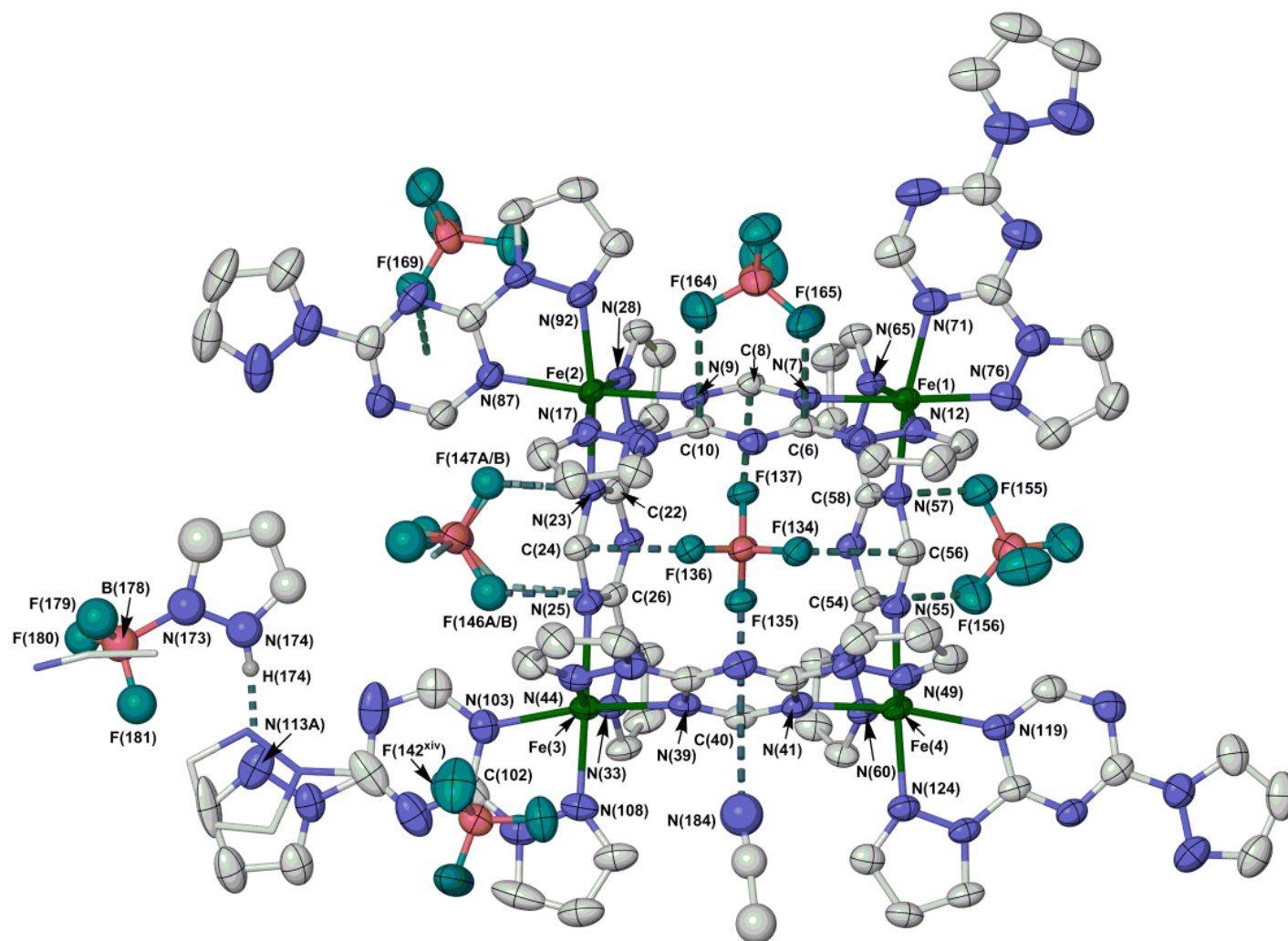


Figure S11 The molecular assembly in $[\{\text{Fe}(L^1)\}_4(\mu-L^1)_4][\text{BF}_4]_8 \cdot \frac{1}{2}\text{PzBF}_3 \cdot n\text{MeCN}$, with a partial numbering scheme. Both orientations of the disordered pyrazolyl substituent and anion, and the partial MeCN solvent overlying the pyrazole \rightarrow BF₃ half-molecule, are shown. Anions and solvent that do not interact directly with the complex, and all C-bound H atoms, are omitted. Displacement ellipsoids are at the 50 % probability level, except for the minor disorder sites mentioned which are de-emphasized for clarity. Symmetry code: (xiv) 1-x, 1-y, 1-z.

Colour code: C, white; H, pale grey; B, pink; F, cyan; Fe, green; N, blue. The view is the same as in Figure 1 of the main article.

Table S5 Selected bond lengths (Å) and angles (°) for $[\{\text{Fe}(L^1)\}_4(\mu-L^1)_4][\text{BF}_4]_{8 \cdot 1/2} \text{PzBF}_3 \cdot n \text{MeCN}$. See Figure S11 for the atom numbering scheme, while definitions of Ψ , V_{Oh} , Σ and Θ are given on page S19.

| | | | | | | | |
|-------------------------|------------|-------------------------|------------|-------------------------|------------|-------------------------|------------|
| Fe(1)–N(7) | 2.263(3) | Fe(2)–N(9) | 2.289(3) | Fe(3)–N(25) | 2.325(4) | Fe(4)–N(41) | 2.263(4) |
| Fe(1)–N(12) | 2.097(4) | Fe(2)–N(17) | 2.112(4) | Fe(3)–N(33) | 2.109(4) | Fe(4)–N(49) | 2.137(4) |
| Fe(1)–N(57) | 2.210(3) | Fe(2)–N(23) | 2.296(3) | Fe(3)–N(39) | 2.256(4) | Fe(4)–N(55) | 2.276(3) |
| Fe(1)–N(65) | 2.089(3) | Fe(2)–N(28) | 2.118(4) | Fe(3)–N(44) | 2.113(4) | Fe(4)–N(60) | 2.116(3) |
| Fe(1)–N(71) | 2.158(4) | Fe(2)–N(87) | 2.175(4) | Fe(3)–N(103) | 2.177(4) | Fe(4)–N(119) | 2.179(4) |
| Fe(1)–N(76) | 2.114(4) | Fe(2)–N(92) | 2.107(4) | Fe(3)–N(108) | 2.112(4) | Fe(4)–N(124) | 2.125(4) |
| | | | | | | | |
| N(7)–Fe(1)–N(12) | 74.21(13) | N(9)–Fe(2)–N(17) | 74.01(14) | N(25)–Fe(3)–N(33) | 72.68(13) | N(41)–Fe(4)–N(49) | 73.64(14) |
| N(7)–Fe(1)–N(57) | 95.05(13) | N(9)–Fe(2)–N(23) | 96.04(12) | N(25)–Fe(3)–N(39) | 93.27(12) | N(41)–Fe(4)–N(55) | 94.69(13) |
| N(7)–Fe(1)–N(65) | 91.97(13) | N(9)–Fe(2)–N(28) | 93.02(13) | N(25)–Fe(3)–N(44) | 89.94(13) | N(41)–Fe(4)–N(60) | 91.68(13) |
| N(7)–Fe(1)–N(71) | 98.54(14) | N(9)–Fe(2)–N(87) | 161.77(14) | N(25)–Fe(3)–N(103) | 100.19(14) | N(41)–Fe(4)–N(119) | 160.56(13) |
| N(7)–Fe(1)–N(76) | 165.31(14) | N(9)–Fe(2)–N(92) | 94.61(13) | N(25)–Fe(3)–N(108) | 165.87(14) | N(41)–Fe(4)–N(124) | 94.11(14) |
| N(12)–Fe(1)–N(57) | 95.92(13) | N(17)–Fe(2)–N(23) | 91.25(13) | N(33)–Fe(3)–N(39) | 96.31(13) | N(49)–Fe(4)–N(55) | 91.45(13) |
| N(12)–Fe(1)–N(65) | 163.13(14) | N(17)–Fe(2)–N(28) | 158.74(13) | N(33)–Fe(3)–N(44) | 159.93(15) | N(49)–Fe(4)–N(60) | 158.13(14) |
| N(12)–Fe(1)–N(71) | 97.12(14) | N(17)–Fe(2)–N(87) | 92.55(14) | N(33)–Fe(3)–N(103) | 99.69(14) | N(49)–Fe(4)–N(119) | 92.60(14) |
| N(12)–Fe(1)–N(76) | 92.75(15) | N(17)–Fe(2)–N(92) | 101.83(15) | N(33)–Fe(3)–N(108) | 94.18(15) | N(49)–Fe(4)–N(124) | 104.19(14) |
| N(57)–Fe(1)–N(65) | 75.32(13) | N(23)–Fe(2)–N(28) | 73.10(13) | N(39)–Fe(3)–N(44) | 74.23(14) | N(55)–Fe(4)–N(60) | 73.32(13) |
| N(57)–Fe(1)–N(71) | 163.27(14) | N(23)–Fe(2)–N(87) | 96.52(13) | N(39)–Fe(3)–N(103) | 161.55(14) | N(55)–Fe(4)–N(119) | 99.42(13) |
| N(57)–Fe(1)–N(76) | 92.97(14) | N(23)–Fe(2)–N(92) | 165.01(14) | N(39)–Fe(3)–N(108) | 93.37(15) | N(55)–Fe(4)–N(124) | 163.71(14) |
| N(65)–Fe(1)–N(71) | 94.43(14) | N(28)–Fe(2)–N(87) | 103.25(14) | N(44)–Fe(3)–N(103) | 93.10(15) | N(60)–Fe(4)–N(119) | 105.11(14) |
| N(65)–Fe(1)–N(76) | 101.97(15) | N(38)–Fe(2)–N(92) | 95.84(14) | N(44)–Fe(3)–N(108) | 103.87(15) | N(60)–Fe(4)–N(124) | 92.74(14) |
| N(71)–Fe(1)–N(76) | 76.01(16) | N(87)–Fe(2)–N(92) | 75.81(14) | N(103)–Fe(3)–N(108) | 76.43(17) | N(119)–Fe(4)–N(124) | 75.68(14) |
| | | | | | | | |
| Ψ [Fe(1)] | 80.65(8) | Ψ [Fe(2)] | 84.40(8) | Ψ [Fe(3)] | 79.04(8) | Ψ [Fe(4)] | 79.48(9) |
| V_{Oh} [Fe(1)] | 12.845(14) | V_{Oh} [Fe(2)] | 13.258(14) | V_{Oh} [Fe(3)] | 13.233(14) | V_{Oh} [Fe(4)] | 13.196(13) |
| Σ [Fe(1)] | 95.2(5) | Σ [Fe(2)] | 102.0(5) | Σ [Fe(3)] | 100.7(5) | Σ [Fe(4)] | 103.4(5) |
| Θ [Fe(1)] | 240 | Θ [Fe(2)] | 288 | Θ [Fe(3)] | 269 | Θ [Fe(4)] | 312 |

Despite showing small differences, the V_{Oh} , Σ and Θ values for Fe(1)–Fe(4) all lie within the ranges expected for a high-spin complex of the $[\text{Fe}(\text{NN})_3]^{2+}$ type, where NN is a diimine chelate.¹²

Table S6 Second sphere dipole...dipole interactions in the crystal structure of $[\{\text{Fe}(L^1)\}_4(\mu-L^1)_4][\text{BF}_4]_8 \cdot \frac{1}{2}\text{PzBF}_3 \cdot n\text{MeCN}$ (Å, °). See Figure S11 for the atom numbering scheme. Symmetry code: (xiv) $1-x, 1-y, 1-z$.

| | D-H | H...A | D...A | D-H...A |
|---|------|-------|-------------------|---------|
| Anion... π contacts – encapsulated anion | | | | |
| C(8)...F(137) | – | – | 2.613(4) | – |
| C(24)...F(136) | – | – | 2.604(4) | – |
| C(40)...F(135) | – | – | 2.642(4) | – |
| C(56)...F(134) | – | – | 2.627(5) | – |
| Anion... π contacts – peripheral anions | | | | |
| C(6)...F(165) | – | – | 2.808(4) | – |
| C(10)...F(164) | – | – | 2.889(4) | – |
| C(22)...F(147A)/F(147B) | – | – | 2.791(6)/2.760(8) | – |
| C(26)...F(146A)/F(146B) | – | – | 2.745(7)/2.791(7) | – |
| C(54)...F(156) | – | – | 3.010(4) | – |
| C(58)...F(155) | – | – | 2.775(4) | – |
| X{N(85)–C(90)}...N(169) ^a | – | – | 2.924 | – |
| C(102)...F(142 ^{xiv}) | – | – | 2.744(5) | – |
| <i>n</i> ... π contacts – lattice solvent | | | | |
| X{N(37)–C(42)}...N(184) ^a | – | – | 2.911 | – |
| Hydrogen bond | | | | |
| N(174)–H(174)...N(13A) | 0.88 | 2.09 | 2.940(10) | 161.7 |

^aThe closest contact in this host:guest interaction is to the centroid 'X' of the triazinyl ring listed (Figure S11).

Table S7 Metric parameters for the intermolecular π ... π interactions in $[\{\text{Fe}(L^1)\}_4(\mu-L^1)_4][\text{BF}_4]_8 \cdot \frac{1}{2}\text{PzBF}_3 \cdot n\text{MeCN}$ (Å, °). See Figure S11 for the atom numbering scheme, and Figure S13 for a plot of these interactions. Symmetry codes: (ii) $x, 1+y, z$; (xv) $1+x, 1+y, z$; (xvi) $-x, 1-y, 1-z$; (xvii) $2-x, 1-y, -z$

| | Dihedral angle | Interplanar distance | Horizontal offset |
|--|------------------|----------------------|-------------------|
| [N(80)–C(84)]...[N(123 ⁱⁱ)...C(127 ⁱⁱ)] (I) | 8.3(3) | 3.352(16) | 1.3 |
| [N(69)–C(74), N(80)–C(84)]...[N(112A ^{xv})...C(116A ^{xv})]/[N(112B ^{xv})...C(116B ^{xv})] (II) | 5.0(5)/2.9(13) | 3.30(4)/3.34(15) | 0.8/1.4 |
| [N(96)–C(100)]...[N(112A ^{xvi})...C(116A ^{xvi})]/[N(112B ^{xvi})...C(116B ^{xvi})] (III) | 15.2(5)/13.3(14) | 3.25(2)/3.23(9) | 1.1/1.8 |
| [N(117)–C(122), N(128)–C(132)]...[N(117 ^{xvii})–C(122 ^{xvii}), N(128 ^{xvii})–C(132 ^{xvii})] (IV) | 0 | 3.27(2) | 2.5 |

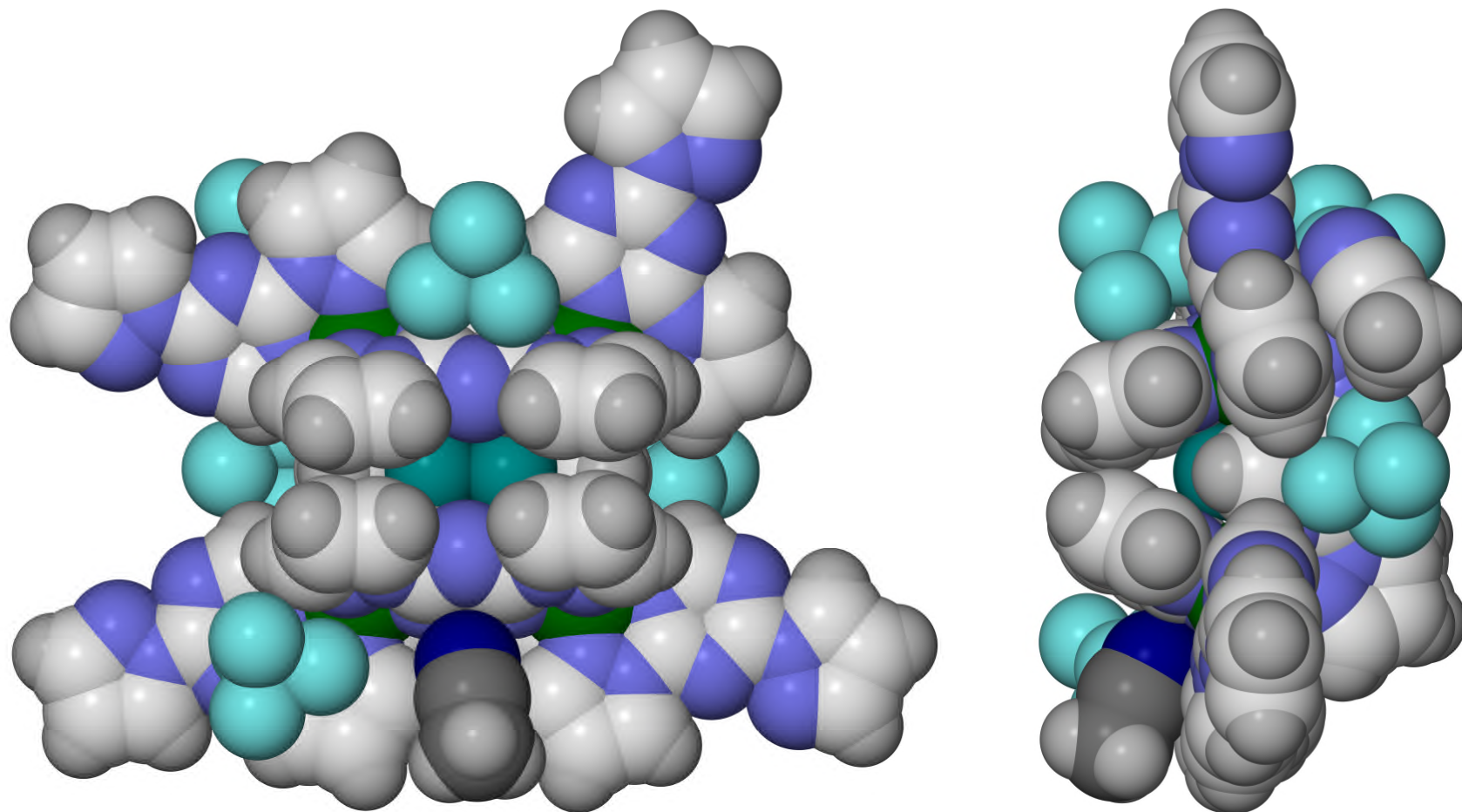


Figure S12 Space-filling views of the supramolecular assembly in $[\{\text{Fe}(L^1)\}_4(\mu-L^1)_4][\text{BF}_4]_8 \cdot \frac{1}{2}\text{PzBF}_3 \cdot n\text{MeCN}$, showing the encapsulated BF_4^- ion and the peripherally bound guest species. Only one orientation is shown of disordered residues in the model, and the half-occupied pyrazole $\rightarrow\text{BF}_3$ residue is not included. For clarity, in-cavity and peripheral anions forming secondary interactions with the molecular square are shown with dark and pale colouration, respectively. The MeCN molecule forming the short $n \dots \pi$ interaction (which is 70 % occupied in the crystal) is plotted in dark grey.

Colour code: C, white or dark grey; H, pale gray; B, pink; F, pale or dark cyan; Fe, green; N, blue.

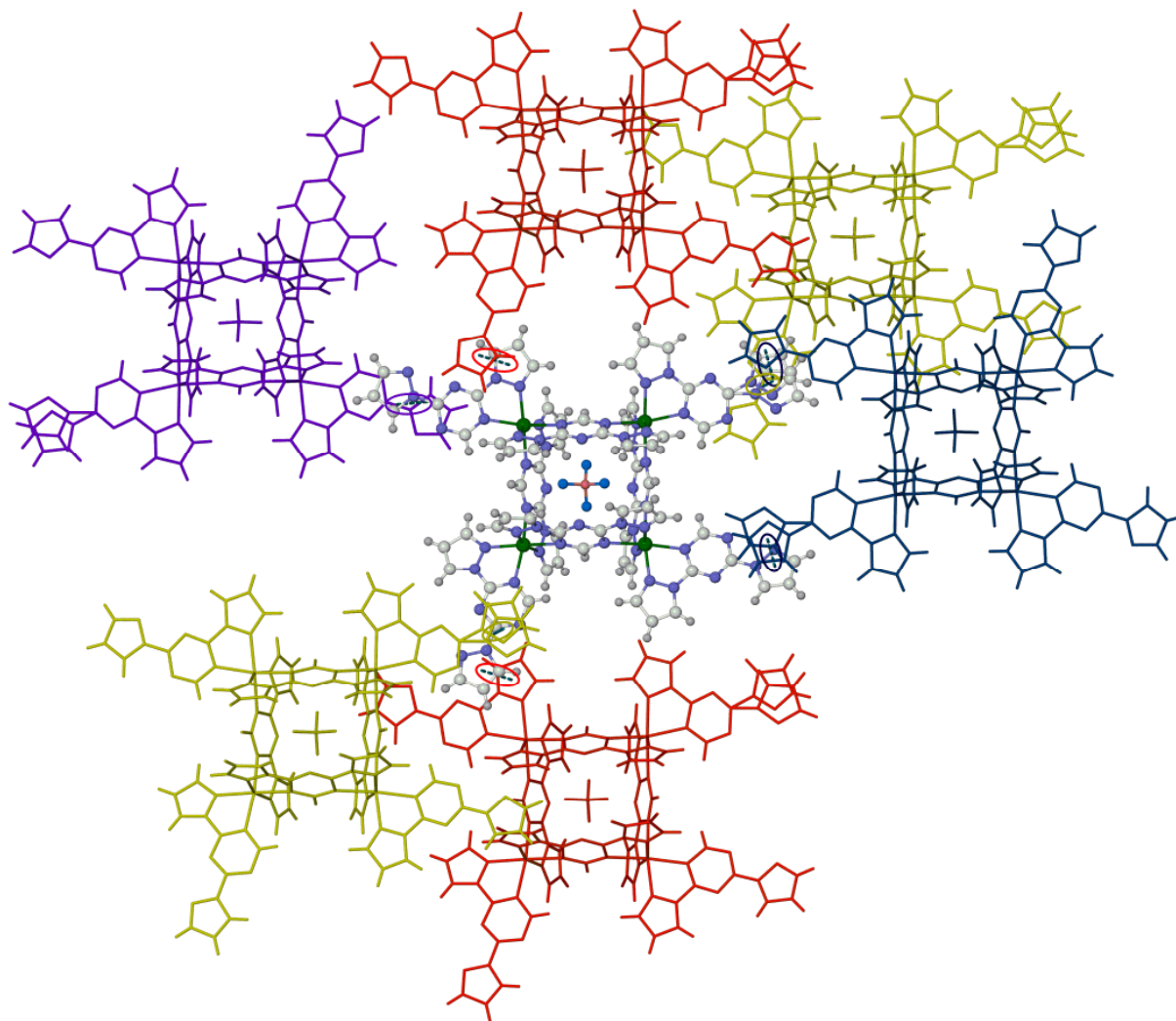


Figure S13 Partial packing diagram of $[\{\text{Fe}(L^1)\}_4(\mu-L^1)_4][\text{BF}_4]_{8 \cdot 1/2}\text{PzBF}_3 \cdot n\text{MeCN}$, showing the association of the complex molecules by intermolecular $\pi \dots \pi$ interactions. The encapsulated BF_4 ions are shown but other anions, solvent molecules and the pyrazole $\rightarrow \text{BF}_3$ residue are omitted for clarity.

The interactions and interacting molecules are colour coded, according to the numbered interactions in Table S7: **(I)** red; **(II)** yellow; **(III)** dark blue; **(IV)** purple.

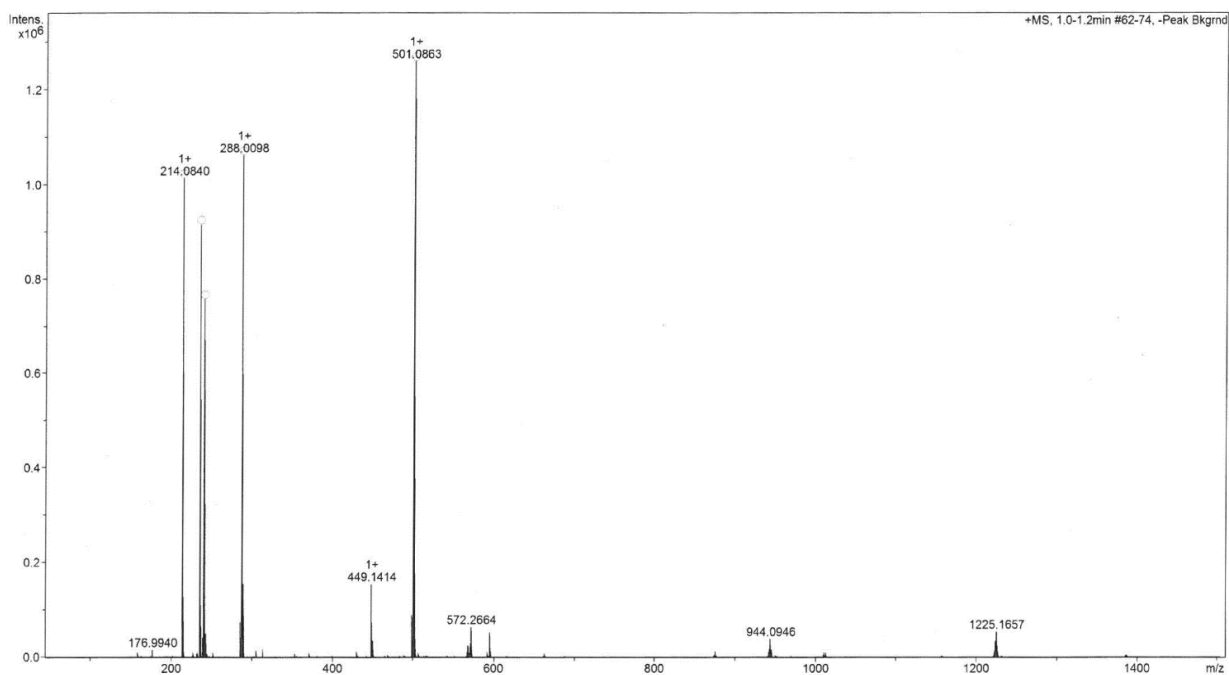


Figure S14 Electrospray mass spectrum of $[\text{Fe}_4(\text{L}^1)_4(\mu\text{-L}^1)_4][\text{BF}_4]_8$. The molecular ion is at $m/z = 1225$ ($[\text{Fe}_4(\text{L}^1)_8(\text{BF}_4)_6]^{2+}$). Other peak assignments are in the Experimental Section.

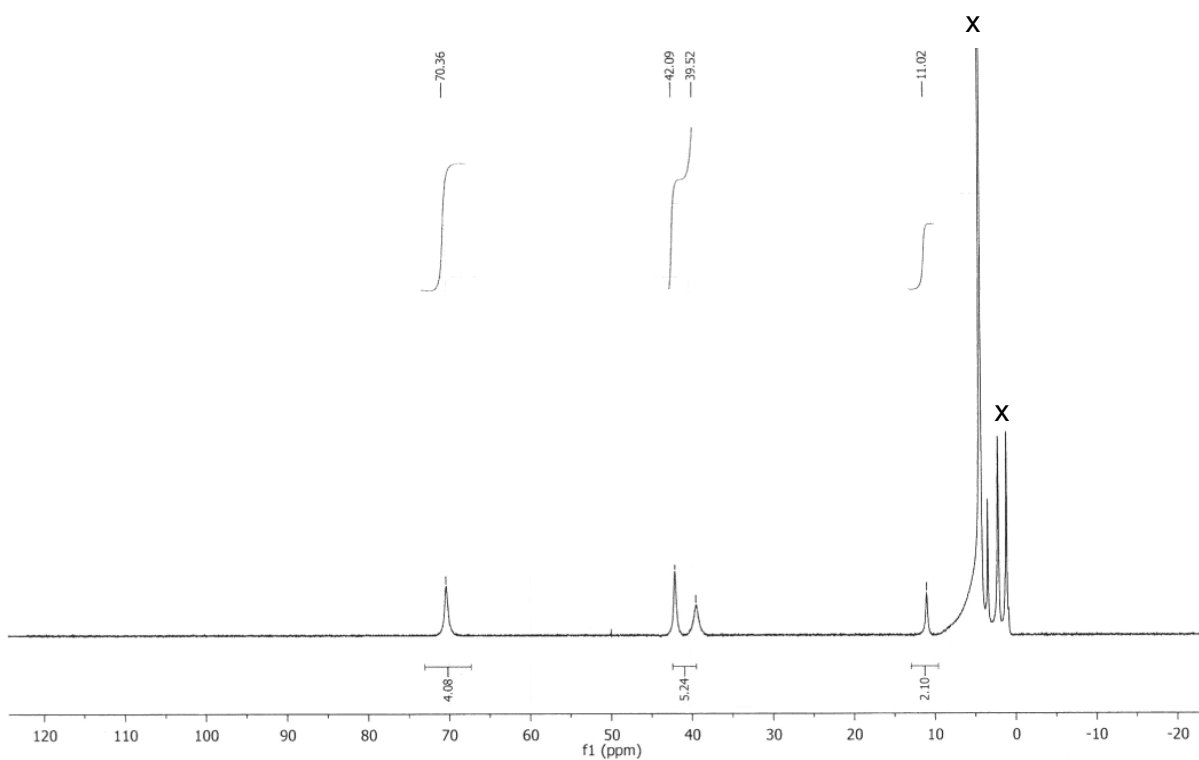


Figure S15 ^1H NMR spectrum of $[\{\text{Fe}(\text{L}^1)\}_4(\mu\text{-L}^1)_4][\text{BF}_4]_8 \cdot \frac{1}{2}\text{PzBF}_3$ (CD_3NO_2).

Since only one L^1 environment is present in the spectrum, the terminal and bridging L^1 ligands in the molecule must undergo rapid chemical exchange in solution.

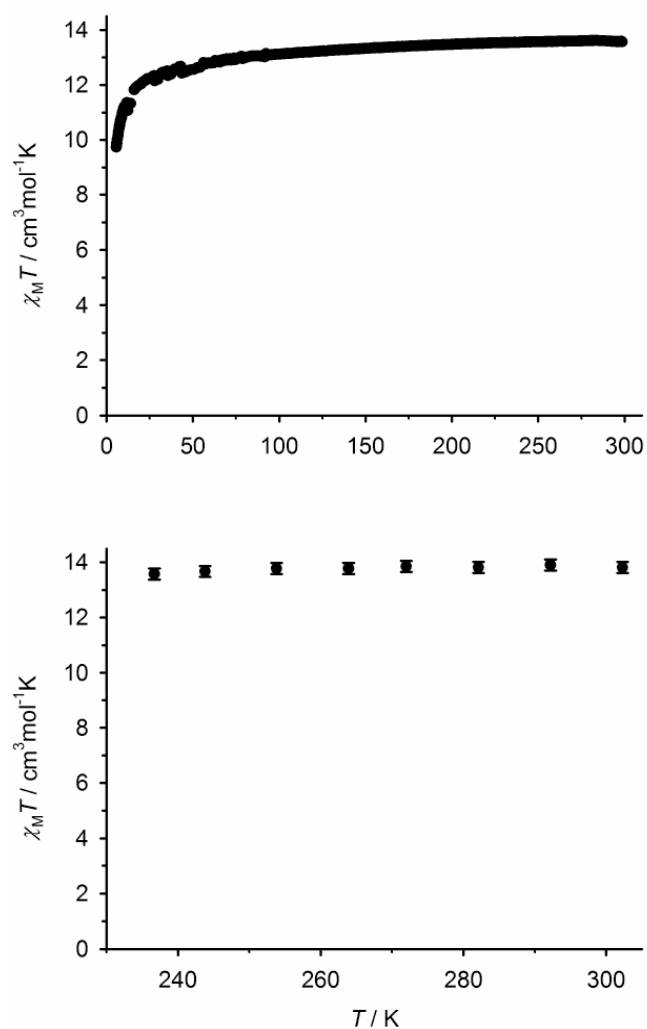


Figure S16 Magnetic susceptibility data for $[\{\text{Fe}(L^1)\}_4(\mu-L^1)_4][\text{BF}_4]_8 \cdot \frac{1}{2} \text{PzBF}_3$ in the solid (top) and in CD_3NO_2 solution (bottom).

The room temperature magnetic moment is consistent with a molecule containing four high-spin iron(II) centres, which each contribute $3.5 \pm 0.2 \text{ cm}^3 \text{mol}^{-1} \text{K}$ to the $\chi_M T$ value.⁷ The decrease in $\chi_M T$ below 50 K in the solid state data arises from zero-field splitting of the high-spin iron sites (*cf* Figures S19 and S20).⁸

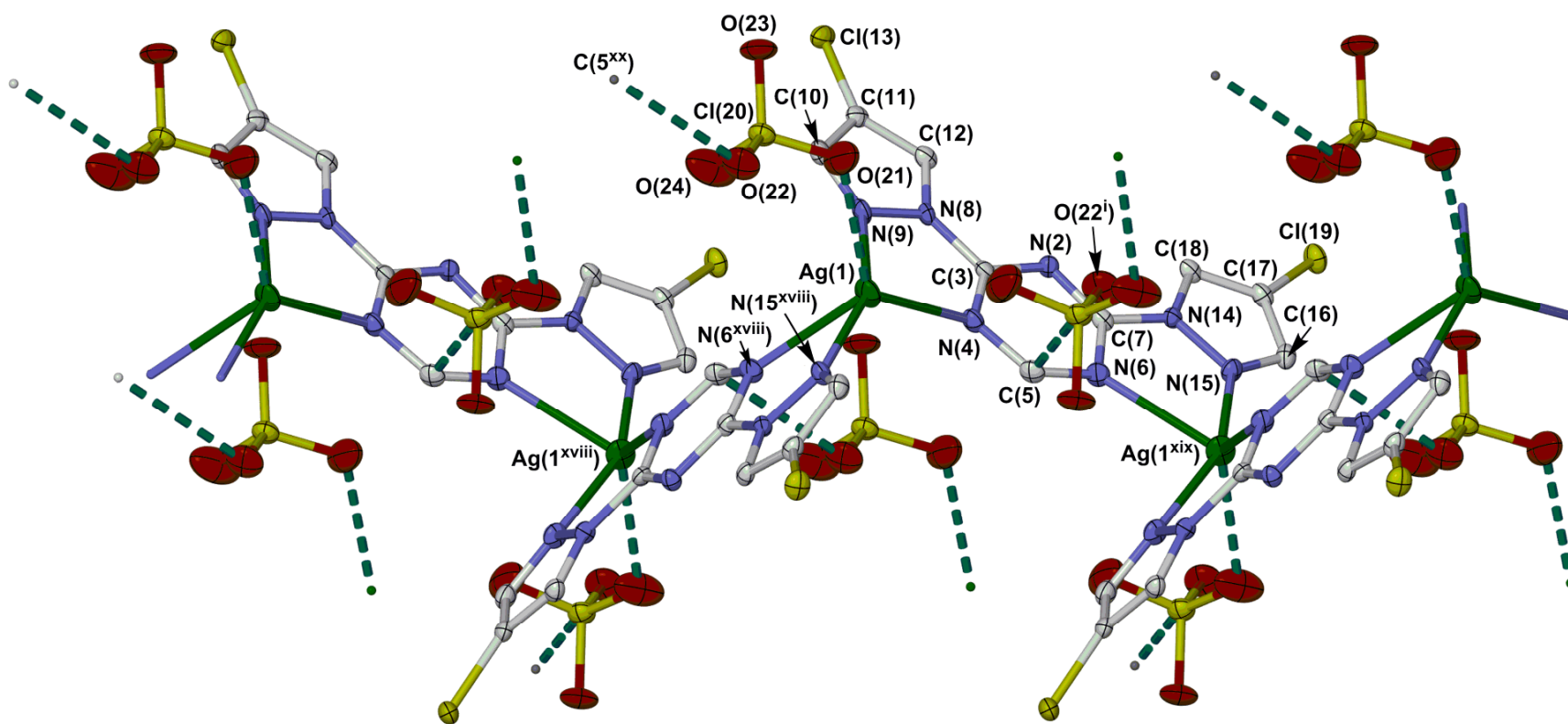


Figure S17 A fraction of a polymer chain in $[\text{Ag}(\mu\text{-}L^2)]\text{ClO}_4$, showing the full atom numbering scheme. Displacement ellipsoids are at the 50 % probability level, and H atoms are omitted for clarity. Symmetry codes: (i) $1/2-x, -1/2+y, 1/2-z$; (xviii) $3/2-x, 1/2+y, 1/2-z$; (xix) $3/2-x, -1/2+y, 1/2-z$; (xx) $1/2-x, 1/2+y, 1/2-z$.

Colour code: C, white; Ag, green; Cl, yellow; N, blue; O, red.

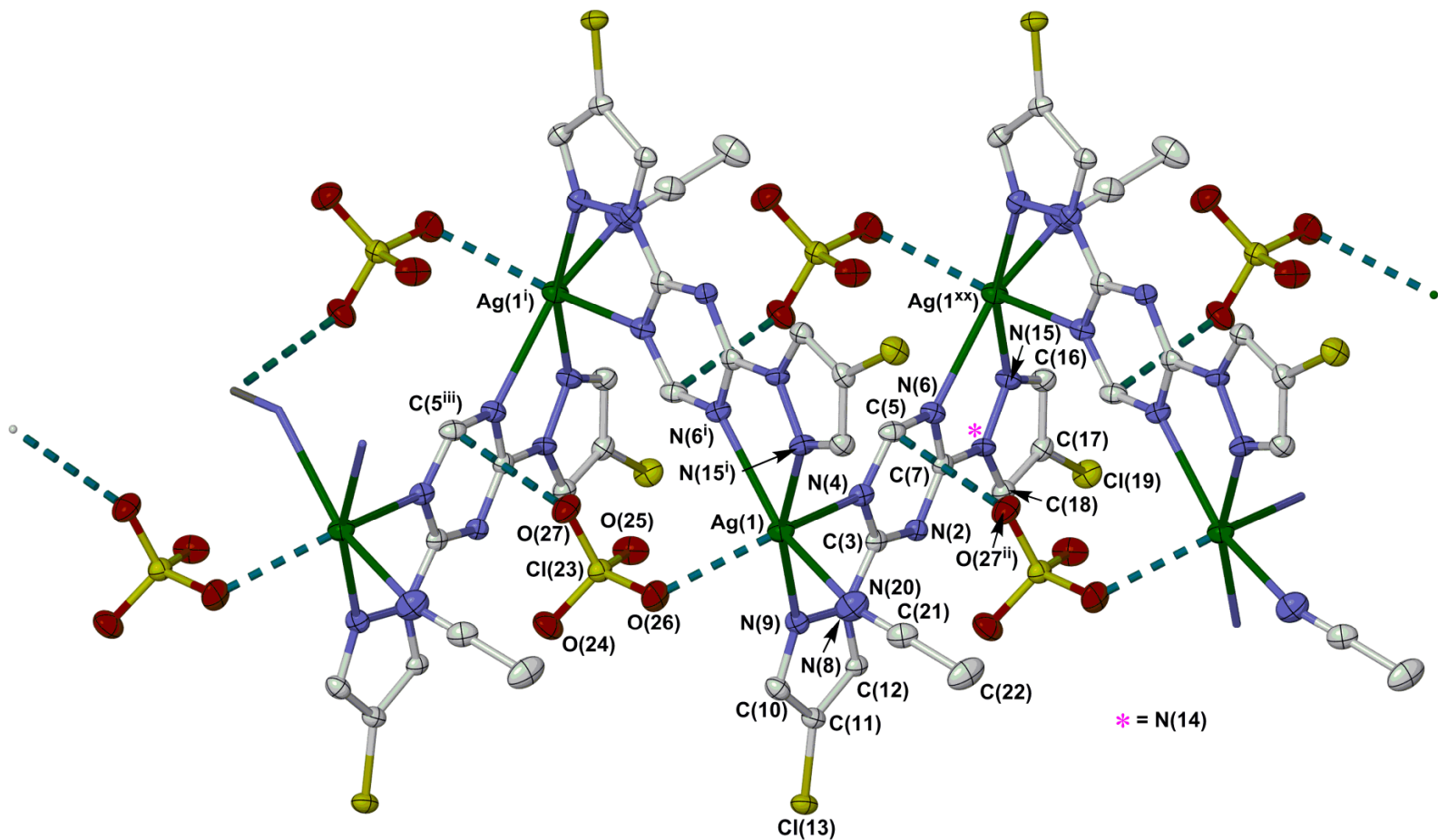


Figure S18 A fraction of a polymer chain in $[\text{Ag}(\text{NCMe})(\mu\text{-L}^2)]\text{ClO}_4$, showing the full atom numbering scheme. Displacement ellipsoids are at the 50 % probability level, and H atoms are omitted for clarity. Symmetry codes: (i) $1/2-x, -1/2+y, 1/2-z$; (ii) $x, 1+y, z$; (iii) $x, -1+y, z$; (xx) $1/2-x, 1/2+y, 1/2-z$.

Colour code: C, white; Ag, green; Cl, yellow; N, blue; O, red.

Table S8 Selected bond lengths (Å) and angles (°) for the coordination polymers [Ag(μ -L²)]ClO₄ and [Ag(NCMe)(μ -L²)]ClO₄. See Figures S17 and S18 for the atom numbering schemes, and page S19 for a definition of Ψ . Symmetry code: (xviii) ³/₂-x, ¹/₂+y, ¹/₂-z; (i) ¹/₂-x, -¹/₂+y, ¹/₂-z.

| [Ag(μ -L ⁵)]ClO ₄ | | [Ag(NCMe)(μ -L ⁵)]ClO ₄ | |
|---|------------|---|-----------|
| Ag(1)–N(4) | 2.403(3) | Ag(1)–N(4) | 2.479(2) |
| Ag(1)–N(6 ^{xviii}) | 2.490(3) | Ag(1)–N(6 ⁱ) | 2.553(2) |
| Ag(1)–N(9) | 2.403(3) | Ag(1)–N(9) | 2.445(2) |
| Ag(1)–N(15 ^{xviii}) | 2.301(3) | Ag(1)–N(15 ⁱ) | 2.433(2) |
| Ag(1)–O(21) | 2.643(4) | Ag(1)–N(20) | 2.414(3) |
| | | Ag(1)–O(26) | 2.670(2) |
| Ag(1)...Ag(1 ^{xviii}) | 6.7596(4) | Ag(1)...Ag(1 ⁱ) | 6.9050(3) |
| N(4)–Ag(1)–N(6 ^{xviii}) | 107.44(10) | N(4)–Ag(1)–N(6 ⁱ) | 87.53(7) |
| N(4)–Ag(1)–N(9) | 67.84(10) | N(4)–Ag(1)–N(9) | 66.06(8) |
| N(4)–Ag(1)–N(15 ^{xviii}) | 126.85(10) | N(4)–Ag(1)–N(15 ⁱ) | 105.11(8) |
| N(4)–Ag(1)–O(21) | 127.03(10) | N(4)–Ag(1)–N(20) | 105.04(9) |
| N(6 ^{aa})–Ag(1)–N(9) | 91.77(9) | N(4)–Ag(1)–O(26) | 138.02(7) |
| N(6 ^{aa})–Ag(1)–N(15 ^{xviii}) | 67.76(10) | N(6 ^v)–Ag(1)–N(9) | 126.70(8) |
| N(6 ^{aa})–Ag(1)–O(21) | 117.60(11) | N(6 ^v)–Ag(1)–N(15 ⁱ) | 64.79(8) |
| N(9)–Ag(1)–N(15 ^{xviii}) | 157.03(10) | N(6 ^v)–Ag(1)–N(20) | 146.63(8) |
| N(9)–Ag(1)–O(21) | 83.79(11) | N(6 ^v)–Ag(1)–O(26) | 90.52(7) |
| N(15 ^{aa})–Ag(1)–O(21) | 96.25(10) | N(9)–Ag(1)–N(15 ⁱ) | 163.04(9) |
| Ψ | 107.22(4) | N(9)–Ag(1)–N(20) | 86.39(9) |
| | | N(9)–Ag(1)–O(26) | 82.19(8) |
| | | N(15 ^v)–Ag(1)–N(20) | 82.00(9) |
| | | N(15 ^v)–Ag(1)–O(26) | 111.80(8) |
| | | N(20)–Ag(1)–O(26) | 99.32(8) |
| | | Ψ | 77.04(4) |

Table S9 Anion... π contacts in the coordination polymers [Ag(μ -L²)]ClO₄ and [Ag(NCMe)(μ -L²)]ClO₄ (Å). See Figures S17 and S18 for the atom numbering scheme. Symmetry codes: (i) ¹/₂-x, -¹/₂+y, ¹/₂-z; (ii) x, 1+y, z.

| | D...A |
|---|----------|
| [Ag(μ -L ⁵)]ClO ₄ | |
| C(5)...O(22 ⁱ) | 2.858(5) |
| [Ag(NCMe)(μ -L ⁵)]ClO ₄ | |
| C(5)...O(27 ⁱⁱ) | 3.086(4) |

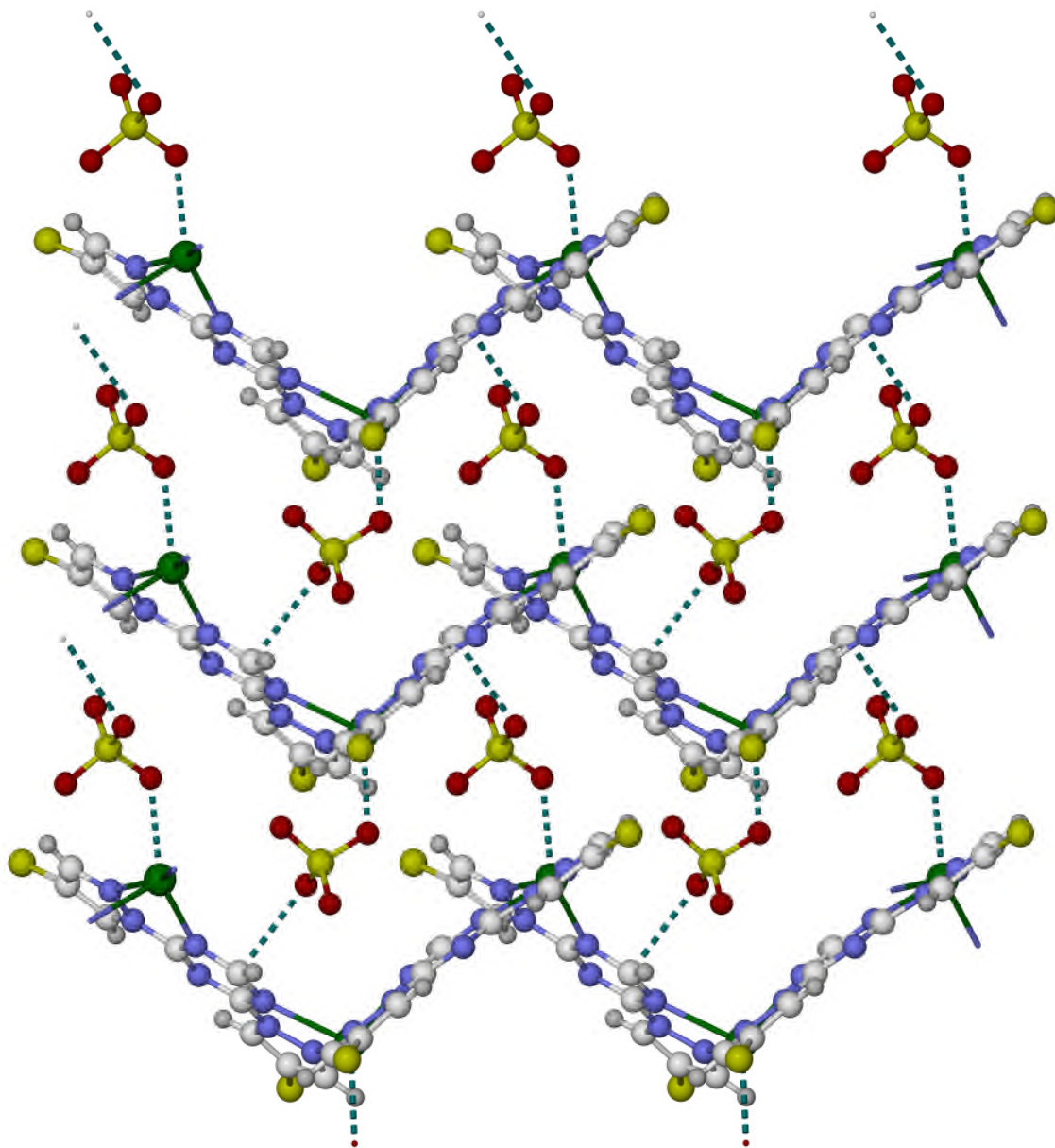


Figure S19 Packing diagram of $[\text{Ag}(\mu\text{-}L^2)]\text{ClO}_4$, showing the association of the polymer chains into 2D sheets through $\text{Ag}\cdots\text{O}$ and $\text{anion}\cdots\pi$ interactions. The view is along the $(1\ \bar{1}\ 2)$ vector, with the unit cell b axis horizontal.

Colour code: C, white; H, pale grey; Ag, green; Cl, yellow; N, blue; O, red.

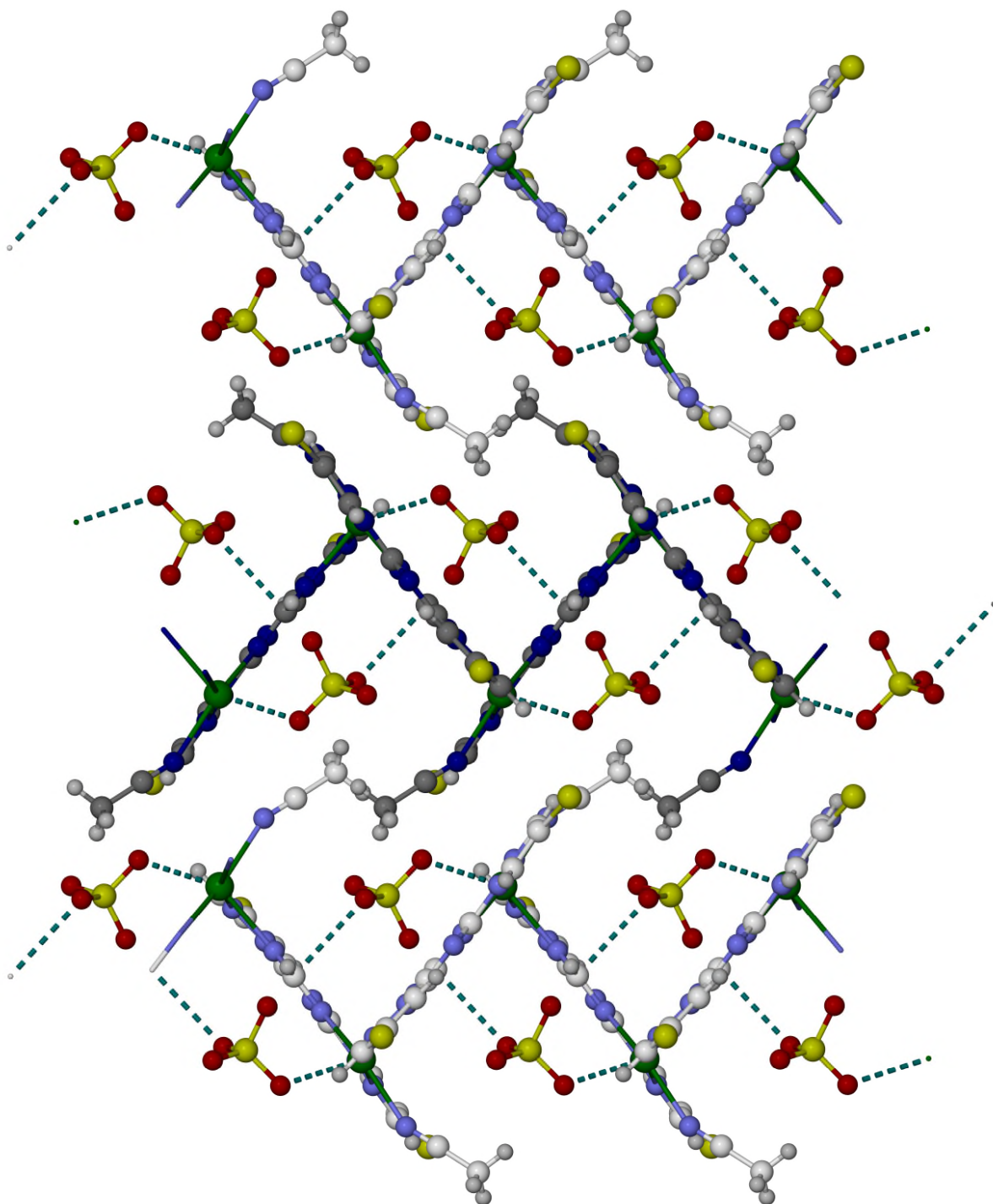


Figure S20 Packing diagram of $[\text{Ag}(\text{NCMe})(\mu\text{-}L^2)]\text{ClO}_4$, highlighting that this coordination polymer packs as discrete chains in its lattice, with only intra-chain anion... π interactions. One chain is highlighted with dark colouration, for clarity. The view is along the (101) vector, with the unit cell b axis horizontal.

Colour code: C, white or dark grey; H, pale grey; Ag, green; Cl, yellow; N, pale or dark blue; O, red.

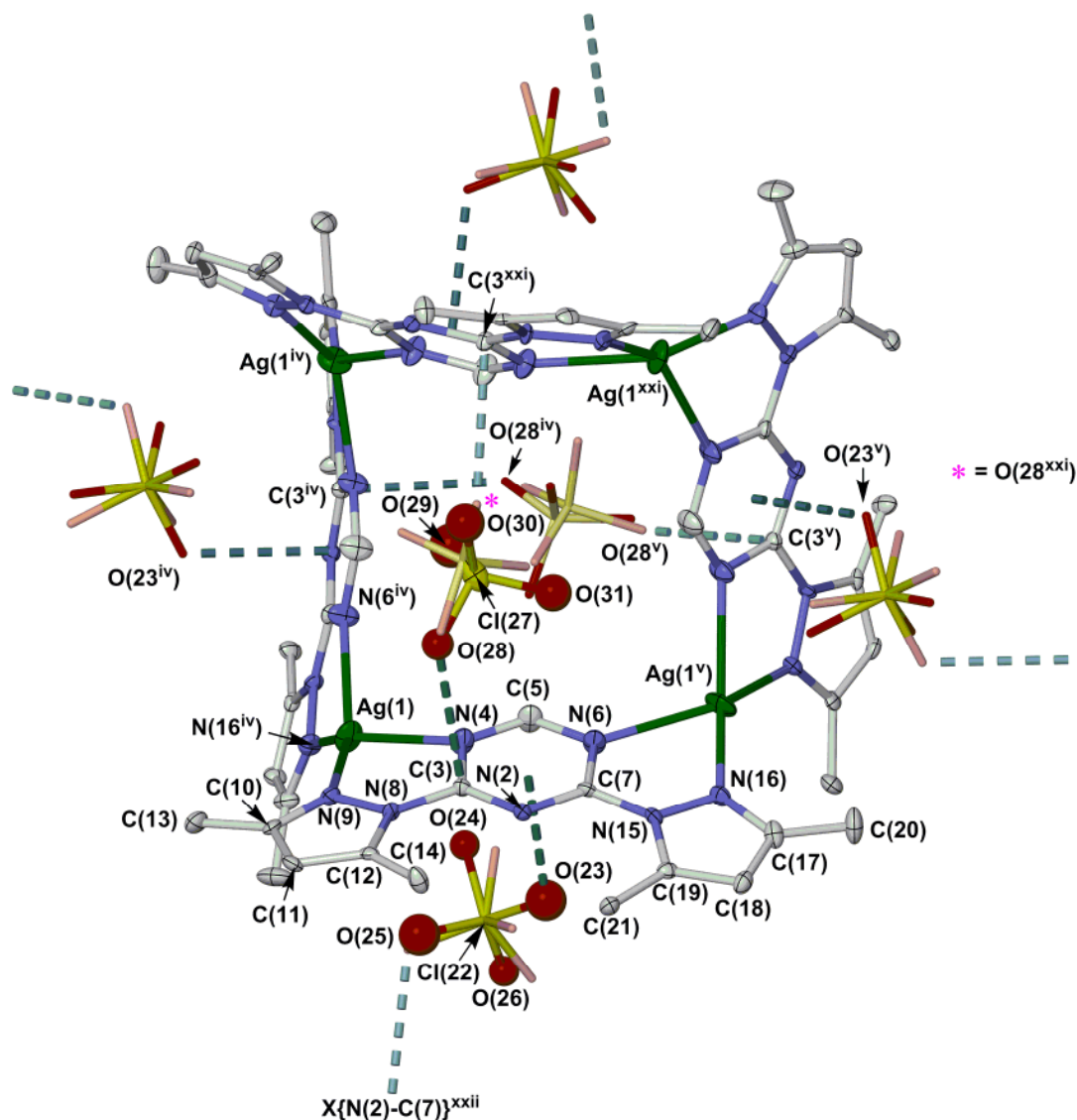


Figure S21 View of the molecular square assembly in solvent-free $[Ag_4(\mu-L^3)_4][ClO_4]_4$, showing the full atom numbering scheme. Displacement ellipsoids are at the 50 % probability level, except for symmetry equivalent sites for the anions which are de-emphasised for clarity, and all H atoms are omitted. Symmetry codes: (iv) $1-y, x, 1-z$; (v) $y, 1-x, 1-z$; (xxi) $1-x, 1-y, z$; (xxii) $1-x, -y, z$.

Colour code: C, white; Ag, green; Cl, yellow; N, blue; O, red.

Anion... π interactions are drawn to the centroid 'X' of the triazine ring acceptor, or to an individual C atom, whichever is the shorter distance (Table S11).

The encapsulated anions and their disorder sites are all equivalent by symmetry, and are held in place by one short anion... π interaction and two weak C-H...O contacts (Table S11). The C-H...O interactions are not shown in this Figure, since H atoms are omitted from the diagram (Figure S25).

Table S10 Selected bond lengths (Å) and angles (°) for the unsolvated form of $[\text{Ag}_4(\mu\text{-L}^3)_4][\text{ClO}_4]_4$. See Figure S21 for the atom numbering scheme, while the definition of Ψ is given on page S19. Symmetry code: (iv) $1-y, x, 1-z$.

| | |
|--|------------|
| Ag(1)–N(4) | 2.388(4) |
| Ag(1)–N(6 ^{iv}) | 2.414(4) |
| Ag(1)–N(9) | 2.225(4) |
| Ag(1)–N(16 ^{iv}) | 2.230(3) |
| Ag(1)...Ag(1 ^{iv}) | 6.7083(5) |
| N(4)–Ag(1)–N(6 ^{iv}) | 107.06(13) |
| N(4)–Ag(1)–N(9) | 69.48(13) |
| N(4)–Ag(1)–N(16 ^{iv}) | 139.56(13) |
| N(6 ^{iv})–Ag(1)–N(9) | 143.17(13) |
| N(6 ^{iv})–Ag(1)–N(16 ^{iv}) | 68.53(13) |
| N(9)–Ag(1)–N(16 ^{iv}) | 138.27(13) |
| Ψ | 71.10(8) |

Table S11 Intermolecular second-sphere interactions in $[\text{Ag}_4(\mu\text{-L}^3)_4][\text{ClO}_4]_4$ (Å, °). See Figure S21 for the atom numbering scheme. Symmetry code: (iv) $1-y, x, 1-z$.

| | D–H | H...A | D...A | D–H...A |
|-----------------------------------|------|-------|-----------|---------|
| Anion... π contacts | | | | |
| C(3)...O(28) | – | – | 2.929(12) | – |
| X{N(2)–C(7)}...O(23) ^a | – | – | 2.859 | – |
| Hydrogen bonds | | | | |
| C(5)–H(5)...O(29 ^{iv}) | 0.95 | 2.32 | 3.193(14) | 154.3 |
| C(5)–H(5)...O(31) | 0.95 | 2.31 | 3.334(10) | 1175.7 |

^aThe closest contact in this host:guest interaction is to the centroid ‘X’ of the triazinyl ring listed (Figure S21).

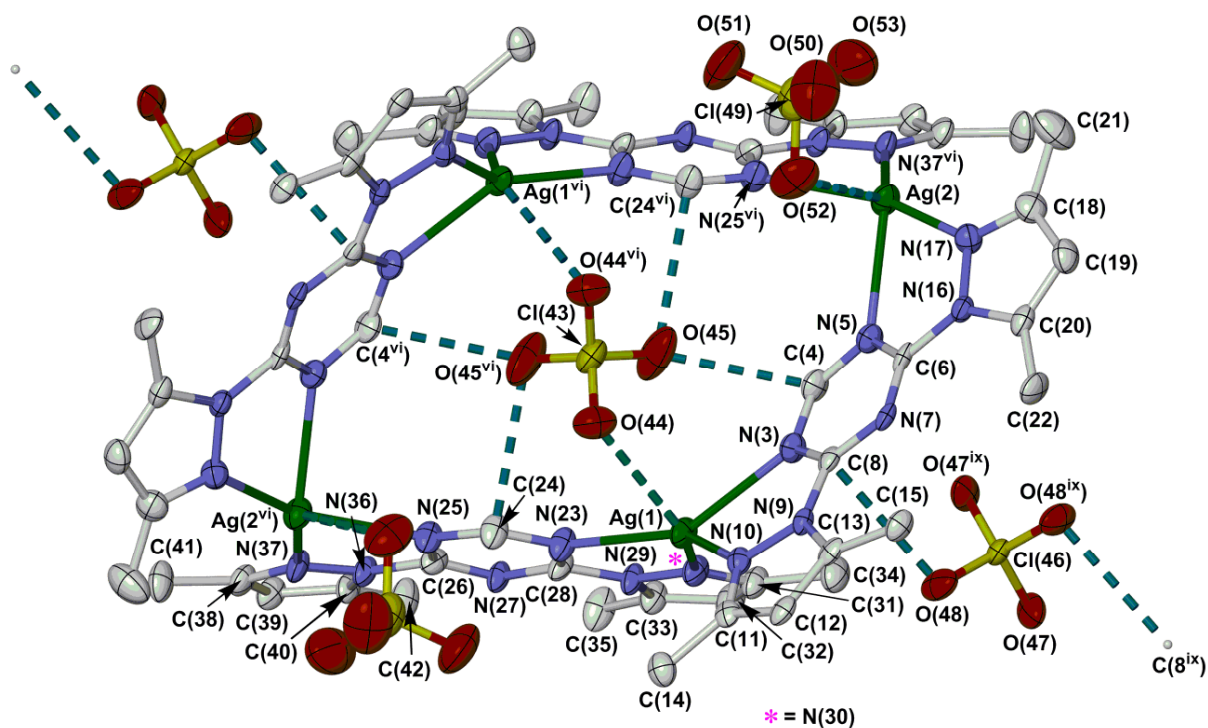


Figure S22 View of the molecular square assembly in $[\text{Ag}_4(\mu\text{-L}^3)_4][\text{ClO}_4]_4 \cdot 3.2\text{MeNO}_2 \cdot 1.2\text{H}_2\text{O}$, showing the full atom numbering scheme. The view is the same as in Figure 7 of the main article. Displacement ellipsoids are at the 50 % probability level, and H atoms are omitted for clarity. Symmetry codes: (vi) $1-x, y, 3/2-z$; (ix) $1-x, y, 1/2-z$.

Colour code: C, white; Ag, green; Cl, yellow; N, blue; O, red.

The encapsulated anion (which has crystallographic C_2 symmetry) forms two Ag...O interactions, and two short and two long anion... π interactions, to the metallacyclic host (Figure S25, Table S13).

Table S12 Selected bond lengths (Å) and angles (°) for $[\text{Ag}_4(\mu\text{-}L^3)_4][\text{ClO}_4]_4 \cdot 3.2\text{MeNO}_2 \cdot 1.2\text{H}_2\text{O}$. See Figure S22 the atom numbering scheme, while the definition of Ψ is given on page S19. Symmetry code:

(vi) $1-x, y, 3/2-z$.

| | | | |
|-------------------|------------|---|------------|
| Ag(1)–N(3) | 2.466(5) | Ag(2)–N(5) | 2.522(6) |
| Ag(1)–N(10) | 2.246(5) | Ag(2)–N(17) | 2.231(6) |
| Ag(1)–N(23) | 2.415(6) | Ag(2)–N(25 ^{vi}) | 2.474(6) |
| Ag(1)–N(30) | 2.296(6) | Ag(2)–N(37 ^{vi}) | 2.238(6) |
| Ag(1)–O(44) | 2.746(6) | Ag(2)–O(52) | 2.802(7) |
| Ag(1)...Ag(2) | 6.8360(8) | Ag(1)...Ag(2 ^{vi}) | 6.7796(8) |
| N(3)–Ag(1)–N(10) | 68.07(18) | N(5)–Ag(2)–N(17) | 66.98(19) |
| N(3)–Ag(1)–N(23) | 145.7(2) | N(5)–Ag(2)–N(25 ^{vi}) | 98.23(19) |
| N(3)–Ag(1)–N(30) | 107.0(2) | N(5)–Ag(2)–N(37 ^{vi}) | 128.2(2) |
| N(3)–Ag(1)–O(44) | 86.20(18) | N(5)–Ag(1)–O(52) | 83.00(19) |
| N(10)–Ag(1)–N(23) | 140.3(2) | N(17)–Ag(2)–N(25 ^{vi}) | 152.9(2) |
| N(10)–Ag(1)–N(30) | 136.43(19) | N(17)–Ag(2)–N(37 ^{vi}) | 139.3(2) |
| N(10)–Ag(1)–O(44) | 91.17(18) | N(17)–Ag(1)–O(52) | 81.5(2) |
| N(23)–Ag(1)–N(30) | 67.11(19) | N(25 ^{vi})–Ag(2)–N(37 ^{vi}) | 67.71(19) |
| N(23)–Ag(1)–O(44) | 76.52(19) | N(25 ^{vi})–Ag(1)–O(52) | 74.0(2) |
| N(30)–Ag(1)–O(44) | 132.34(19) | N(37 ^{vi})–Ag(1)–O(52) | 132.74(19) |
| Ψ [Ag(1)] | 114.21(12) | Ψ [Ag(2)] | 50.48(14) |

Table S13 Anion... π contacts in $[\text{Ag}_4(\mu\text{-}L^3)_4][\text{ClO}_4]_4 \cdot 3.2\text{MeNO}_2 \cdot 1.2\text{H}_2\text{O}$ (Å). See Figure S22 for the atom numbering scheme. Symmetry code: (vi) $1-x, y, 3/2-z$.

| | D...A |
|------------------------------|-----------|
| C(4)...O(45) | 2.844(10) |
| C(8)...O(48) | 2.998(8) |
| C(24)...O(45 ^{vi}) | 3.066(11) |

There are no noteworthy C–H...O hydrogen bonds in this structure.

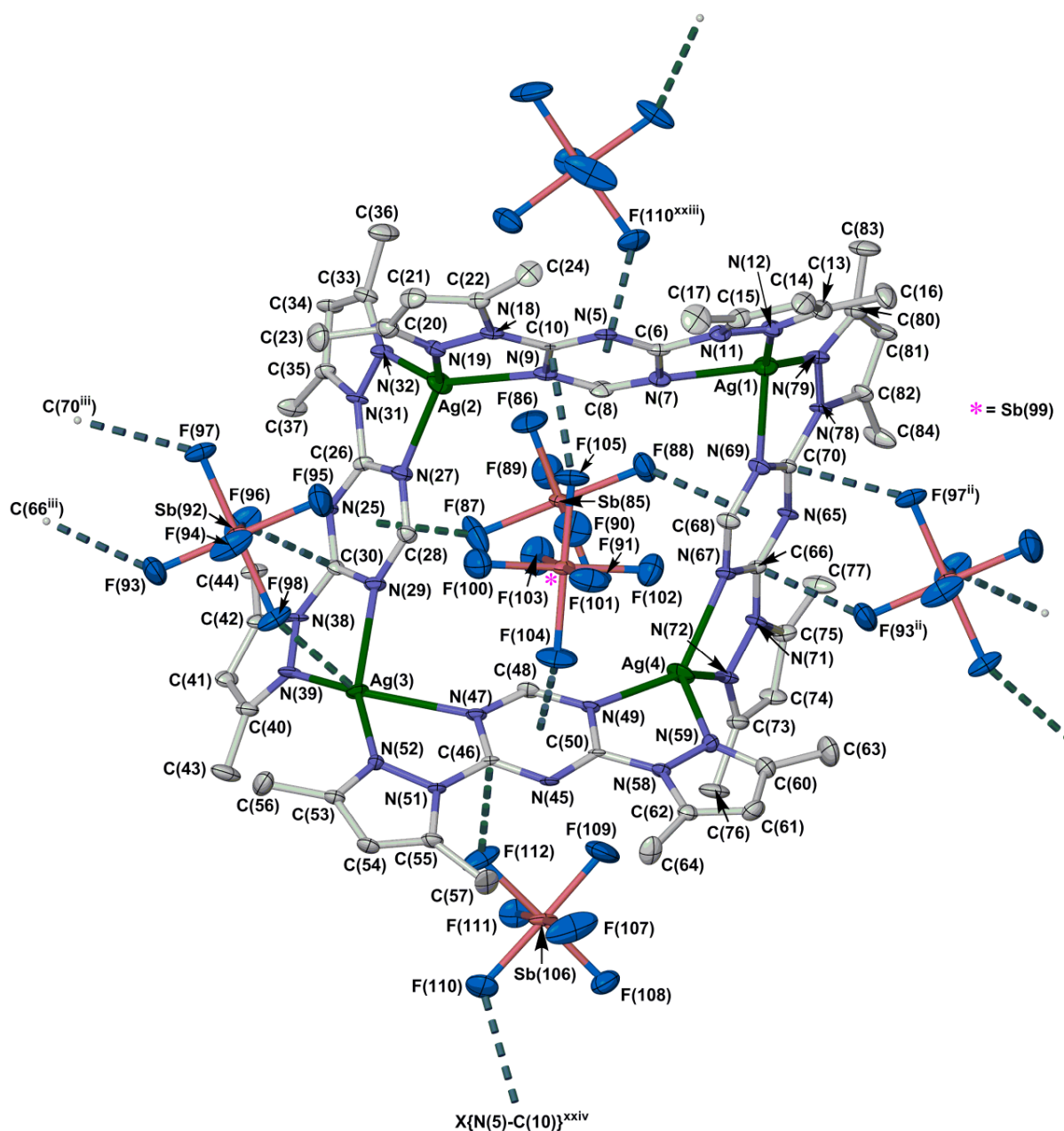


Figure S23 View of the molecular square assembly in $[Ag_4(\mu-L^3)_4][SbF_6]_2 \cdot MeNO_2$, showing the full atom numbering scheme. Displacement ellipsoids are at the 50 % probability level, and all H atoms are omitted for clarity. Symmetry codes: (ii) $x, 1+y, z$; (iii) $x, -1+y, z$; (xxiii) $1/2+x, 1/2-y, 1/2+z$; (xxiv) $-1/2+x, 1/2-y, -1/2+z$.

Colour code: C, white; Ag, green; F, cyan; N, blue; Sb, pink.

Anion... π interactions are drawn to the centroid 'X' of the triazine ring acceptor, or to an individual C atom, whichever is the shorter distance (Table S15).

In contrast to the perchlorate salts with this arrangement of guest anions, the SbF_6^- ions in this structure are not disordered. Each in-cavity SbF_6^- ion forms two short anion... π interactions, to triazinyl acceptors on opposite sides of the host cavity. A weak C-H...F interaction between C(28) and F(103) is not shown, since H atoms are omitted from the diagram (Figure S26).

Table S14 Selected bond lengths (Å) and angles (°) for [Ag₄(μ-L³)₄][SbF₆]₄·MeNO₂. See Figure S23 for the atom numbering scheme, while the definition of Ψ is given on page S19.

| | | | |
|-------------------|------------|-------------------|------------|
| Ag(1)–N(7) | 2.486(5) | Ag(3)–N(29) | 2.448(4) |
| Ag(1)–N(12) | 2.196(4) | Ag(3)–N(39) | 2.247(5) |
| Ag(1)–N(69) | 2.425(4) | Ag(3)–N(47) | 2.510(5) |
| Ag(1)–N(79) | 2.201(5) | Ag(3)–N(52) | 2.222(4) |
| Ag(2)–N(9) | 2.360(5) | Ag(3)–F(98) | 2.759(4) |
| Ag(2)–N(19) | 2.239(4) | Ag(4)–N(49) | 2.307(4) |
| Ag(2)–N(27) | 2.328(4) | Ag(4)–N(59) | 2.267(5) |
| Ag(2)–N(32) | 2.263(4) | Ag(4)–N(67) | 2.324(4) |
| | | Ag(4)–N(72) | 2.246(5) |
| Ag(1)...Ag(2) | 6.7062(6) | Ag(2)...Ag(3) | 6.5880(5) |
| Ag(1)...Ag(4) | 6.6918(6) | Ag(3)...Ag(4) | 6.7605(6) |
| N(7)–Ag(1)–N(12) | 69.06(16) | N(29)–Ag(3)–N(39) | 68.05(15) |
| N(7)–Ag(1)–N(69) | 96.53(14) | N(29)–Ag(3)–N(47) | 94.60(15) |
| N(7)–Ag(1)–N(79) | 148.09(16) | N(29)–Ag(3)–N(52) | 149.58(15) |
| N(12)–Ag(1)–N(69) | 142.28(16) | N(29)–Ag(3)–F(98) | 80.37(14) |
| N(12)–Ag(1)–N(79) | 138.91(17) | N(39)–Ag(3)–N(47) | 137.28(16) |
| N(69)–Ag(1)–N(79) | 69.06(15) | N(39)–Ag(3)–N(52) | 141.66(16) |
| N(9)–Ag(2)–N(19) | 69.53(17) | N(39)–Ag(3)–F(98) | 87.92(14) |
| N(9)–Ag(2)–N(27) | 124.18(15) | N(47)–Ag(3)–N(52) | 67.09(15) |
| N(9)–Ag(2)–N(32) | 140.01(16) | N(47)–Ag(3)–F(98) | 128.88(13) |
| N(19)–Ag(2)–N(27) | 135.19(16) | N(52)–Ag(3)–F(98) | 92.35(14) |
| N(19)–Ag(2)–N(32) | 130.46(17) | N(49)–Ag(4)–N(59) | 69.86(16) |
| N(27)–Ag(2)–N(32) | 69.84(15) | N(49)–Ag(4)–N(67) | 134.36(15) |
| | | N(49)–Ag(4)–N(72) | 142.57(16) |
| | | N(59)–Ag(4)–N(67) | 127.97(16) |
| | | N(59)–Ag(4)–N(72) | 121.81(17) |
| | | N(67)–Ag(4)–N(72) | 70.12(15) |
| Ψ [Ag(1)] | 55.04(9) | Ψ [Ag(3)] | 55.55(8) |
| Ψ [Ag(2)] | 100.63(8) | Ψ [Ag(4)] | 96.86(8) |

Table S15 Intermolecular second-sphere interactions in [Ag₄(μ-L³)₄][SbF₆]₄·MeNO₂ (Å, °). See Figure S23 for the atom numbering scheme. Symmetry codes: (ii) *x*, 1+*y*, *z*; (xxiii) ¹/₂+*x*, ¹/₂–*y*, ¹/₂+*z*.

| | D–H | H...A | D...A | D–H...A |
|---|------|-------|----------|---------|
| Anion...π contacts | | | | |
| X{C(5)–C(10)}...F(110 ^{xxiii}) ^a | – | – | 2.834 | – |
| C(10)...F(105) | – | – | 2.880(6) | – |
| X{C(65)–C(70)}...F(87) ^a | – | – | 2.797 | – |
| C(30)...F(96) | – | – | 2.803(7) | – |
| C(46)...F(112) | – | – | 2.855(6) | – |
| X{C(65)–C(70)}...F(104) ^a | – | – | 2.843 | – |
| X{C(65)–C(70)}...F(88) ^a | – | – | 2.769 | – |
| C(66)...F(93 ⁱⁱ) | – | – | 2.750(7) | – |
| C(70)...F(97 ⁱⁱ) | – | – | 2.841(7) | – |
| Hydrogen bond | | | | |
| C(28)–H(28)...F(103) | 0.95 | 2.38 | 3.281(7) | 158.0 |

^aThe closest contact in this host:guest interaction is to the centroid 'X' of the triazinyl ring listed (Figure S23).

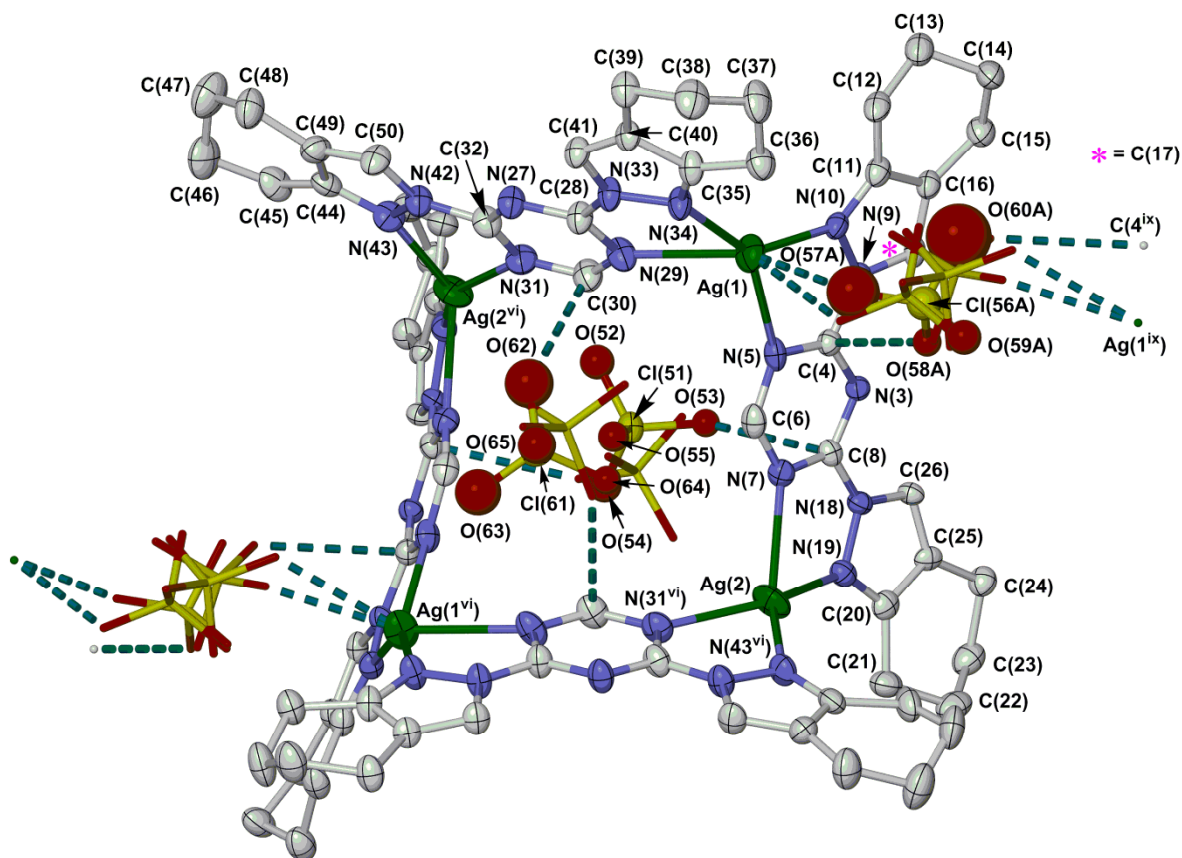


Figure S24 View of the molecular square assembly in $[\text{Ag}_4(\mu\text{-}L^4)][\text{ClO}_4]_4 \cdot \text{MeNO}_2$, showing the full atom numbering scheme. Displacement ellipsoids are at the 50 % probability level, except for symmetry equivalent or disorder sites for the anions which are de-emphasised for clarity, and all H atoms are omitted. Symmetry codes: (vi) $1-x, y, 3/2-z$; (ix) $1-x, y, 1/2-z$.

Colour code: C, white; Ag, green; Cl, yellow; N, blue; O, red.

Each encapsulated anion forms one strong and one weak anion... π interaction, in both of its symmetry-equivalent disorder sites (Table S17). An additional weak C–H...O interaction between C(6) and O(64) is not shown, since H atoms are omitted from the diagram (Figure S26).

Table S16 Selected bond lengths (Å) and angles (°) for [Ag₄(μ-L⁴)₄][ClO₄]₄·MeNO₂. See Figure S24 for the atom numbering scheme, while the definition of Ψ is given on page S19. Symmetry code: (vi) 1-x, y, 3/2-z.

| | | | |
|---------------------------|-------------------|--|-----------|
| Ag(1)–N(5) | 2.466(7) | Ag(2)–N(7) | 2.447(6) |
| Ag(1)–N(10) | 2.219(6) | Ag(2)–N(19) | 2.225(6) |
| Ag(1)–N(29) | 2.566(7) | Ag(2)–N(31 ^{vi}) | 2.378(6) |
| Ag(1)–N(34) | 2.195(6) | Ag(2)–N(43 ^{vi}) | 2.287(6) |
| Ag(1)–O(57A)/O(57B) | 2.74(2)/2.75(2) | | |
| Ag(1)...Ag(2) | 6.9287(11) | Ag(1)...Ag(2 ^{vi}) | 7.0322(9) |
| N(5)–Ag(1)–N(10) | 70.3(2) | N(7)–Ag(2)–N(19) | 71.0(2) |
| N(5)–Ag(1)–N(29) | 89.18(19) | N(7)–Ag(2)–N(31 ^{vi}) | 107.0(2) |
| N(5)–Ag(1)–N(34) | 148.5(2) | N(7)–Ag(2)–N(43 ^{vi}) | 126.5(2) |
| N(5)–Ag(1)–O(57A)/O(57B) | 91.8(6)/84.5(5) | N(19)–Ag(2)–N(31 ^{vi}) | 151.6(2) |
| N(10)–Ag(1)–N(29) | 120.1(2) | N(19)–Ag(2)–N(43 ^{vi}) | 134.3(2) |
| N(10)–Ag(1)–N(34) | 140.2(2) | N(31 ^x)–Ag(2)–N(43 ^{vi}) | 70.7(2) |
| N(10)–Ag(1)–O(57A)/O(57B) | 86.6(5)/93.6(5) | | |
| N(29)–Ag(1)–N(34) | 69.3(2) | | |
| N(29)–Ag(1)–O(57A)/O(57B) | 151.8(6)/141.2(5) | | |
| N(34)–Ag(1)–O(57A)/O(57B) | 96.9(4)/97.9(5) | | |
| Ψ [Ag(1)] | 66.50(15) | Ψ [Ag(2)] | 76.39(13) |

Table S17 Intermolecular second-sphere interactions in [Ag₄(μ-L⁴)₄][ClO₄]₄·MeNO₂ (Å, °). See Figure S24 for the atom numbering scheme. Symmetry code: (vi) 1-x, y, 3/2-z.

| | D–H | H...A | D...A | D–H...A |
|------------------------------|------|-------|-----------|---------|
| Anion...π contacts | | | | |
| C(4)...O(58A) | – | – | 3.065(14) | – |
| C(6)...O(55) | – | – | 3.092(18) | – |
| C(8)...O(53) | – | – | 2.871(15) | – |
| C(30)...O(62) | – | – | 2.89(3) | – |
| C(30)...O(64 ^{vi}) | – | – | 3.038(16) | – |
| Hydrogen bonds | | | | |
| C(6)–H(6)...O(64) | 0.95 | 2.45 | 3.371(15) | 164.5 |

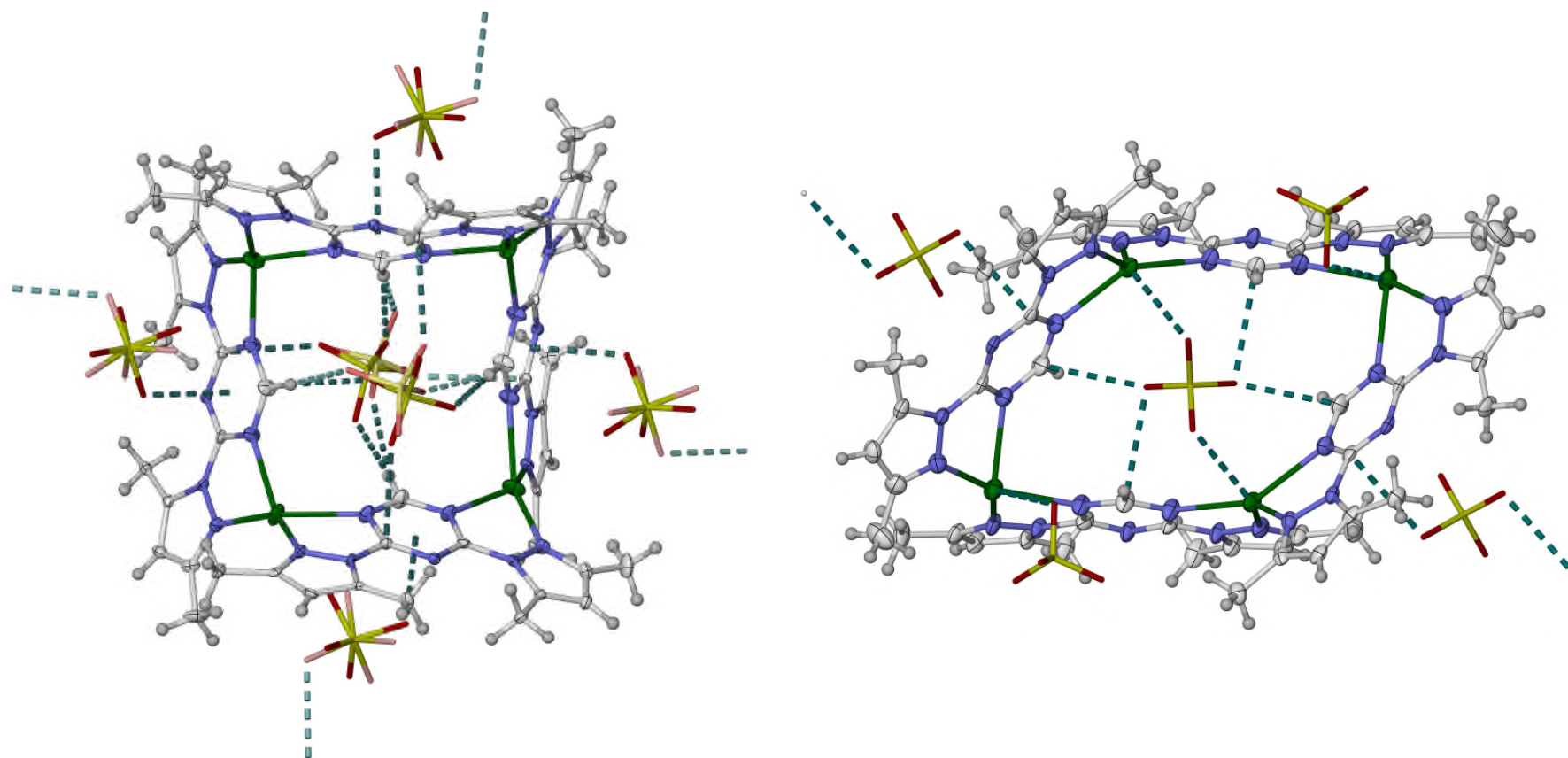


Figure S25 Views of the assemblies in $[Ag_4(\mu-L^3)_4][ClO_4]_4$ (left) and $[Ag_4(\mu-L^3)_4][ClO_4]_4 \cdot 3.2MeNO_2 \cdot 1.2H_2O$ (right), showing their full complement of secondary interactions. Different disorder orientations of the anions in the left hand diagram, and the secondary interactions to them, are distinguished by pale or dark colouration. Colour code: C, white; H, pale grey; Ag, green; Cl, pale or dark yellow; N, blue; O, pale or dark red.

The right hand view is the same as in Figure S22, but is included here again for completeness.

Anion... π interactions in the left hand diagram are drawn to the centroid of the triazine ring acceptor, or to an individual C atom, whichever is the shorter distance (Table S11). All anion... π interactions in the right hand diagram are formed to an individual C atom.

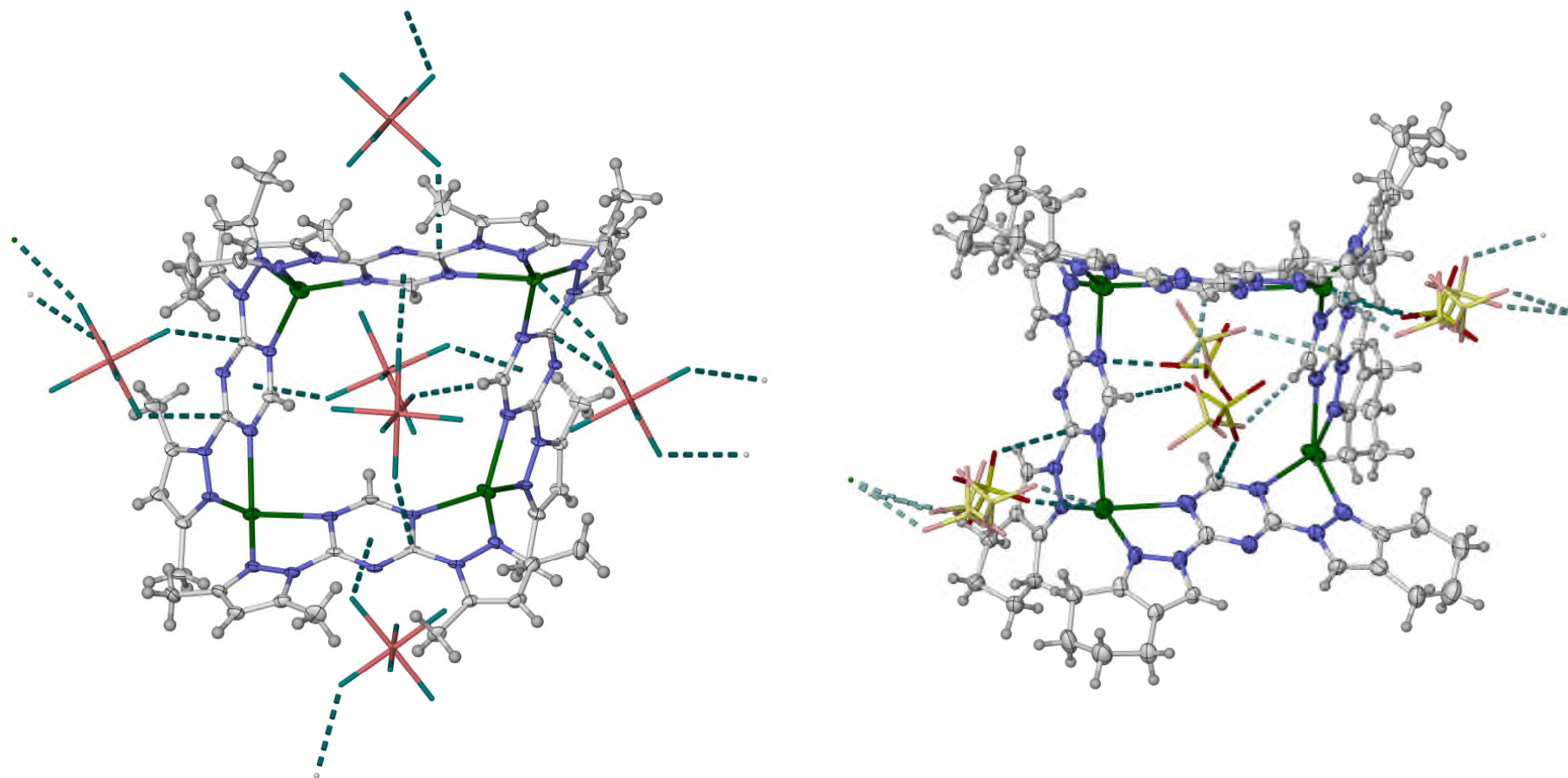


Figure S26 Views of the assemblies in $[Ag_4(\mu-L^3)_4][SbF_6]_4 \cdot MeNO_2$ (left) and $[Ag_4(\mu-L^4)_4][ClO_4]_4 \cdot MeNO_2$ (right), showing their full complement of secondary interactions. Different disorder orientations of the anions in the right hand diagram, and the secondary interactions to them, are distinguished by pale or dark colouration. Colour code: C, white; H, pale grey; Ag, green; Cl, pale or dark yellow; F, cyan; N, blue; O, pale or dark red; Sb, pink.

Anion... π interactions in the left hand diagram are drawn to the centroid of the triazine ring acceptor, or to an individual C atom, whichever is the shorter distance (Table S15). All anion... π interactions in the right hand diagram are formed to an individual C atom.

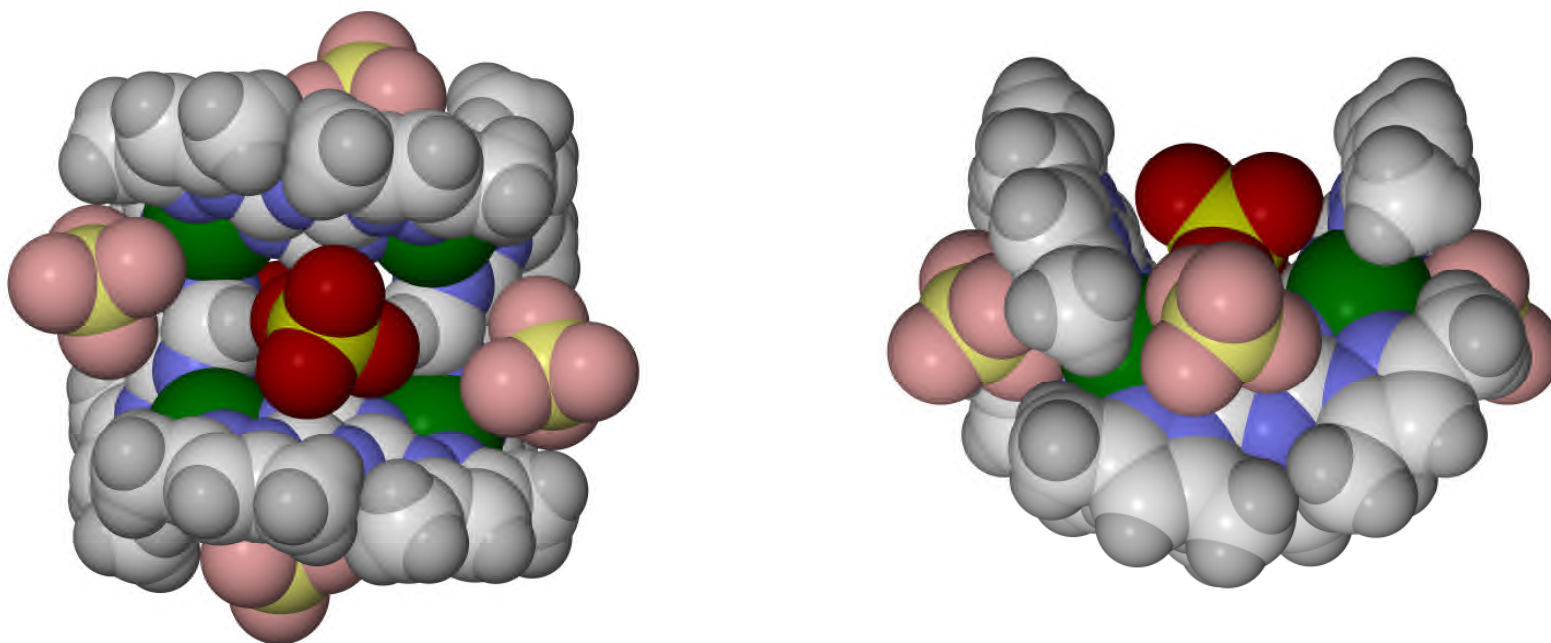


Figure S27 Space-filling views of the host:guest assembly in solvent-free $[\text{Ag}_4(\mu\text{-}L^3)_4][\text{ClO}_4]_4$. For clarity, in-cavity and peripheral perchlorate ions forming secondary interactions with the molecular square are shown with dark and pale colouration, respectively. Colour code: C, white; H, pale grey; Ag, green; Cl, pale or dark yellow; N, blue; O, pale or dark red.

This assembly has crystallographic S_4 symmetry, and so gives identical views from either side of its open face (*cf* Figure S28). The anions are all crystallographically disordered about C_2 axes, but this disorder is not shown in the Figure.

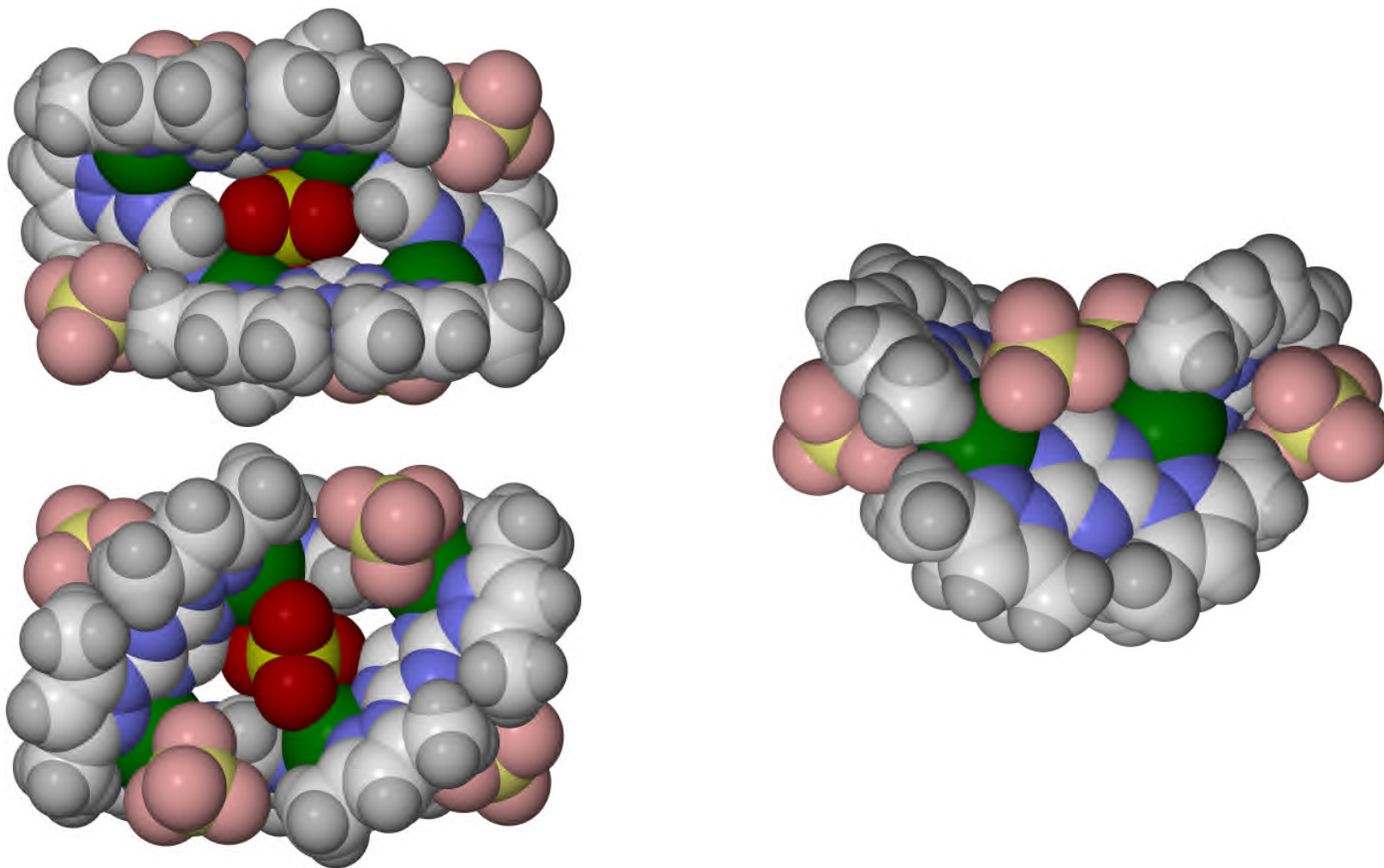


Figure S28 Space-filling views of the host:guest assembly in $[\text{Ag}_4(\mu\text{-}L^3)_4][\text{ClO}_4]_4 \cdot 3.2\text{MeNO}_2 \cdot 1.2\text{H}_2\text{O}$. Details as for Figure S27. Colour code: C, white; H, pale grey; Ag, green; Cl, pale or dark yellow; N, blue; O, pale or dark red.

The two views on the left show the opposite sides on the open face of the molecular square. Some of the exocyclic perchlorate ions bridge to neighbouring metallocycles in the lattice (not shown). The lattice solvent, which does not form a second sphere interaction with the complex, is not included.

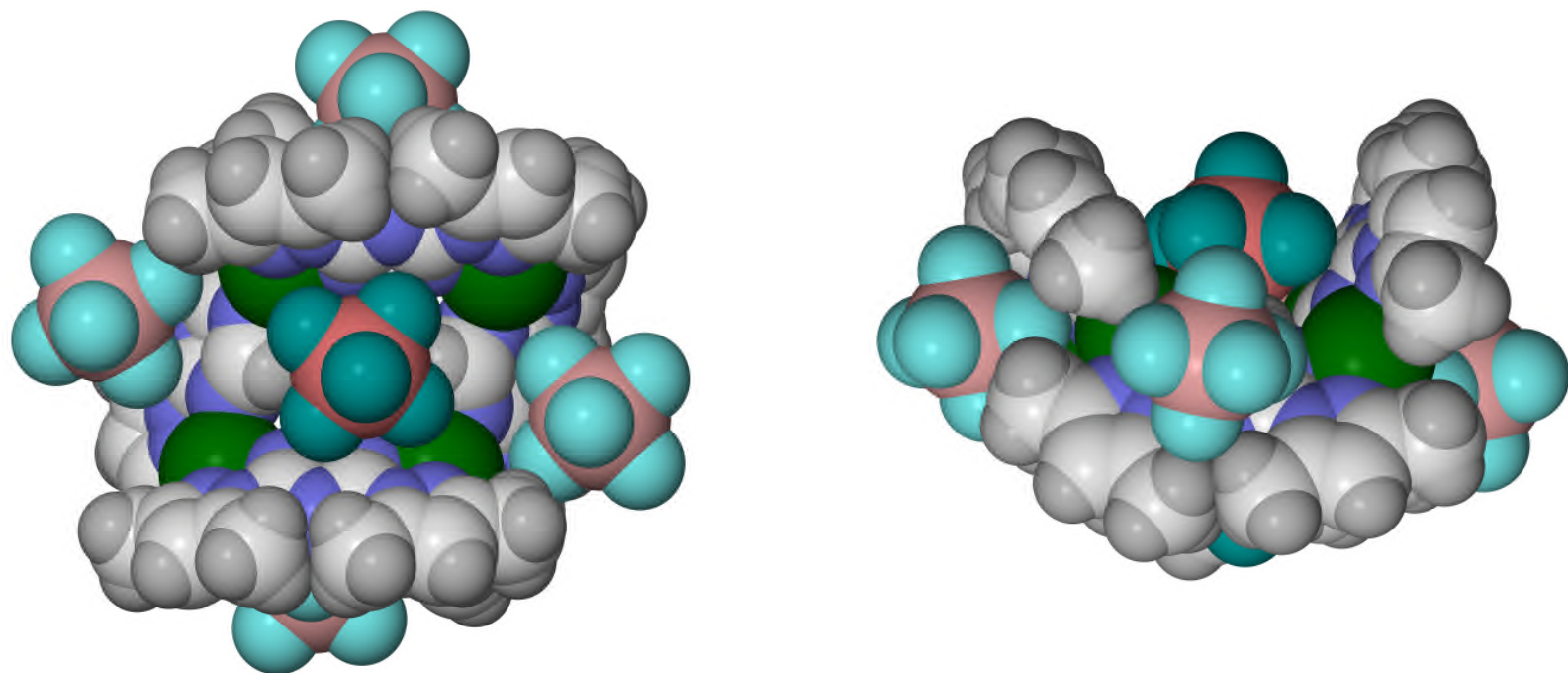


Figure S29 Space-filling views of the host:guest assembly in $[\text{Ag}_4(\mu\text{-}L^3)_4][\text{SbF}_6]_4 \cdot \text{MeNO}_2$. For clarity, in-cavity and peripheral anions forming secondary interactions with the molecular square are shown with dark and pale colouration, respectively.

Colour code: C, white; H, pale grey; Ag, green; B, pale or dark pink; F, pale or dark cyan; N, blue.

All the exocyclic hexafluoroantimonate ions bridge to neighbouring metallocycles in the lattice (not shown). The lattice solvent, which does not form a second sphere interaction with the complex, is not included.

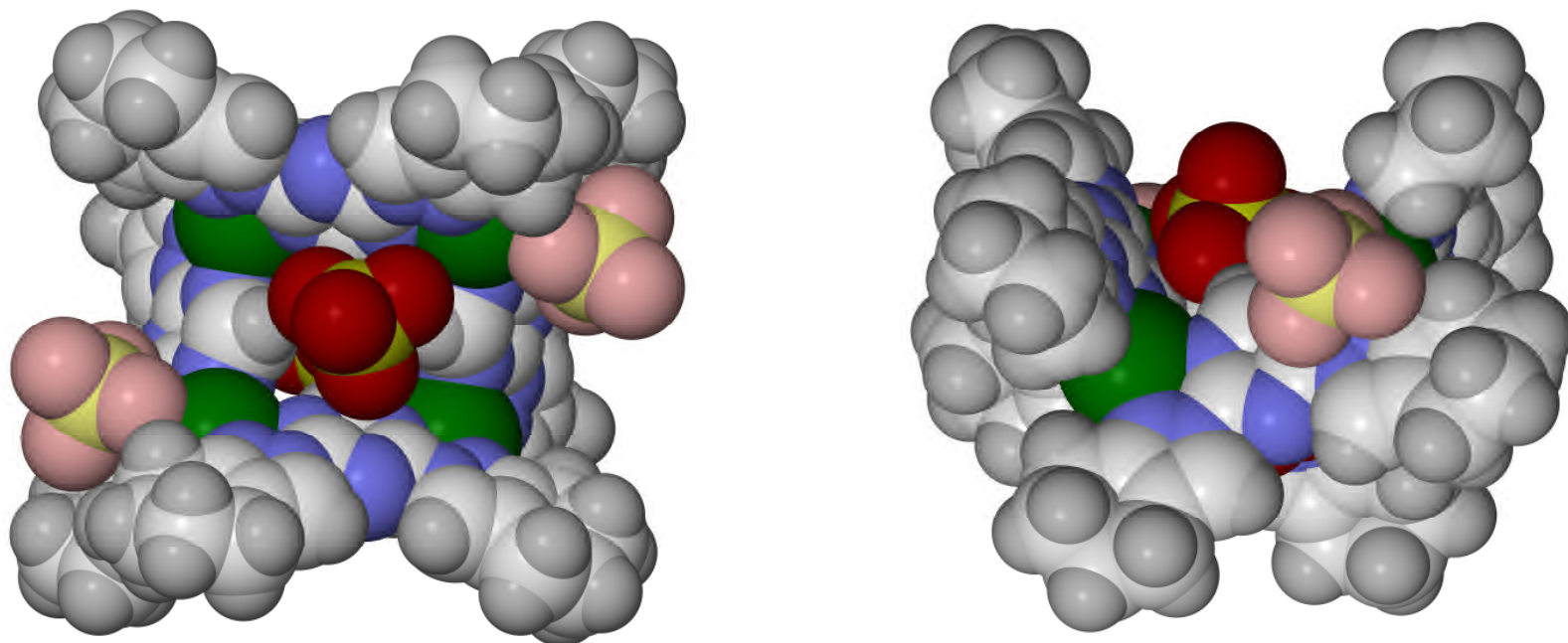


Figure S30 Space-filling views of the host:guest assembly in $[\text{Ag}_4(\mu\text{-}L^4)][\text{ClO}_4]_4 \cdot \text{MeNO}_2$. For clarity, in-cavity and peripheral perchlorate ions forming secondary interactions with the molecular square are shown with dark and pale colouration, respectively.

Colour code: C, white; H, pale grey; Ag, green; Cl, pale or dark yellow; N, blue; O, pale or dark red.

All the anions are all crystallographically disordered about C_2 axes, which is not shown in the Figure. Moieties that do not form second-sphere interactions with the complex are also not included.

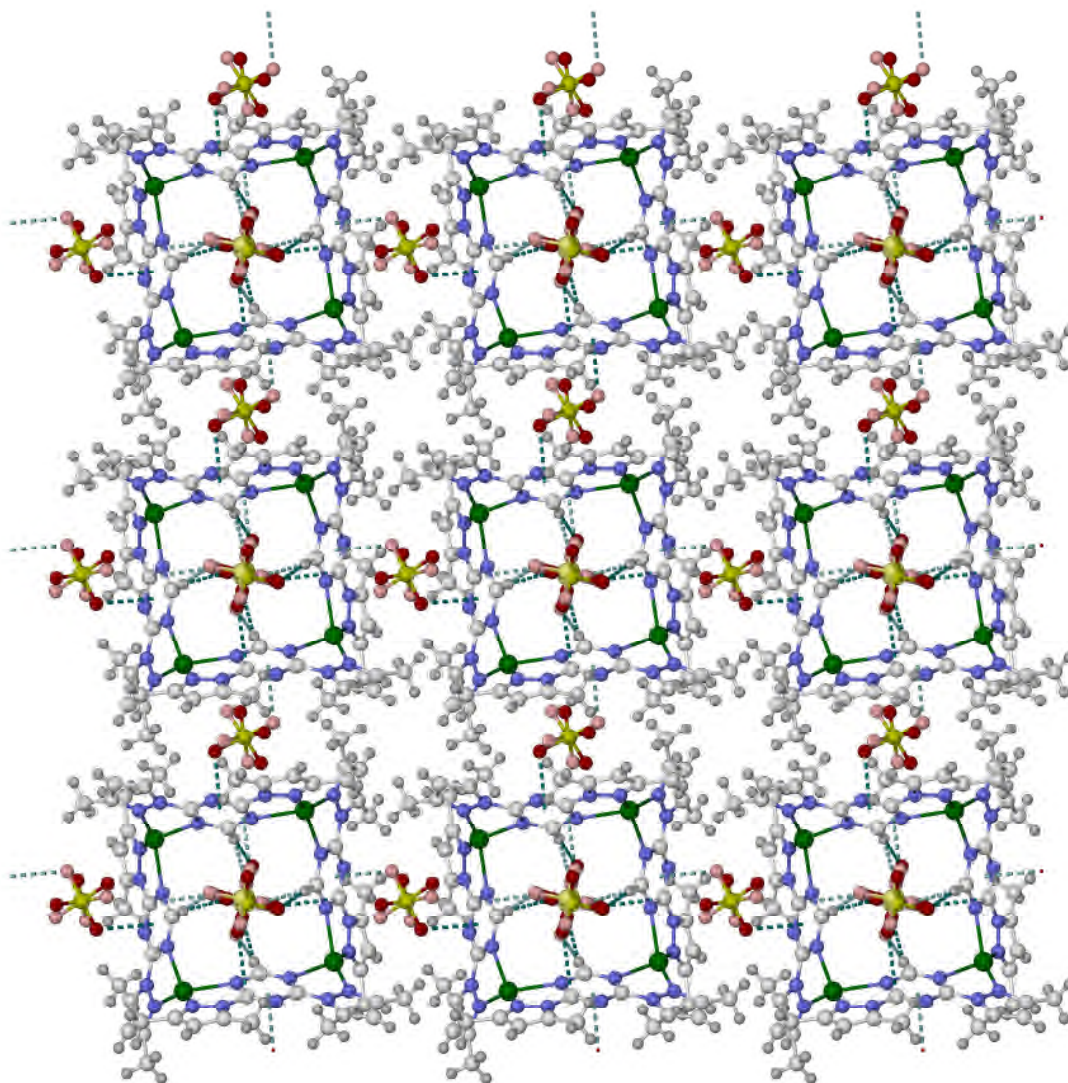


Figure S31 Packing diagram of $[\text{Ag}_4(\mu\text{-L}^3)_4][\text{ClO}_4]_4$, showing a layer of complex molecules in the lattice. The view is along the (001) crystal vector, with the unit cell a axis horizontal. Different disorder orientations of the ClO_4^- anions are distinguished with pale or dark colouration (Figures S21 and S25).

Colour code: C, white; H, pale grey; Ag, green; Cl, pale or dark yellow; N, blue; O, pale or dark red.

Each of the peripheral anions is disordered over two sites, each of them positioned to form an anion... π contact to just one neighbouring cation. Hence, the anions do not form bridging anion... π interactions in this lattice.

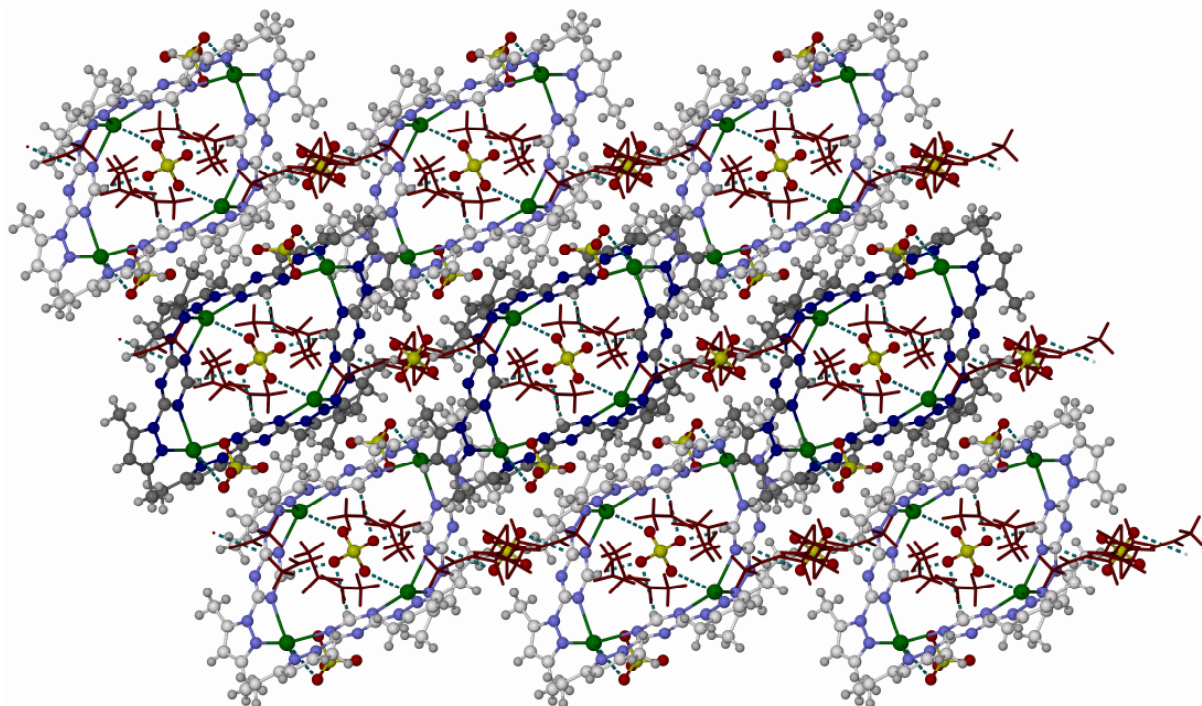


Figure S32 Packing diagram of $[\text{Ag}_4(\mu\text{-L}^3)_4][\text{ClO}_4]_4 \cdot 3.2\text{MeNO}_2 \cdot 1.2\text{H}_2\text{O}$, showing the arrangement of the cations into chains *via* anion... π contacts to bridging perchlorate ions. The view is along the (010) crystal vector, with the unit cell *c* axis horizontal. One supramolecular chain is highlighted with dark colouration, and the solvent molecules are de-emphasised for clarity.

Colour code: C, white or dark grey; H, pale grey; Ag, green; Cl, yellow; N{complex}, blue; O{anion}, red; MeNO₂, maroon.

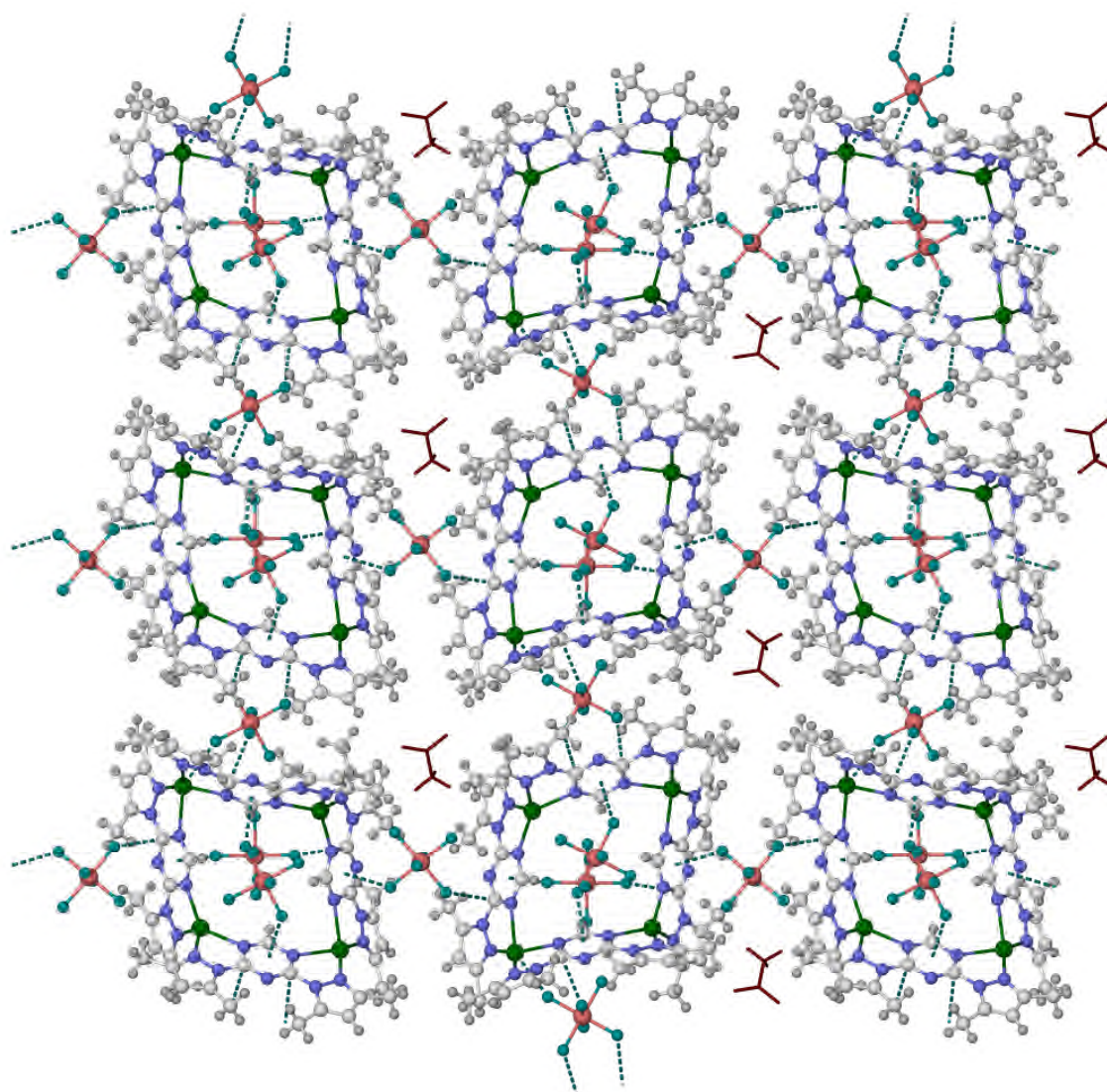


Figure S33 Packing diagram of $[\text{Ag}_4(\mu\text{-L}^3)_4][\text{SbF}_6]_4 \cdot \text{MeNO}_2$, showing the arrangement of the cations into layers *via* anion... π contacts to bridging SbF_6^- ions. The view is along the $(10\bar{1})$ crystal vector, with the unit cell b axis vertical. Solvent molecules are de-emphasised for clarity.

Colour code: C, white; H, pale grey; Ag, green; Cl, yellow; F, cyan; N, blue; Sb, pink; MeNO_2 , maroon.

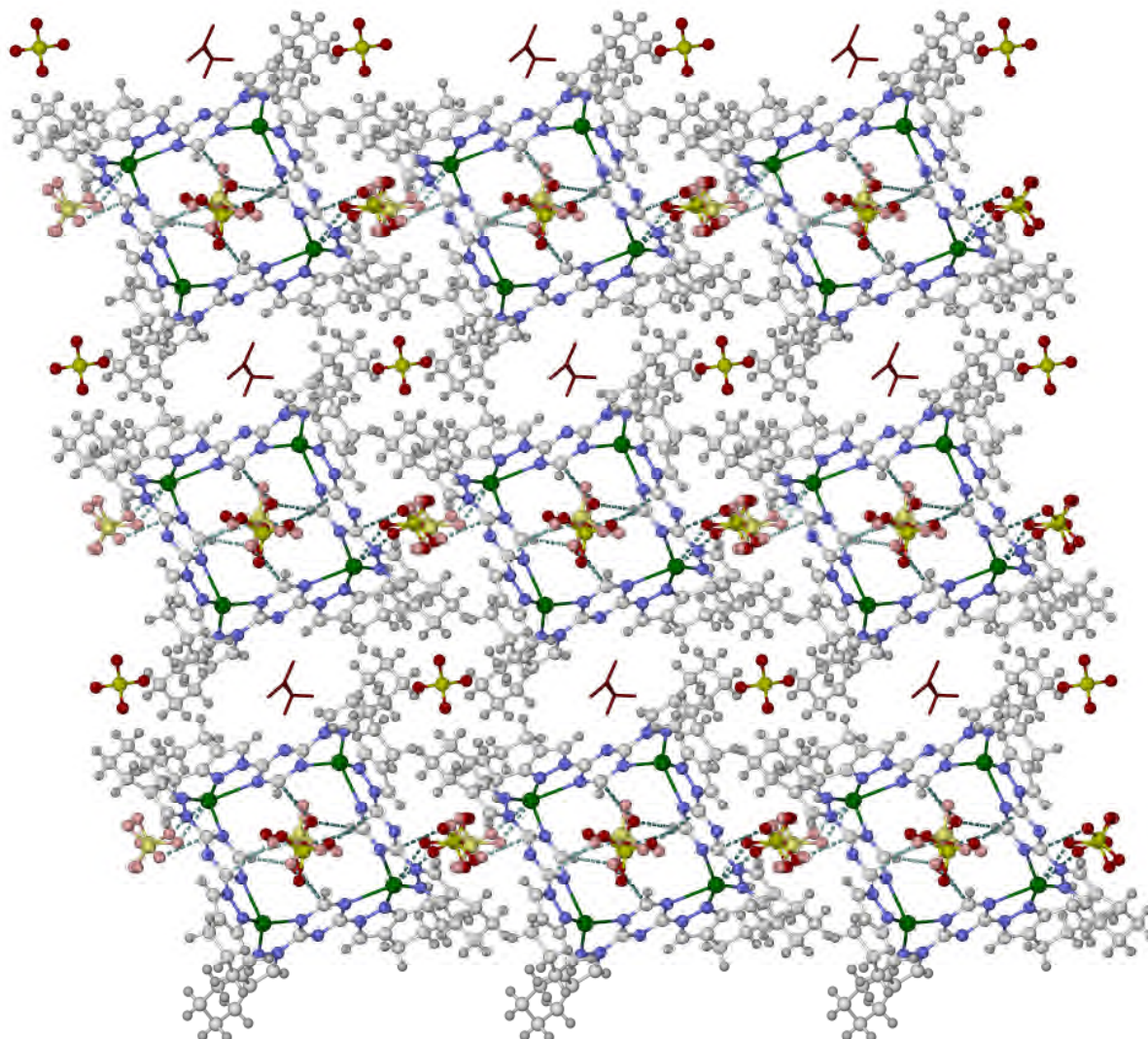


Figure S34 Packing diagram of $[\text{Ag}_4(\mu\text{-}L^4)]_4[\text{ClO}_4]_4 \cdot \text{MeNO}_2$, showing a layer of complex molecules in the lattice. The view is along the (010) crystal vector, with the unit cell c axis horizontal. Different disorder orientations of the ClO_4^- anions are distinguished with pale or dark colouration (Figures S24 and S26), and the solvent molecules are de-emphasised for clarity.

Colour code: C, white; H, pale grey; Ag, green; Cl, pale or dark yellow; N, blue; O, pale or dark red; MeNO_2 , maroon.

Both orientations of the disordered, peripheral half-anion are shown, and the pale/dark colouration is used to distinguish the symmetry equivalents of those two disorder sites about their crystallographic C_2 axis. Each of the four sites of that anion is positioned to interact with just one neighbouring cation, through an $\text{Ag}\cdots\text{O}$ interaction and/or an anion $\cdots\pi$ contact. Hence, these anions do not form bridging interactions between cations in this lattice.

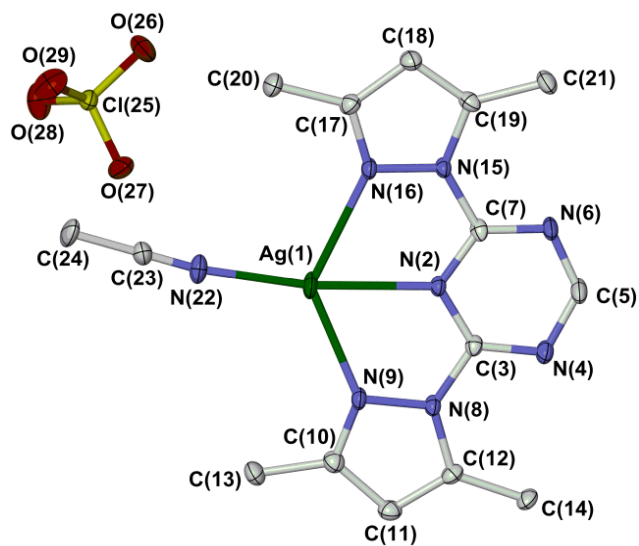


Figure S35 View of the asymmetric unit of $[\text{Ag}(\text{NCMe})L^3]\text{ClO}_4$, showing the full atom numbering scheme. Displacement ellipsoids are at the 50 % probability level, and H atoms are omitted for clarity.

Colour code: C, white; Ag, green; Cl, yellow; N, blue; O, red.

Table S18 Selected bond lengths (Å) and angles (°) for mononuclear $[\text{Ag}(\text{NCMe})L^3]\text{ClO}_4$. See Figure S35 for the atom numbering scheme.

| | | | |
|------------------|------------|-------------------|------------|
| Ag(1)–N(2) | 2.392(2) | Ag(1)–N(16) | 2.511(2) |
| Ag(1)–N(9) | 2.377(2) | Ag(1)–N(22) | 2.154(3) |
| N(2)–Ag(1)–N(9) | 66.75(8) | N(9)–Ag(1)–N(16) | 131.39(8) |
| N(2)–Ag(1)–N(16) | 64.64(8) | N(9)–Ag(1)–N(22) | 122.27(10) |
| N(2)–Ag(1)–N(22) | 167.71(10) | N(16)–Ag(1)–N(22) | 105.92(10) |

There are no anion... π contacts in $[\text{Ag}(\text{NCMe})L^6]\text{ClO}_4$.

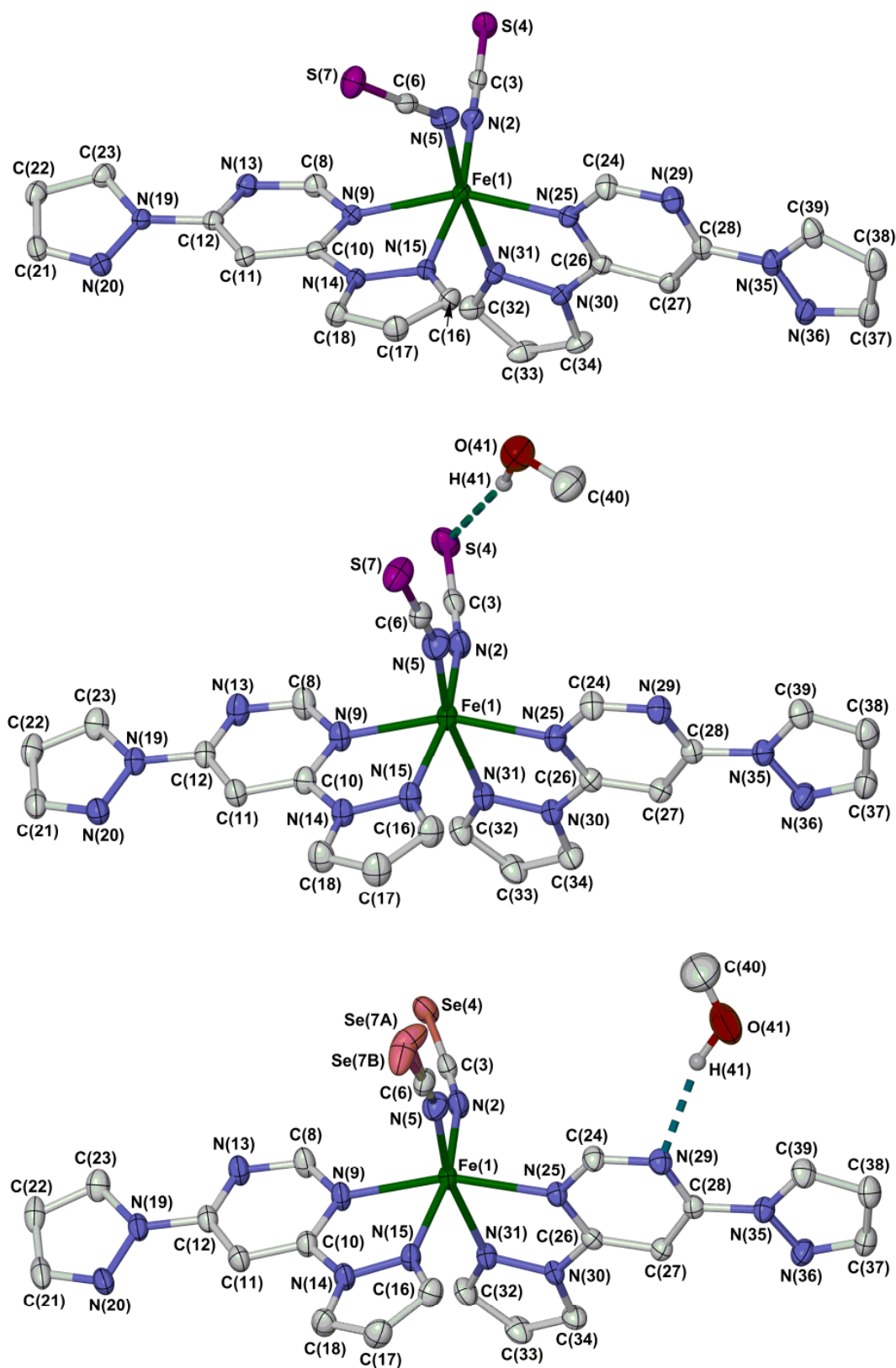


Figure S36 Views of the asymmetric units of $[\text{Fe}(\text{NCS})_2(\text{L}^5)_2]$ (top), $[\text{Fe}(\text{NCS})_2(\text{L}^5)_2]\cdot\text{MeOH}$ (middle) and $[\text{Fe}(\text{NCSe})_2(\text{L}^5)_2]\cdot\text{MeOH}$ (bottom), showing the full atom numbering schemes. Displacement ellipsoids are at the 50 % probability level, and C-bound H atoms are omitted for clarity. The views of the methanol solvates are the same as in Fig. 1 of the main article.

Colour code: C, white; H, pale grey; Fe, green; N, blue; O, red; S, purple; Se, pink.

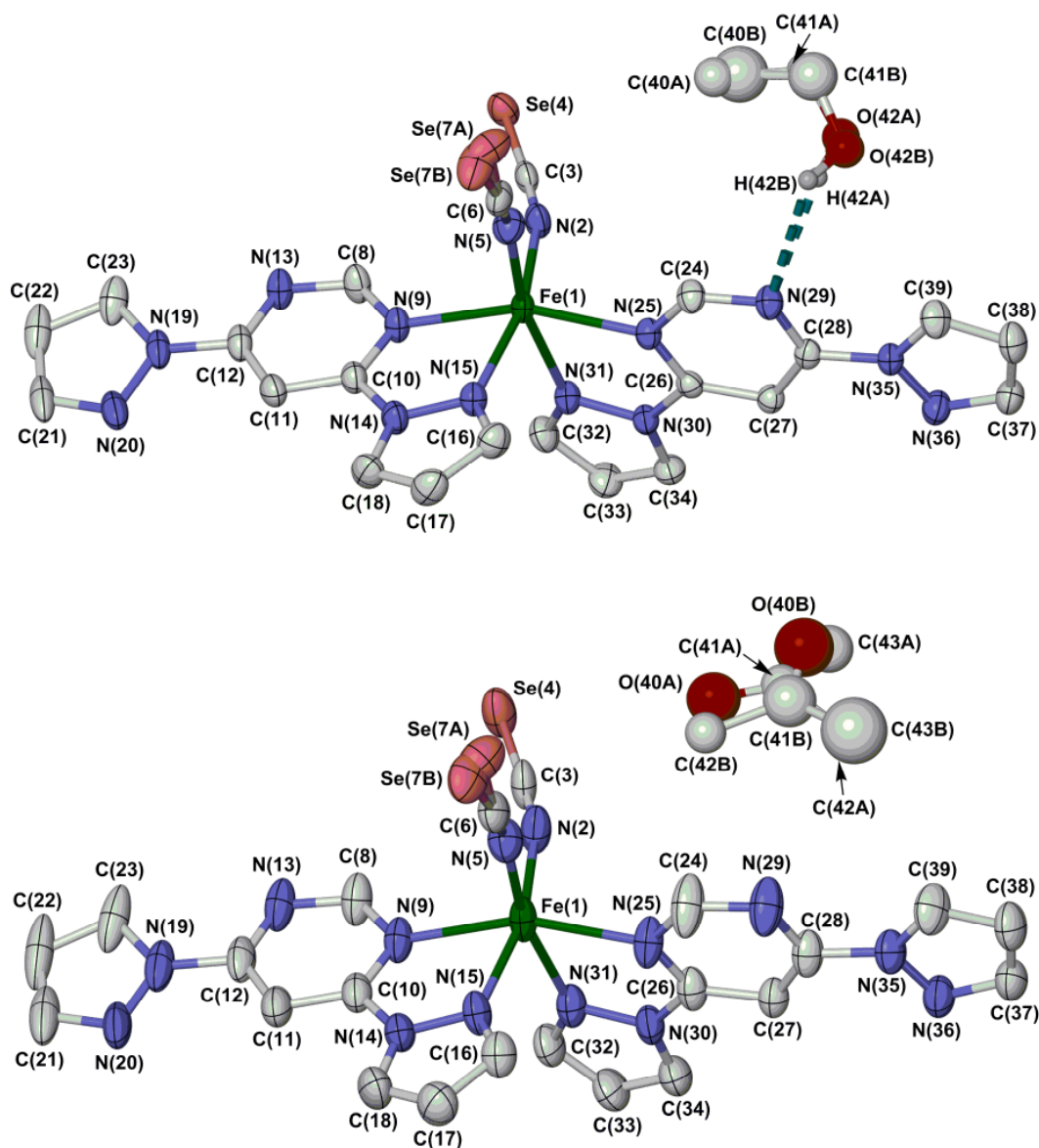


Figure S37 Views of the asymmetric units of $[\text{Fe}(\text{NCS})_2(\text{L}^5)_2] \cdot \frac{1}{2}\text{EtOH}$ (top) and $[\text{Fe}(\text{NCSe})_2(\text{L}^5)_2] \cdot \frac{1}{2}\text{Me}_2\text{CO}$ (bottom), showing the atom numbering schemes. Displacement ellipsoids are at the 50 % probability level, and C-bound H atoms are omitted for clarity.

Colour code: C, white; H, pale grey; Fe, green; N, blue; O, red; Se, pink.

Table S19 Selected bond lengths (Å) and angles (°) for the mononuclear complexes [Fe(NCE)₂(L⁵)₂] (E = S, Se). See Figures S36 and S37 for the atom numbering scheme, while definitions of V_{Oh} , Ψ , Σ and Θ are given on page S19.

| | [Fe(NCS) ₂ (L ⁵) ₂] | [Fe(NCS) ₂ (L ⁵) ₂]·MeOH | [Fe(NCSe) ₂ (L ⁵) ₂]·MeOH | [Fe(NCSe) ₂ (L ⁵) ₂]·½EtOH | [Fe(NCS) ₂ (L ⁵) ₂]·½Me ₂ CO |
|-------------------|--|---|--|---|--|
| Fe(1)–N(2) | 2.1056(16) | 2.103(2) | 2.105(2) | 2.101(2) | 2.108(4) |
| Fe(1)–N(5) | 2.0679(16) | 2.054(2) | 2.055(2) | 2.057(2) | 2.057(4) |
| Fe(1)–N(9) | 2.2092(15) | 2.2023(18) | 2.2064(19) | 2.209(2) | 2.216(3) |
| Fe(1)–N(15) | 2.1916(15) | 2.1841(19) | 2.1772(19) | 2.185(2) | 2.185(4) |
| Fe(1)–N(25) | 2.1976(14) | 2.2138(17) | 2.2325(17) | 2.234(2) | 2.233(3) |
| Fe(1)–N(31) | 2.1693(15) | 2.1847(19) | 2.1695(19) | 2.167(2) | 2.166(4) |
| N(2)–Fe(1)–N(5) | 93.98(6) | 93.55(9) | 94.14(9) | 93.72(10) | 93.38(17) |
| N(2)–Fe(1)–N(9) | 94.28(6) | 92.12(7) | 91.12(7) | 90.40(8) | 90.87(14) |
| N(2)–Fe(1)–N(15) | 166.98(6) | 165.56(7) | 164.92(7) | 164.14(8) | 164.35(13) |
| N(2)–Fe(1)–N(25) | 103.46(6) | 100.98(7) | 100.58(7) | 102.72(8) | 103.12(14) |
| N(2)–Fe(1)–N(31) | 89.48(6) | 89.24(8) | 90.28(8) | 90.56(9) | 91.30(16) |
| N(5)–Fe(1)–N(9) | 97.37(6) | 101.20(8) | 101.07(8) | 101.13(9) | 100.34(14) |
| N(5)–Fe(1)–N(15) | 87.31(6) | 90.69(8) | 89.93(8) | 89.44(9) | 89.30(16) |
| N(5)–Fe(1)–N(25) | 96.75(6) | 93.59(8) | 92.12(7) | 92.20(9) | 92.07(15) |
| N(5)–Fe(1)–N(31) | 170.53(6) | 166.34(8) | 164.92(8) | 164.96(9) | 164.93(14) |
| N(9)–Fe(1)–N(15) | 72.71(5) | 73.51(7) | 73.85(7) | 73.73(8) | 73.48(14) |
| N(9)–Fe(1)–N(25) | 156.43(6) | 159.60(7) | 161.72(7) | 160.69(8) | 160.75(17) |
| N(9)–Fe(1)–N(31) | 91.15(5) | 92.05(7) | 93.24(7) | 93.24(8) | 93.90(13) |
| N(15)–Fe(1)–N(25) | 89.23(5) | 92.51(7) | 93.75(7) | 92.68(8) | 92.17(14) |
| N(15)–Fe(1)–N(31) | 91.30(6) | 89.88(7) | 89.50(7) | 90.35(8) | 90.04(15) |
| N(25)–Fe(1)–N(31) | 73.85(5) | 72.75(6) | 72.88(7) | 72.79(8) | 72.91(14) |
| Fe(1)–N(2)–C(3) | 177.98(16) | 169.06(18) | 163.12(17) | 163.05(19) | 163.6(3) |
| Fe(1)–N(5)–C(6) | 141.10(15) | 163.4(2) | 161.0(2) | 162.3(2) | 164.6(4) |
| V_{Oh} | 12.910(6) | 12.932(7) | 12.950(7) | 12.952(8) | 12.973(17) |
| Ψ | 104.84(4) | 99.27(4) | 93.18(4) | 95.54(5) | 96.1(9) |
| Σ | 75.7(2) | 71.3(3) | 70.1(3) | 71.0(3) | 71.5(5) |
| Θ | 204 | 217 | 220 | 229 | 228 |

Table S20 Hydrogen bond parameters for the solvate crystals of the mononuclear complexes $[\text{Fe}(\text{NCE})_2(L^5)_2]$ (E = S, Se) (\AA , $^\circ$). See Figures S36 and S37 for the atom numbering scheme.

| | D–H | H...A | D...A | D–H...A |
|--|-----------|-----------|--------------------|-------------|
| $[\text{Fe}(\text{NCS})_2(L^5)_2] \cdot \text{MeOH}$ O(41)–H(41)...S(4) | 0.999(19) | 2.45(2) | 3.433(2) | 167(3) |
| $[\text{Fe}(\text{NCSe})_2(L^5)_2] \cdot \text{MeOH}$ O(41)–H(41)...N(29) | 0.93(2) | 2.09(3) | 2.998(3) | 164(5) |
| $[\text{Fe}(\text{NCSe})_2(L^5)_2] \cdot \frac{1}{2} \text{EtOH}$ O(41A)–H(41A)/O(41B)–H(41B)...N(29) | 0.84 | 2.27/2.37 | 3.062(9)/2.977(13) | 157.6/129.6 |

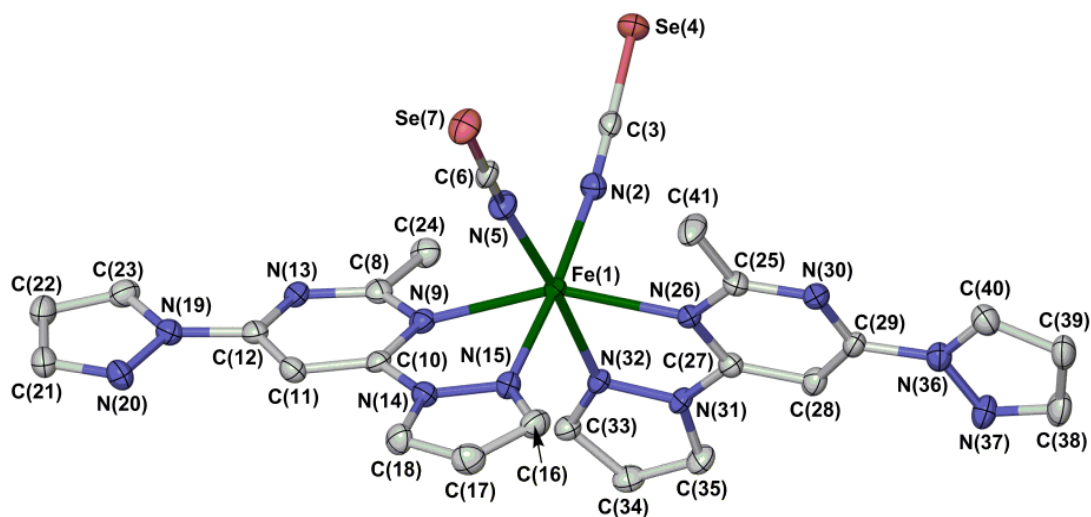


Figure 38 View of the asymmetric unit of $[\text{Fe}(\text{NCSe})_2(\text{L}^6)_2]$, showing the atom numbering scheme. Displacement ellipsoids are at the 50 % probability level, and H atoms are omitted for clarity.

Colour code: C, white; Fe, green; N, blue; Se, pink.

Table S21 Selected bond lengths (\AA) and angles ($^\circ$) for the mononuclear complex $[\text{Fe}(\text{NCSe})_2(\text{L}^6)_2]$. See Figure S38 for the atom numbering scheme, while definitions of V_{Oh} , Ψ , Σ and Θ are given on page S14.

| | | | |
|------------------|------------|-------------------|------------|
| Fe(1)–N(2) | 2.115(3) | Fe(1)–N(15) | 2.157(3) |
| Fe(1)–N(5) | 2.085(3) | Fe(1)–N(26) | 2.271(3) |
| Fe(1)–N(9) | 2.305(3) | Fe(1)–N(32) | 2.151(3) |
| N(2)–Fe(1)–N(5) | 88.59(11) | N(5)–Fe(1)–N(32) | 175.03(11) |
| N(2)–Fe(1)–N(9) | 106.30(10) | N(9)–Fe(1)–N(15) | 72.35(10) |
| N(2)–Fe(1)–N(15) | 174.19(11) | N(9)–Fe(1)–N(26) | 155.59(9) |
| N(2)–Fe(1)–N(26) | 90.30(10) | N(9)–Fe(1)–N(32) | 87.65(10) |
| N(2)–Fe(1)–N(32) | 94.76(10) | N(15)–Fe(1)–N(26) | 92.82(10) |
| N(5)–Fe(1)–N(9) | 87.88(10) | N(15)–Fe(1)–N(32) | 90.84(10) |
| N(5)–Fe(1)–N(15) | 85.72(11) | N(26)–Fe(1)–N(32) | 72.95(10) |
| N(5)–Fe(1)–N(26) | 110.77(11) | Fe(1)–N(2)–C(3) | 170.7(3) |
| | | Fe(1)–N(5)–C(6) | 158.8(3) |
| V_{Oh} | 13.101(11) | Σ | 90.7(4) |
| Ψ | 109.94(7) | Θ | 222 |

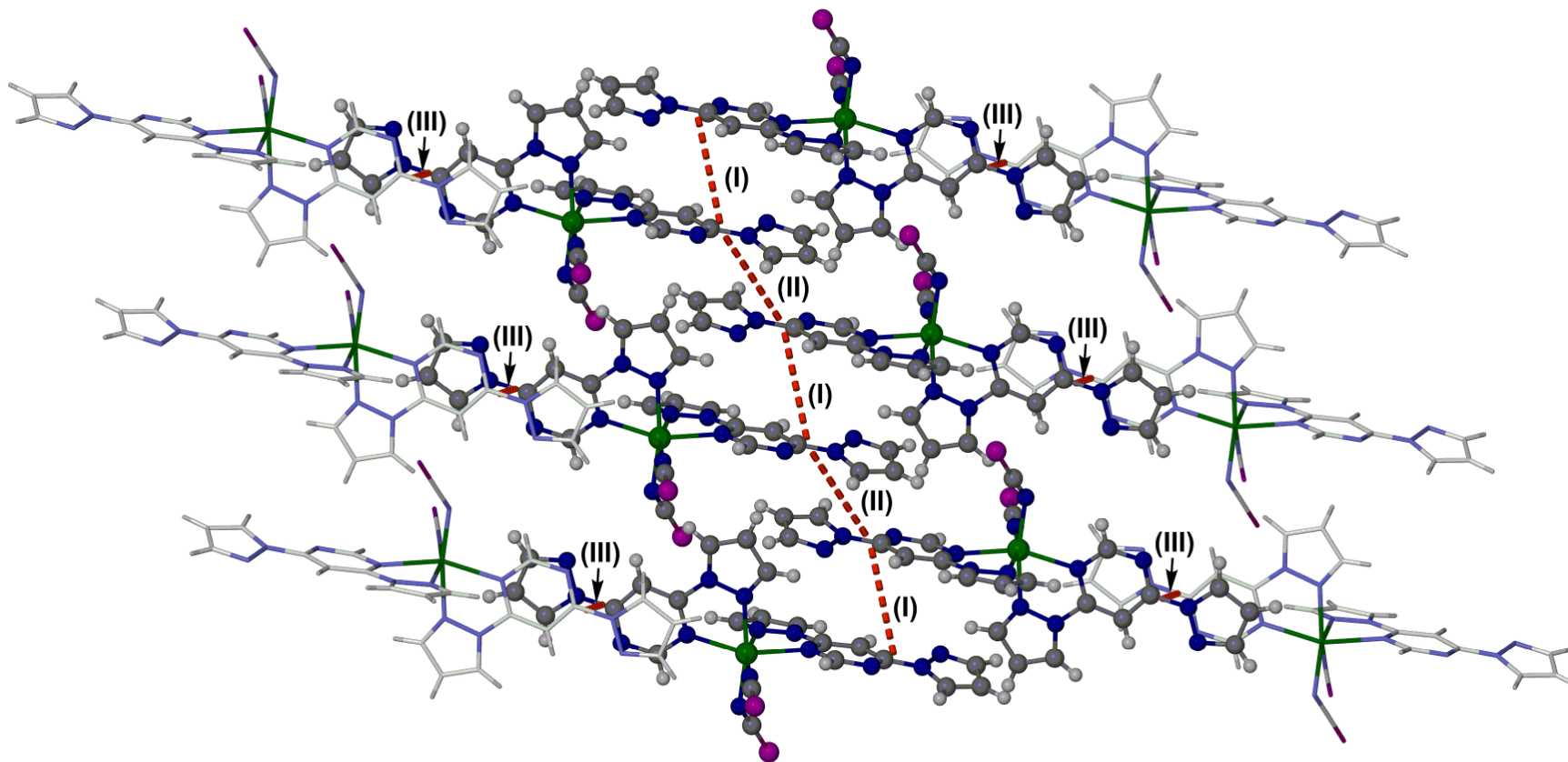


Figure S39 Partial packing diagram of $[\text{Fe}(\text{NCS})_2(\text{L}^5)_2]$, showing association of the molecules into stacks *via* intermolecular $\pi\cdots\pi$ interactions [(I) and (II)]. Neighbouring stacks are linked by a pairwise $\pi\cdots\pi$ interaction (III) involving the other ligand in the molecule. The molecules in the main stack are highlighted with dark colouration. The labels on the stacking interactions (shown in red) correspond to those in Table S22.

Colour code: C, white or dark grey; H, pale grey; Fe, green; N, pale or dark blue; S, purple.

The same packing motif occurs in $[\text{Fe}(\text{NCSe})_2(\text{L}^6)_2]$, which is isomorphous with this compound.

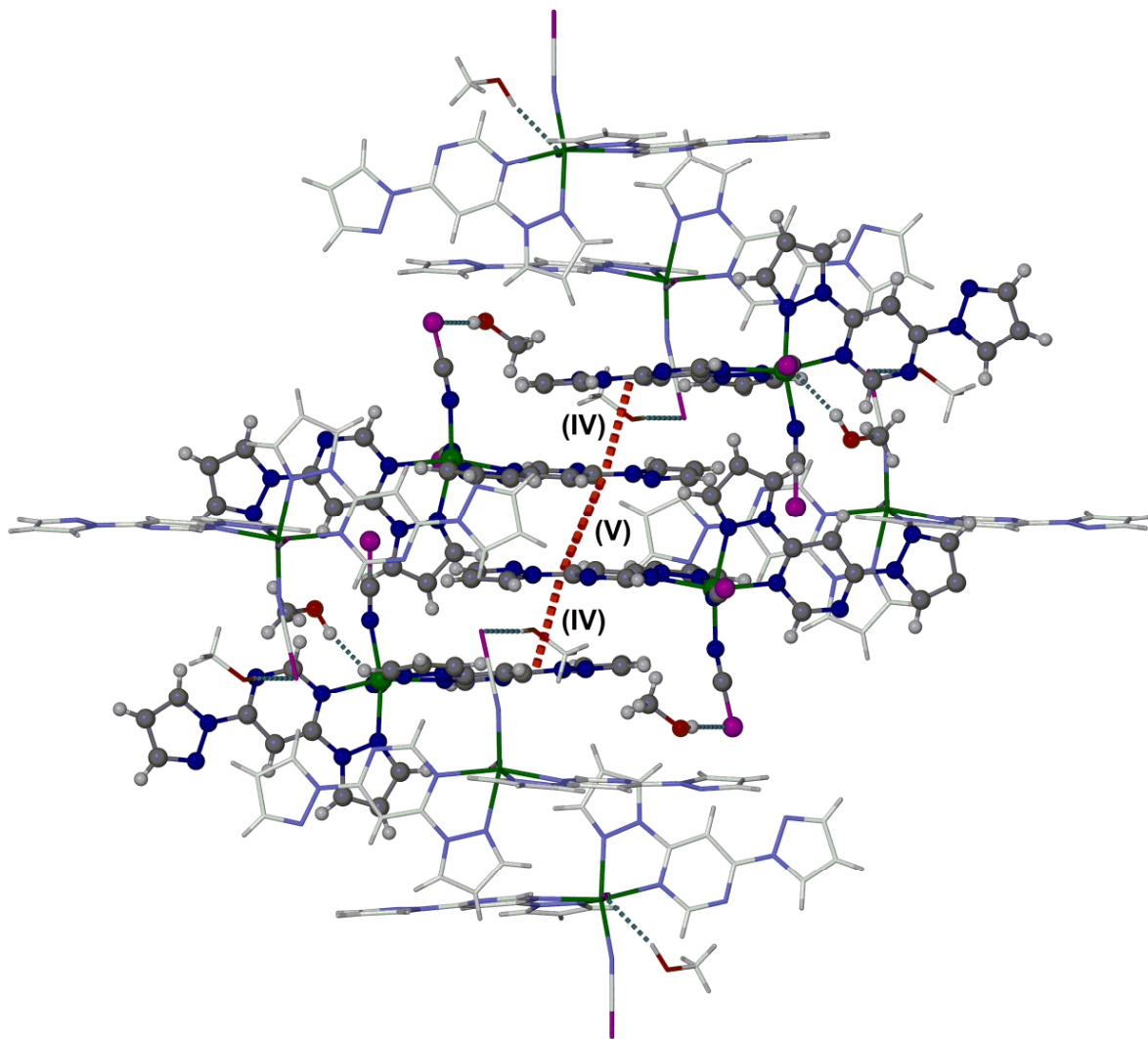


Figure S40 Partial packing diagram of $[\text{Fe}(\text{NCS})_2(L^5)_2] \cdot \text{MeOH}$, showing association of the molecules into tetrads through $\pi \dots \pi$ stacking. The four stacked molecules are highlighted with dark colouration. The labels on the stacking interactions (shown in red) correspond to those in Table S23.

Colour code: C, white or dark grey; H, pale grey; Fe, green; N, pale or dark blue; O, red; S, purple.

Each molecule is also involved in a second $\pi \dots \pi$ tetrad, perpendicular to the one in the Figure.

The same packing motif occurs in $[\text{Fe}(\text{NCSe})_2(L^5)_2] \cdot \text{MeOH}$, $[\text{Fe}(\text{NCSe})_2(L^5)_2] \cdot \frac{1}{2}\text{EtOH}$ and $[\text{Fe}(\text{NCSe})_2(L^5)_2] \cdot \frac{1}{2}\text{Me}_2\text{CO}$ which are isomorphous with this compound.

Table S22 Intermolecular $\pi\dots\pi$ interactions in the solvent-free mononuclear complexes $[\text{Fe}(\text{NCS})_2(L^5)_2]$ and $[\text{Fe}(\text{NCSe})_2(L^6)_2]$ (\AA , $^\circ$). See Figure S39 for the atom numbering, and the labelling of these interactions. Symmetry codes: (xvi) $-x, 1-y, 1-z$; (xxv) $1-x, -y, 2-z$; (xxvi) $2-x, -y, 2-z$; (xxvii) $1-x, -y, 1-z$; (xxviii) $2-x, -y, 1-z$.

| | Interplanar distance | Dihedral angle | Horizontal offset |
|--|----------------------|----------------|-------------------|
| $[\text{Fe}(\text{NCS})_2(L^5)_2]$ | | | |
| $[\text{C}(8)\text{-N}(13), \text{N}(19)\text{-C}(23)]\dots[\text{C}(8^{\text{xxv}})\text{-N}(13^{\text{xxv}}), \text{N}(19^{\text{xxv}})\text{-C}(23^{\text{xxv}})]$ (I) | 3.021(6) | 0 | 3.70 |
| $[\text{C}(8)\text{-N}(13), \text{N}(19)\text{-C}(23)]\dots[\text{C}(8^{\text{xxvi}})\text{-N}(13^{\text{xxvi}}), \text{N}(19^{\text{xxvi}})\text{-C}(23^{\text{xxvi}})]$ (II) | 3.363(7) | 0 | 3.29 |
| $[\text{C}(24)\text{-N}(29), \text{N}(35)\text{-C}(39)]\dots[\text{C}(24^{\text{xvi}})\text{-N}(29^{\text{xvi}}), \text{N}(35^{\text{xvi}})\text{-C}(39^{\text{xvi}})]$ (III) | 3.227(6) | 0 | 1.25 |
| $[\text{Fe}(\text{NCSe})_2(L^6)_2]^a$ | | | |
| $[\text{C}(8)\text{-N}(13), \text{N}(19)\text{-C}(23)]\dots[\text{C}(8^{\text{xxvii}})\text{-N}(13^{\text{xxvii}}), \text{N}(19^{\text{xxvii}})\text{-C}(23^{\text{xxvii}})]$ (I) | 3.348(5) | 0 | 4.28 |
| $[\text{C}(8)\text{-N}(13), \text{N}(19)\text{-C}(23)]\dots[\text{C}(8^{\text{xxviii}})\text{-N}(13^{\text{xxviii}}), \text{N}(19^{\text{xxviii}})\text{-C}(23^{\text{xxviii}})]$ (II) | 3.323(3) | 0 | 2.65 |
| $[\text{C}(24)\text{-N}(29), \text{N}(35)\text{-C}(39)]\dots[\text{C}(24^{\text{xvi}})\text{-N}(29^{\text{xvi}}), \text{N}(35^{\text{xvi}})\text{-C}(39^{\text{xvi}})]$ (III) | 3.397(17) | 0 | 1.30 |

^aThe symmetry codes for this compound are different, because its dataset was merged to a different origin by the diffractometer software.

Table S23 Intermolecular $\pi\dots\pi$ interactions in the solvate crystals of the mononuclear complexes $[\text{Fe}(\text{NCE})_2(L^5)_2]$ (E = S, Se) (\AA , $^\circ$). See Figure S40 for the atom numbering, and the labelling of these interactions. Symmetry codes: (x) $1-x, 2-y, 1-z$; (xxix) $-1/2+x, 3/2-y, 1/2+z$;

| | Interplanar distance | Dihedral angle | Horizontal offset |
|---|----------------------|----------------|-------------------|
| $[\text{Fe}(\text{NCS})_2(L^5)_2]\cdot\text{MeOH}$ | | | |
| $[\text{C}(8)\text{-N}(13), \text{N}(19)\text{-C}(23)]\dots[\text{C}(24^{\text{xxix}})\text{-N}(29^{\text{xxix}}), \text{N}(35^{\text{xxix}})\text{-C}(39^{\text{xxix}})]$ (IV) | 3.450(8) | 9.67(9) | 1.20 |
| $[\text{C}(24)\text{-N}(29), \text{N}(35)\text{-C}(39)]\dots[\text{C}(24^{\text{x}})\text{-N}(29^{\text{x}}), \text{N}(35^{\text{x}})\text{-C}(39^{\text{x}})]$ (V) | 3.393(9) | 0 | 3.67 |
| $[\text{Fe}(\text{NCSe})_2(L^5)_2]\cdot\text{MeOH}$ | | | |
| $[\text{C}(8)\text{-N}(13), \text{N}(19)\text{-C}(23)]\dots[\text{C}(24^{\text{xxix}})\text{-N}(29^{\text{xxix}}), \text{N}(35^{\text{xxix}})\text{-C}(39^{\text{xxix}})]$ (IV) | 3.463(9) | 10.14(9) | 1.13 |
| $[\text{C}(24)\text{-N}(29), \text{N}(35)\text{-C}(39)]\dots[\text{C}(24^{\text{x}})\text{-N}(29^{\text{x}}), \text{N}(35^{\text{x}})\text{-C}(39^{\text{x}})]$ (V) | 3.431(9) | 0 | 3.69 |
| $[\text{Fe}(\text{NCSe})_2(L^5)_2]\cdot\frac{1}{2}\text{EtOH}$ | | | |
| $[\text{C}(8)\text{-N}(13), \text{N}(19)\text{-C}(23)]\dots[\text{C}(24^{\text{xxix}})\text{-N}(29^{\text{xxix}}), \text{N}(35^{\text{xxix}})\text{-C}(39^{\text{xxix}})]$ (IV) | 3.442(10) | 8.92(11) | 1.11 |
| $[\text{C}(24)\text{-N}(29), \text{N}(35)\text{-C}(39)]\dots[\text{C}(24^{\text{x}})\text{-N}(29^{\text{x}}), \text{N}(35^{\text{x}})\text{-C}(39^{\text{x}})]$ (V) | 3.477(11) | 0 | 3.53 |
| $[\text{Fe}(\text{NCSe})_2(L^5)_2]\cdot\frac{1}{2}\text{Me}_2\text{CO}$ | | | |
| $[\text{C}(8)\text{-N}(13), \text{N}(19)\text{-C}(23)]\dots[\text{C}(24^{\text{xxix}})\text{-N}(29^{\text{xxix}}), \text{N}(35^{\text{xxix}})\text{-C}(39^{\text{xxix}})]$ (IV) | 3.434(18) | 7.6(2) | 1.22 |
| $[\text{C}(24)\text{-N}(29), \text{N}(35)\text{-C}(39)]\dots[\text{C}(24^{\text{x}})\text{-N}(29^{\text{x}}), \text{N}(35^{\text{x}})\text{-C}(39^{\text{x}})]$ (V) | 3.50(2) | 0 | 3.57 |

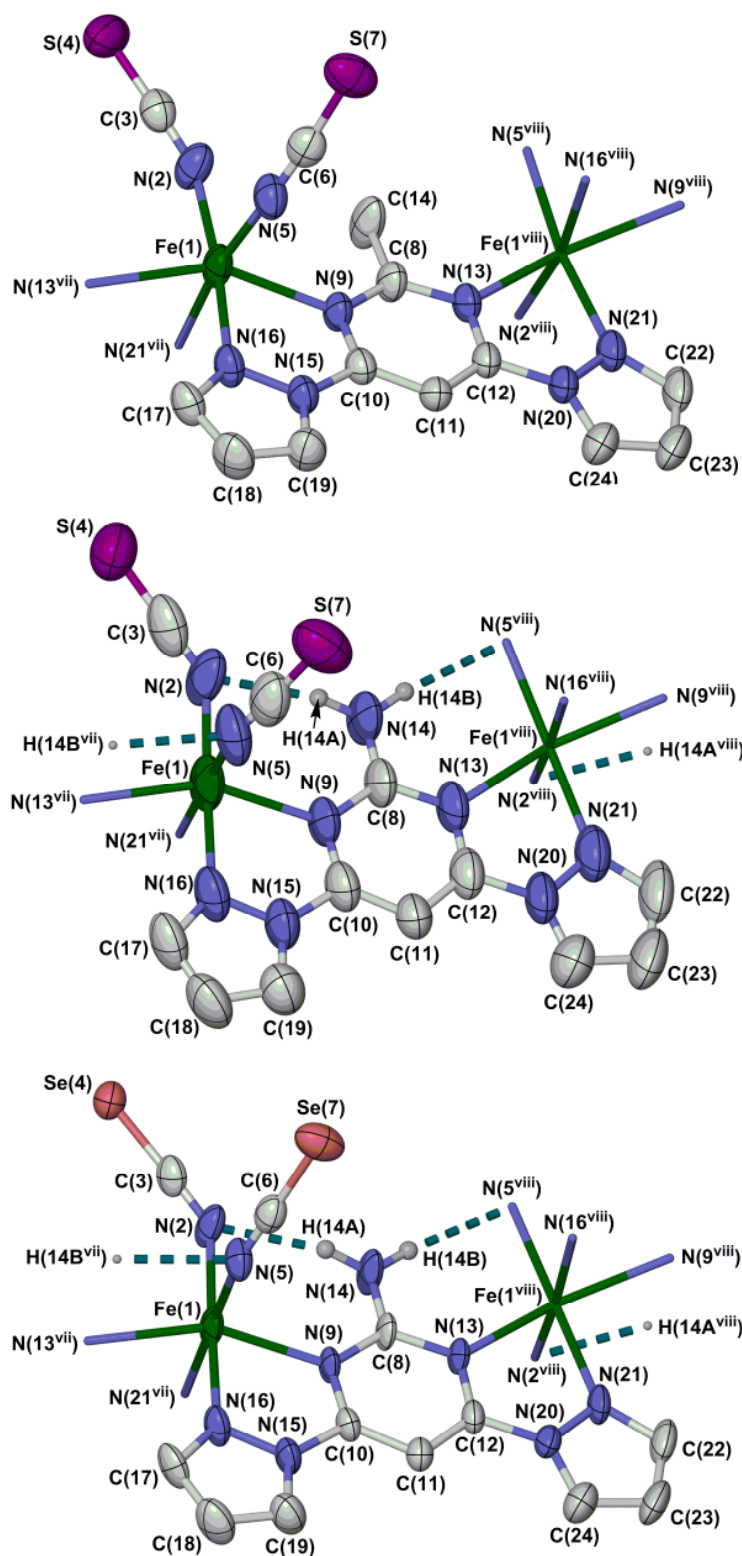


Figure S41 View of the asymmetric units of isostructural $[\text{Fe}(\text{NCS})_2(\mu\text{-}L^6)]$ (top), $[\text{Fe}(\text{NCS})_2(\mu\text{-}L^7)]$ (middle) and $[\text{Fe}(\text{NCSe})_2(\mu\text{-}L^7)]$ (bottom), showing the atom numbering schemes. Displacement ellipsoids are at the 50 % probability level, and C-bound H atoms are omitted for clarity. Symmetry codes: (vii) $1/4+y, 5/4-x, 1/4+z$; (viii) $5/4-y, -1/4+x, -1/4+z$.

Colour code: C, white; H, pale grey; Fe, green; N, blue; S, purple; Se, pink.

Table S24 Selected bond lengths (Å) and angles (°) for the isostructural coordination polymers [Fe(NCE)₂(μ-L)] (E = S, Se; L = L⁶, L⁷). See Figure S41 for the atom numbering scheme, while definitions of V_{Oh}, Ψ, Σ and Θ are given on page S19. Symmetry code: (vii) ^{1/4+y, 5/4-x, 1/4+z}.

| | [Fe(NCS) ₂ (μ-L ⁶)] | [Fe(NCS) ₂ (μ-L ⁷)] | [Fe(NCSe) ₂ (μ-L ⁷)] |
|--|--|--|---|
| Fe(1)–N(2) | 2.051(4) | 2.036(6) | 2.073(5) |
| Fe(1)–N(5) | 2.139(4) | 2.113(6) | 2.131(5) |
| Fe(1)–N(9) | 2.231(3) | 2.202(4) | 2.195(4) |
| Fe(1)–N(13 ^{vii}) | 2.245(3) | 2.206(4) | 2.201(4) |
| Fe(1)–N(16) | 2.194(3) | 2.178(5) | 2.160(5) |
| Fe(1)–N(21 ^{vii}) | 2.184(4) | 2.181(5) | 2.162(5) |
| Fe(1)...Fe(1 ^{vii}) | 6.3590(7) | 6.3435(2) | 6.3467(3) |
| N(2)–Fe(1)–N(5) | 87.87(15) | 86.1(2) | 85.1(2) |
| N(2)–Fe(1)–N(9) | 115.32(12) | 105.67(17) | 105.23(16) |
| N(2)–Fe(1)–N(13 ^{vii}) | 89.19(13) | 96.73(18) | 95.06(17) |
| N(2)–Fe(1)–N(16) | 170.43(12) | 175.6(2) | 174.0(2) |
| N(2)–Fe(1)–N(21 ^{vii}) | 96.21(15) | 94.4(2) | 94.0(2) |
| N(5)–Fe(1)–N(9) | 83.32(12) | 89.68(17) | 89.38(16) |
| N(5)–Fe(1)–N(13 ^{vii}) | 114.05(11) | 106.14(17) | 106.41(16) |
| N(5)–Fe(1)–N(16) | 88.10(13) | 89.69(19) | 88.97(19) |
| N(5)–Fe(1)–N(21 ^{vii}) | 172.19(12) | 179.5(2) | 179.1(2) |
| N(9)–Fe(1)–N(13 ^{vii}) | 151.19(12) | 153.46(18) | 155.37(17) |
| N(9)–Fe(1)–N(16) | 72.78(10) | 73.25(15) | 74.15(15) |
| N(9)–Fe(1)–N(21 ^{vii}) | 88.91(11) | 90.23(16) | 90.55(16) |
| N(13 ^{xx})–Fe(1)–N(16) | 84.53(11) | 85.42(15) | 87.08(16) |
| N(13 ^{xx})–Fe(1)–N(21 ^{vii}) | 72.77(11) | 73.77(17) | 73.96(15) |
| N(16)–Fe(1)–N(21 ^{vii}) | 88.84(13) | 89.83(18) | 91.91(19) |
| Fe(1)–N(2)–C(3) | 152.3(3) | 140.2(4) | 141.4(4) |
| Fe(1)–N(5)–C(6) | 160.2(3) | 153.0(5) | 155.7(4) |
| V _{Oh} | 12.692(12) | 12.722(18) | 12.769(17) |
| Ψ | 88.25(8) | 88.72(11) | 88.81(12) |
| Σ | 109.3(4) | 85.4(6) | 84.5(6) |
| Θ | 271 | 201 | 197 |

Table S25 Hydrogen bond parameters for the coordination polymers [Fe(NCE)₂(μ-L⁷)] (E = S, Se) (Å, °). See Figure S41 for the atom numbering scheme. Symmetry code: (viii) ^{5/4-y, -1/4+x, -1/4+z}.

| | D–H | H...A | D...A | D–H...A |
|--|---------|---------|----------|---------|
| [Fe(NCS) ₂ (μ-L ⁷)] | | | | |
| N(14)–H(14A)...N(2) | 0.90(2) | 2.11(3) | 2.978(6) | 164(7) |
| N(14)–H(14B)...N(5 ^{viii}) | 0.89(2) | 2.16(2) | 3.038(6) | 171(7) |
| [Fe(NCS) ₂ (μ-L ⁷)] | | | | |
| N(14)–H(14A)...N(2) | 0.89(2) | 2.12(3) | 2.986(6) | 164(8) |
| N(14)–H(14B)...N(5 ^{viii}) | 0.90(2) | 2.16(3) | 3.046(6) | 170(8) |

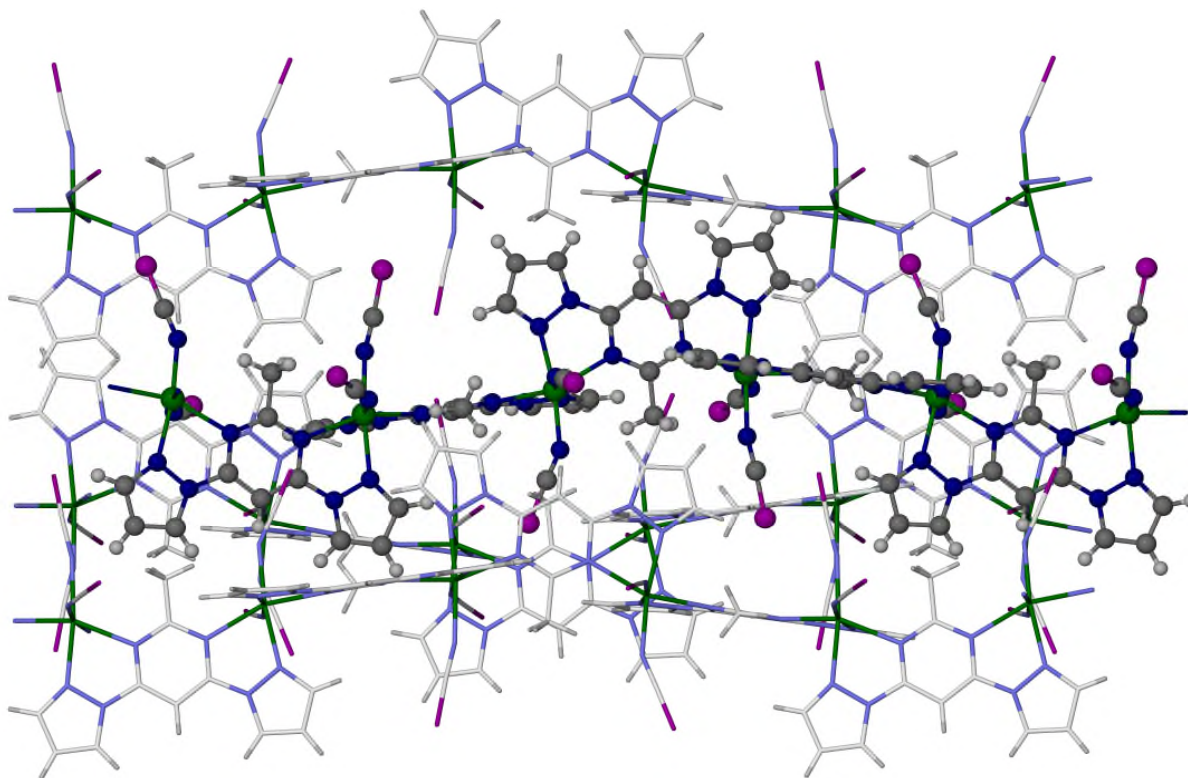


Figure S42 A $[\text{Fe}(\text{NCS})_2(\mu\text{-}L^6)]$ coordination polymer chain surrounded by three of its four nearest neighbours in the lattice (Figure S43), showing the absence of $\pi\dots\pi$ interactions between nearest neighbour chains. The central chain is shown with dark colouration, while the neighbour chains are de-emphasised for clarity.

Colour code: C, white or dark grey; H, pale grey; Fe, green; N, pale or dark blue; S, purple.

The apparently overlapping L^6 ligands on different polymer chains are in fact separated by the length of an NCS ligand, and have no $\pi\dots\pi$ interaction between them.

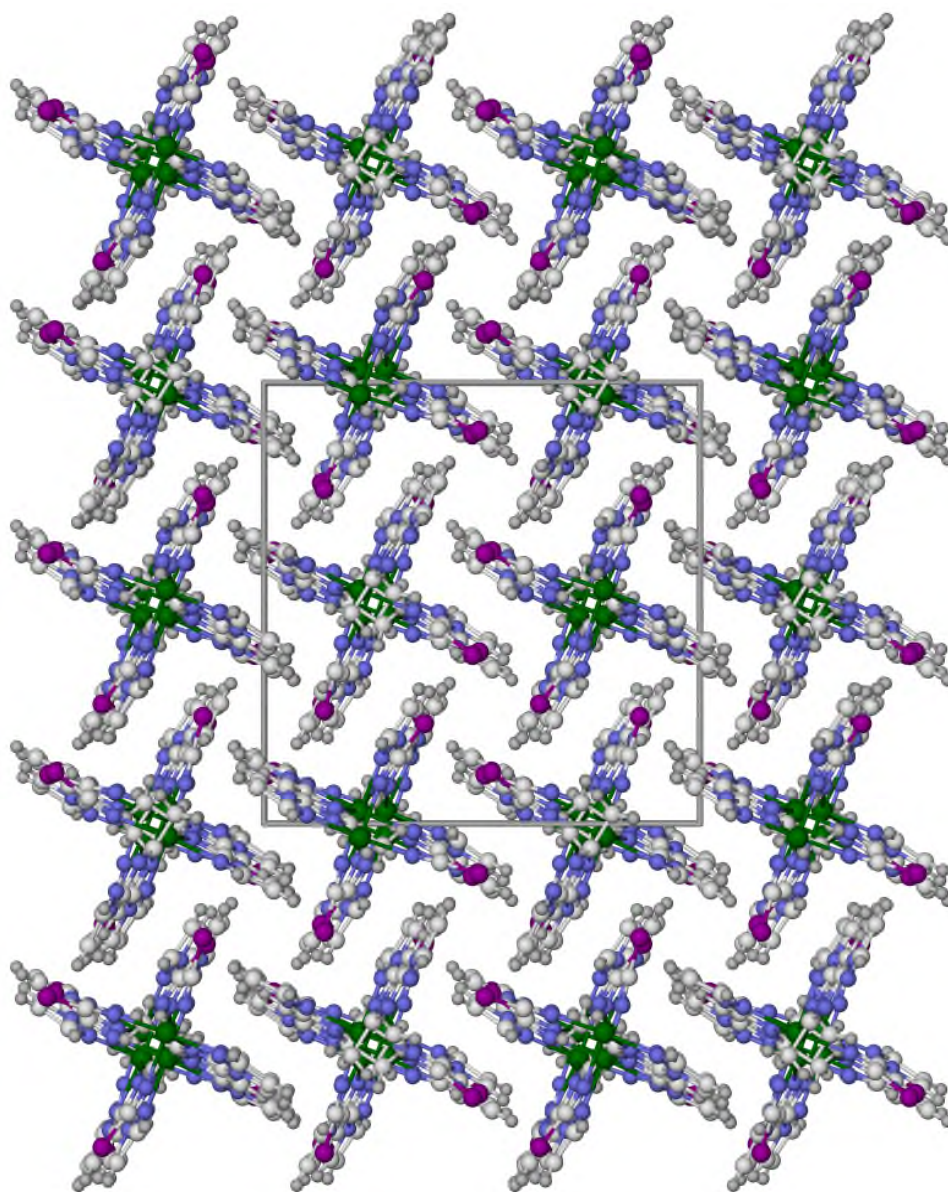


Figure S43 Packing diagram of $[\text{Fe}(\text{NCS})_2(\mu\text{-L}^6)]$, showing the interdigitation of the coordination polymer chains. The view is along the (001) crystal vector.

Colour code: C, white; H, pale grey; Fe, green; N, blue; S, purple.

This four-fold molecular interdigitation resembles the “terpyridine embrace” packing motif, that is often adopted by complexes of terpyridine and terpy-analogue ligands.⁹ However, unlike most terpyridine embrace crystals, nearest neighbour polymer chains are offset such that there are no intermolecular $\pi\cdots\pi$ interactions between them.

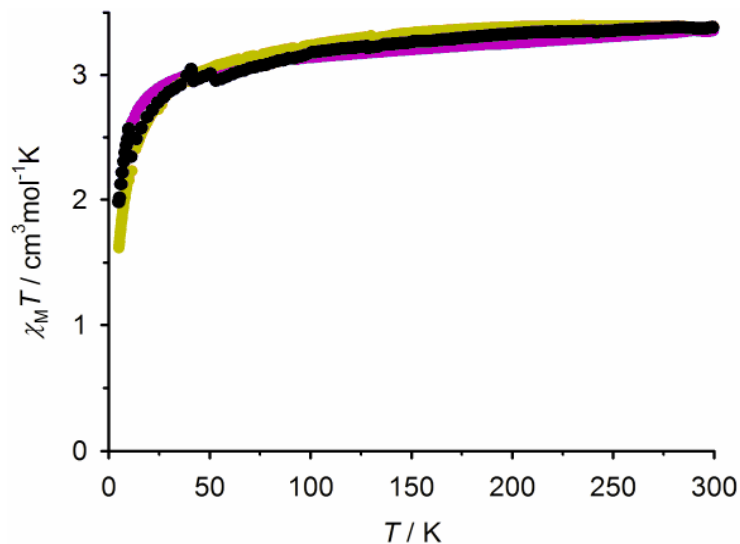


Figure S44 Variable temperature magnetic susceptibility data for: $[\text{Fe}(\text{NCS})_2(\text{L}^5)_2] \cdot \text{MeOH}$ (black); $[\text{Fe}(\text{NCS})_2(\text{L}^5)_2]$ (purple); and $[\text{Fe}(\text{NCSe})_2(\text{L}^5)_2] \cdot \frac{1}{2}\text{Me}_2\text{CO}$ (yellow). Scan rate 5 Kmin^{-1} . Data for $[\text{Fe}(\text{NCSe})_2(\text{L}^5)_2] \cdot \text{MeOH}$ are shown in Figure 6 of the main article.

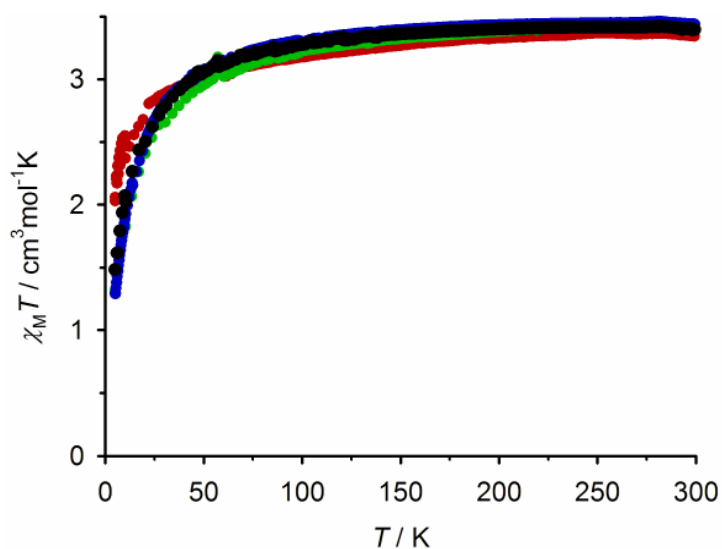


Figure S45 Variable temperature magnetic susceptibility data for: $[\text{Fe}(\text{NCS})_2(\mu\text{-L}^6)]$ (black); $[\text{Fe}(\text{NCSe})_2(\text{L}^6)_2]$ (red); $[\text{Fe}(\text{NCS})_2(\mu\text{-L}^7)]$ (green); and $[\text{Fe}(\text{NCSe})_2(\mu\text{-L}^7)]$ (blue). Scan rate 5 Kmin^{-1} .

All these compounds are high-spin between 5-300 K. The low-temperature decrease in $\chi_M T$ below 50 K reflects zero-field splitting of the high-spin iron(II) centres, and does not imply the onset of thermal spin-crossover.⁸

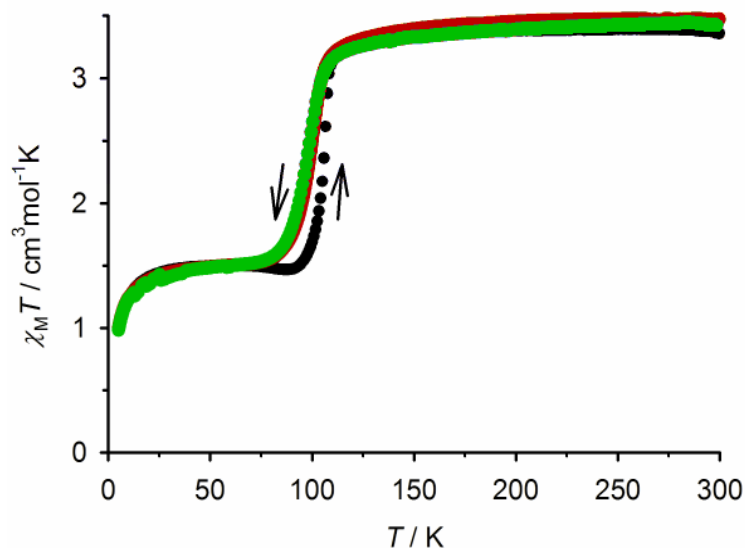


Figure S46 Magnetic data showing the reproducible annealing behaviour of $[\text{Fe}(\text{NCSe})_2(\text{L}^5)_2] \cdot \text{solvent}$. The graphs show three different samples, each of which were annealed at 370 K for 24 hrs. Scan rate 5 Kmin^{-1} .

Black curve: $[\text{Fe}(\text{NCSe})_2(\text{L}^5)_2] \cdot \text{MeOH}$ after heating at 370 K for 24 hrs, measured in cooling and warming mode (these data are also in Figure 6 of the main article).

Red curve: a second sample of $[\text{Fe}(\text{NCSe})_2(\text{L}^5)_2] \cdot \text{MeOH}$ after heating at 370 K for 24 hrs, measured in cooling mode only.

Green curve: $[\text{Fe}(\text{NCSe})_2(\text{L}^5)_2] \cdot \frac{1}{2} \text{Me}_2\text{CO}$ after heating at 370 K for 24 hrs, measured in cooling mode only.

These data prove the reproducibility of the annealed spin-crossover phase of this material, and that it doesn't depend on the solvent present in the initial sample. They also imply the incompleteness of the spin transition does not reflect incomplete desolvation of the samples, but is an inherent feature of the material.

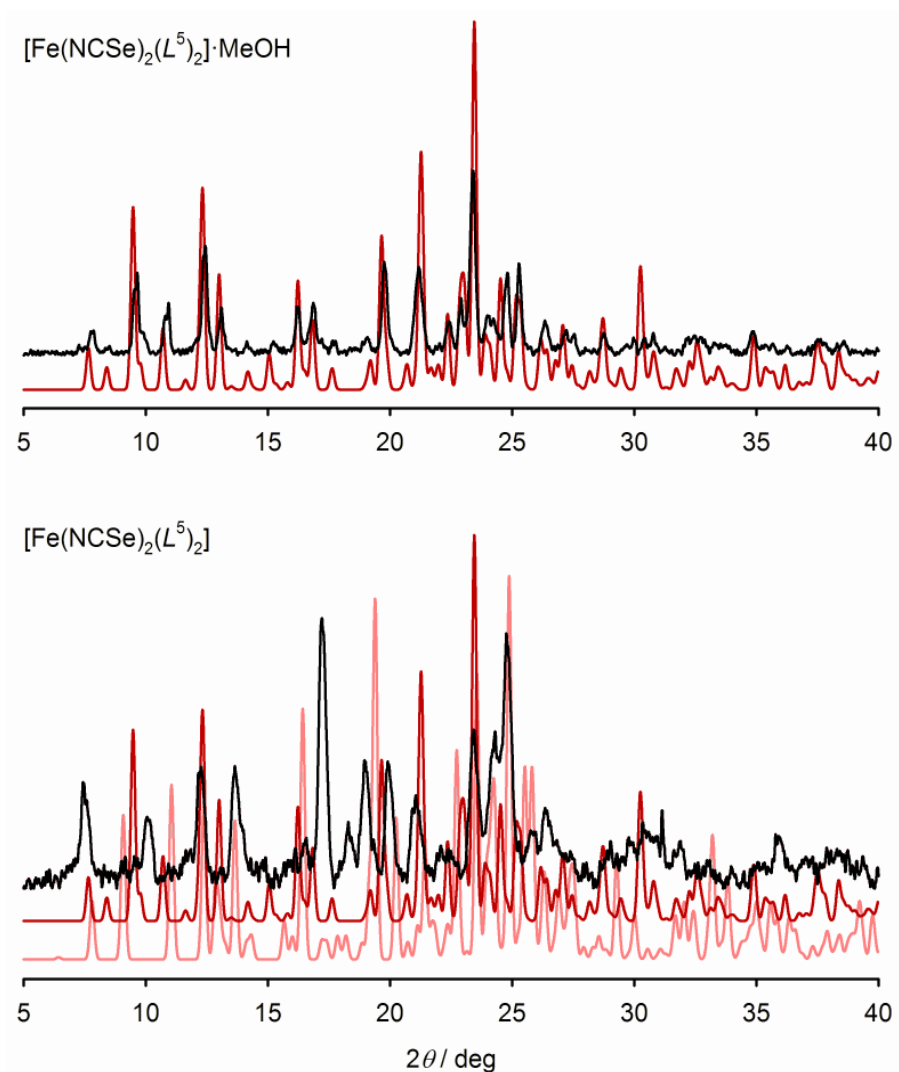


Figure S47 Measured (black) and simulated (red) X-ray powder diffraction data for freshly prepared $[\text{Fe}(\text{NCSe})_2(L^5)_2] \cdot \text{MeOH}$ (top), and the same material after annealing for 24 hrs at 370 K (bottom).

The simulations are based on the crystal structures of $[\text{Fe}(\text{NCSe})_2(L^5)_2] \cdot \text{MeOH}$ (dark red) and the solvent-free phase of $[\text{Fe}(\text{NCSe})_2(L^5)_2]$ with the S atoms replaced by Se (pale red; Figure S48).

The annealed sample $[\text{Fe}(\text{NCSe})_2(L^5)_2]$, which is solvent-free by microanalysis and exhibits spin-crossover on cooling (Figure 6, main article and Figure S46), is poorly crystalline but doesn't apparently correspond to either structure type.

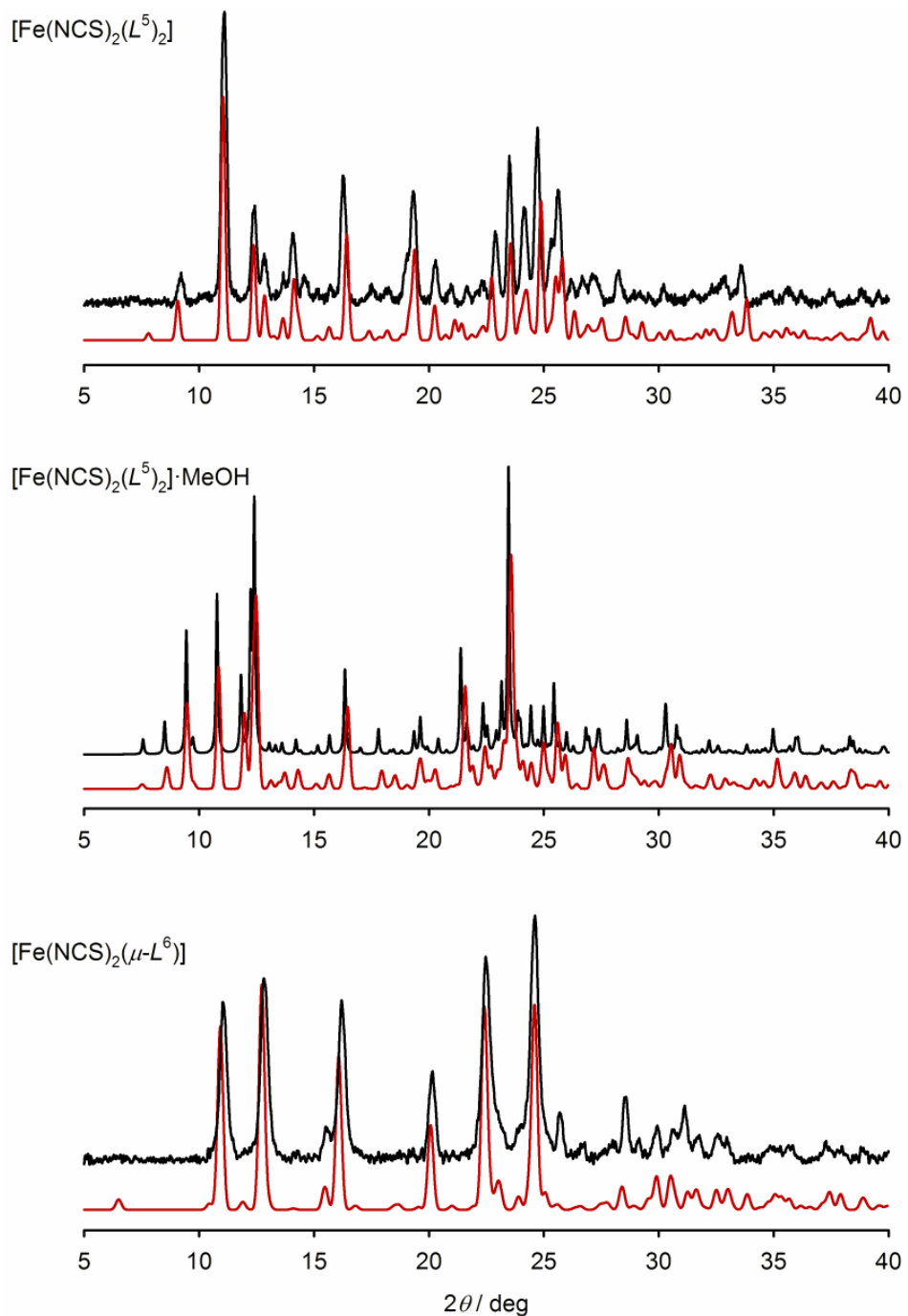


Figure S48 Measured (black) and simulated (red) X-ray powder diffraction data for the iron complexes of $\text{L}^5\text{-L}^7$.

These data are discussed at the end of the Figure, on the next page.

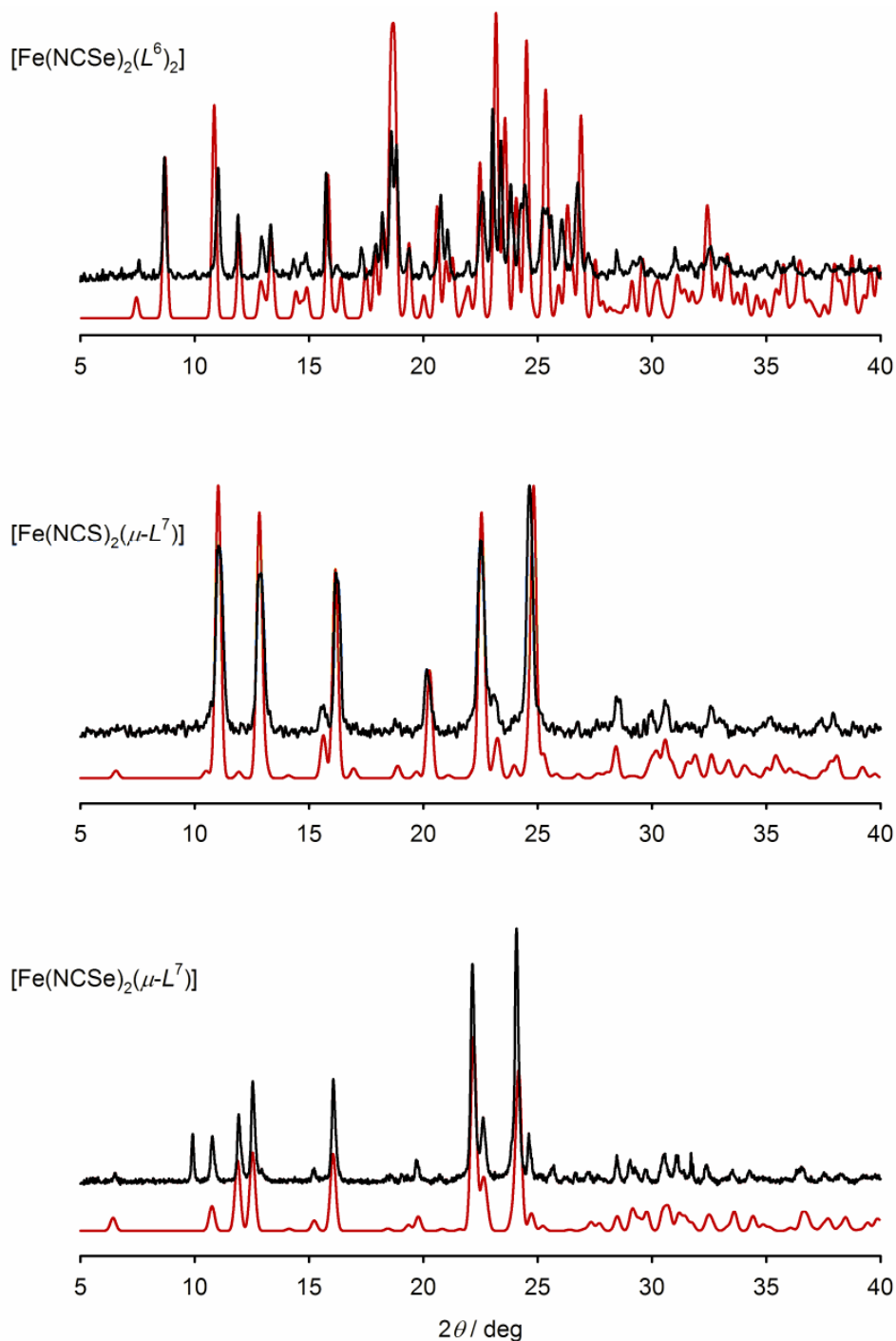


Figure S48 continued.

Agreement between experiment and simulation is excellent for all the compounds, except for a peak at $2\theta = 9.9^\circ$ for $[\text{Fe}(\text{NCSe})_2(\mu-L^7)]$ which does not have a counterpart in the simulation. That might imply $[\text{Fe}(\text{NCSe})_2(\mu-L^7)]$ contains a minor fraction of the mononuclear $[\text{Fe}(\text{NCSe})_2(L^7)_2]$ phase (which is the product obtained from the corresponding reaction of L^6).

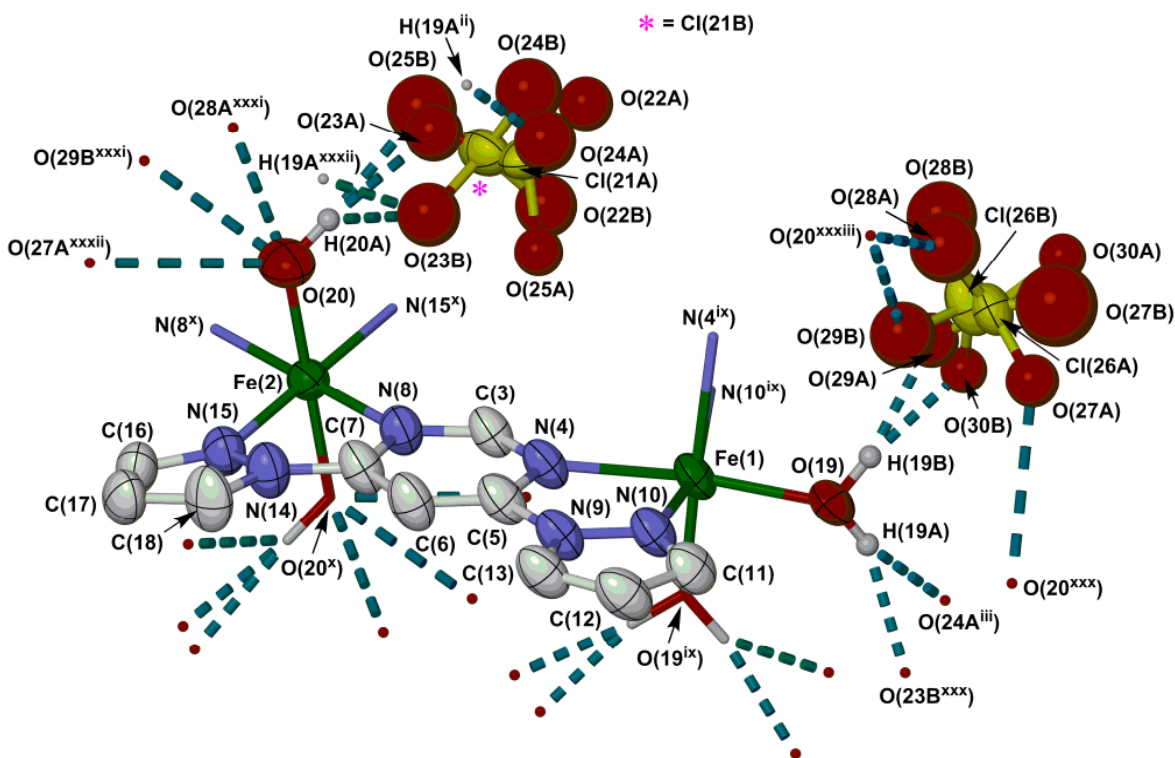


Figure S49 View of the asymmetric unit of the coordination polymer $[\text{Fe}(\text{OH})_2(\mu\text{-L}^5)][\text{ClO}_4]_2$, showing the atom numbering schemes. Displacement ellipsoids are at the 50 % probability level, and C-bound H atoms are omitted for clarity. Symmetry codes: (ii) $x, 1+y, z$; (iii) $x, -1+y, z$; (ix) $1-x, y, 1/2-z$; (x) $1-x, 2-y, 1-z$; (xxx) $1-x, -1+y, 1/2-z$; (xxxi) $x, 2-y, 1/2+z$; (xxxii) $1-x, 1+y, 1/2-z$; (xxxiii) $x, 2-y, -1/2+z$.

Colour code: C, white; H, pale grey; Cl, yellow; Fe, green; N, blue; O, red.

Atom H(20B) was not located during the structure refinement, and may be disordered between the hydrogen bond acceptor groups O(28A^{xxxii})/O(29B^{xxxii}), and O(27A^{xxxii}) (Table S27).

Table S26 Selected bond lengths (Å) and angles (°) for the coordination polymer [Fe(OH₂)₂(μ-L⁵)] [ClO₄]₂. See Figure S49 for the atom numbering scheme, while definitions of *V*_{Oh}, *Ψ*, *Σ* and *Θ* are given on page S19. Symmetry codes: (ix) 1-x, y, 1/2-z; (x) 1-x, 2-y, 1-z.

| | | | |
|----------------------------------|------------|---------------------------------|----------|
| Fe(1)–N(4) | 2.219(6) | Fe(2)–N(8) | 2.207(6) |
| Fe(1)–N(10) | 2.119(6) | Fe(2)–N(15) | 2.178(6) |
| Fe(1)–O(19) | 2.086(6) | Fe(2)–O(20) | 2.086(6) |
| Fe(1)...Fe(2) | 6.3787(13) | | |
| N(4)–Fe(1)–N(4 ^{ix}) | 92.6(3) | N(8)–Fe(2)–N(8 ^x) | 180 |
| N(4)–Fe(1)–N(10) | 74.0(2) | N(8)–Fe(2)–N(15) | 74.3(2) |
| N(4)–Fe(1)–N(10 ^{ix}) | 94.4(2) | N(8)–Fe(2)–N(15 ^x) | 105.7(2) |
| N(4)–Fe(1)–O(19) | 167.5(2) | N(8)–Fe(2)–O(20) | 89.5(3) |
| N(4)–Fe(1)–O(19 ^{ix}) | 89.7(2) | N(8)–Fe(2)–O(20 ^x) | 90.5(3) |
| N(10)–Fe(1)–N(10 ^{ix}) | 163.4(4) | N(15)–Fe(2)–N(15 ^x) | 180 |
| N(10)–Fe(1)–O(19) | 93.7(3) | N(15)–Fe(2)–O(20) | 87.0(3) |
| N(10)–Fe(1)–O(19 ^{ix}) | 98.0(3) | N(15)–Fe(2)–O(20 ^x) | 93.0(3) |
| O(19)–Fe(1)–O(19 ^{ix}) | 90.7(3) | O(20)–Fe(2)–O(20 ^x) | 180 |
| <i>V</i> _{Oh} [Fe(1)] | 12.73(3) | <i>V</i> _{Oh} [Fe(2)] | 12.86(2) |
| <i>Ψ</i> [Fe(1)] | 96.94(8) | <i>Ψ</i> [Fe(2)] | 180 |
| <i>Σ</i> [Fe(1)] | 68.1(9) | <i>Σ</i> [Fe(2)] | 76.8(9) |
| <i>Θ</i> [Fe(1)] | 195 | <i>Θ</i> [Fe(2)] | 147 |

Table S27 Hydrogen bond parameters for the coordination polymer [Fe(OH₂)₂(μ-L⁵)] [ClO₄]₂ (Å, °). See Figure S49 for the atom numbering scheme. Symmetry code: (iii) x, -1+y, z; (xxx) 1-x, -1+y, 1/2-z; (xxxii) x, 2-y, 1/2+z; (xxxiii) 1-x, 1+y, 1/2-z.

| | D–H | H...A | D...A | D–H...A |
|---|---------|------------------|---------------------|----------------|
| O(19)–H(19A)...O(24A ⁱⁱⁱ)/O(23B ^{xxx}) | 0.89(2) | 0.89(2)/1.98(7) | 2.913(15)/2.735(16) | 154(10)/142(9) |
| O(19)–H(19B)...O(29A)/O(30B) | 0.89(2) | 1.94(4)/1.89(4) | 2.804(11)/2.757(13) | 163(10)/164(9) |
| O(20)–H(23A)...O(23A)/O(23B) | 0.89(2) | 2.13(5)/2.13(11) | 2.967(15)/2.651(15) | 156(11)/117(9) |
| O(20)–H(23A)...O(25B) | 0.89(2) | 2.14(3) | 3.037(18) | 178(12) |
| O(20)–H(23B)...O(28A ^{xxxii})/O(29B ^{xxxii}) ^a | – | – | 2.714(15)/2.945(18) | – |
| O(20)–H(23B)...O(27A ^{xxxiii}) | – | – | 3.003(11) | – |

^aAtom H(20B) was not located during the structure refinement.

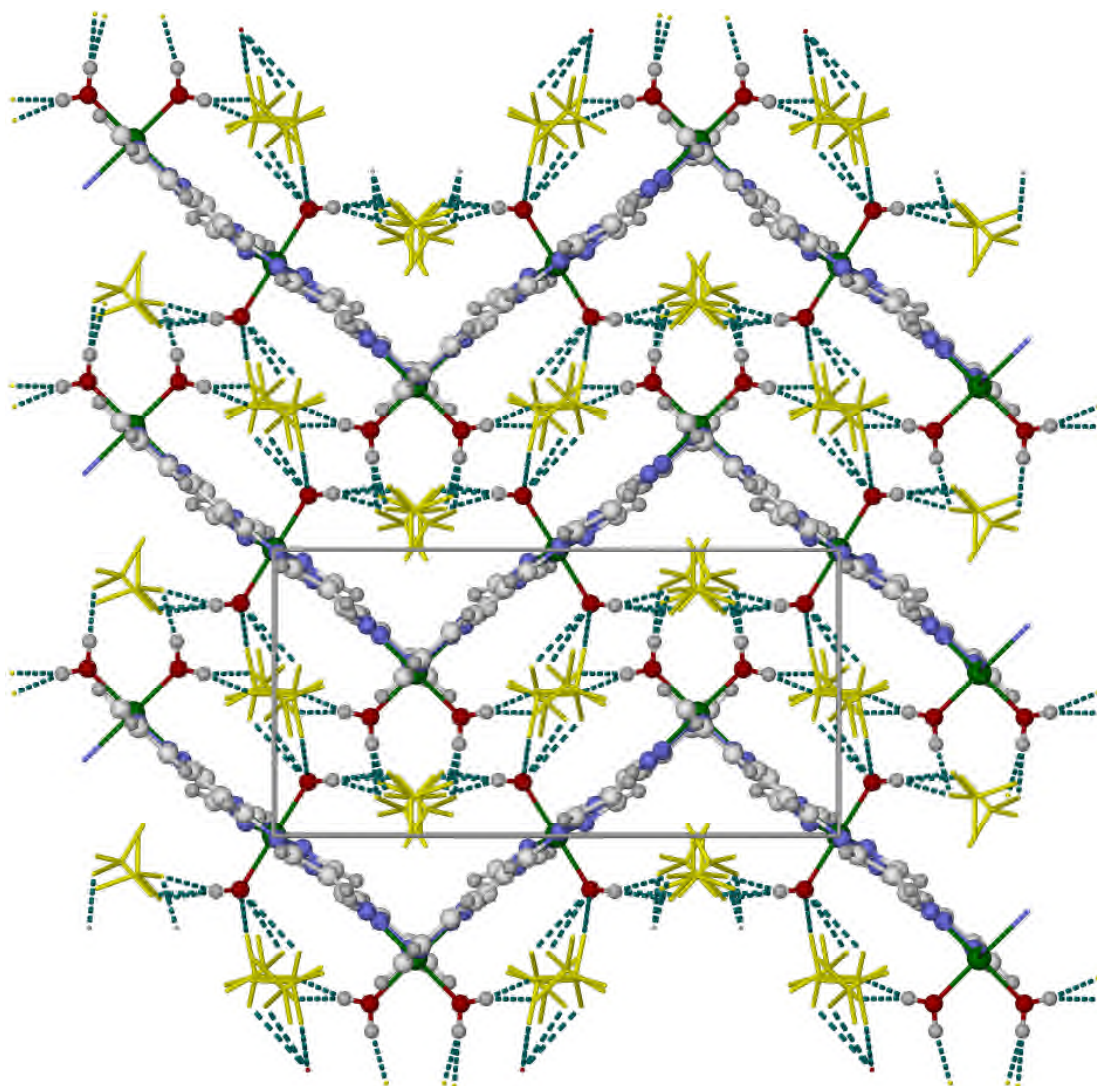


Figure S50 Packing diagram of $[\text{Fe}(\text{OH})_2(\mu\text{-L}^5)][\text{ClO}_4]_2$, showing a hydrogen-bonded layer of polymer chains. The view is along the (100) crystal vector, with c horizontal. Both orientations of each disordered anion are shown, and are de-emphasised for clarity.

Colour code: C, white or dark grey; H, pale grey; Fe, green; N, pale or dark blue; O, red; ClO_4^- , yellow.

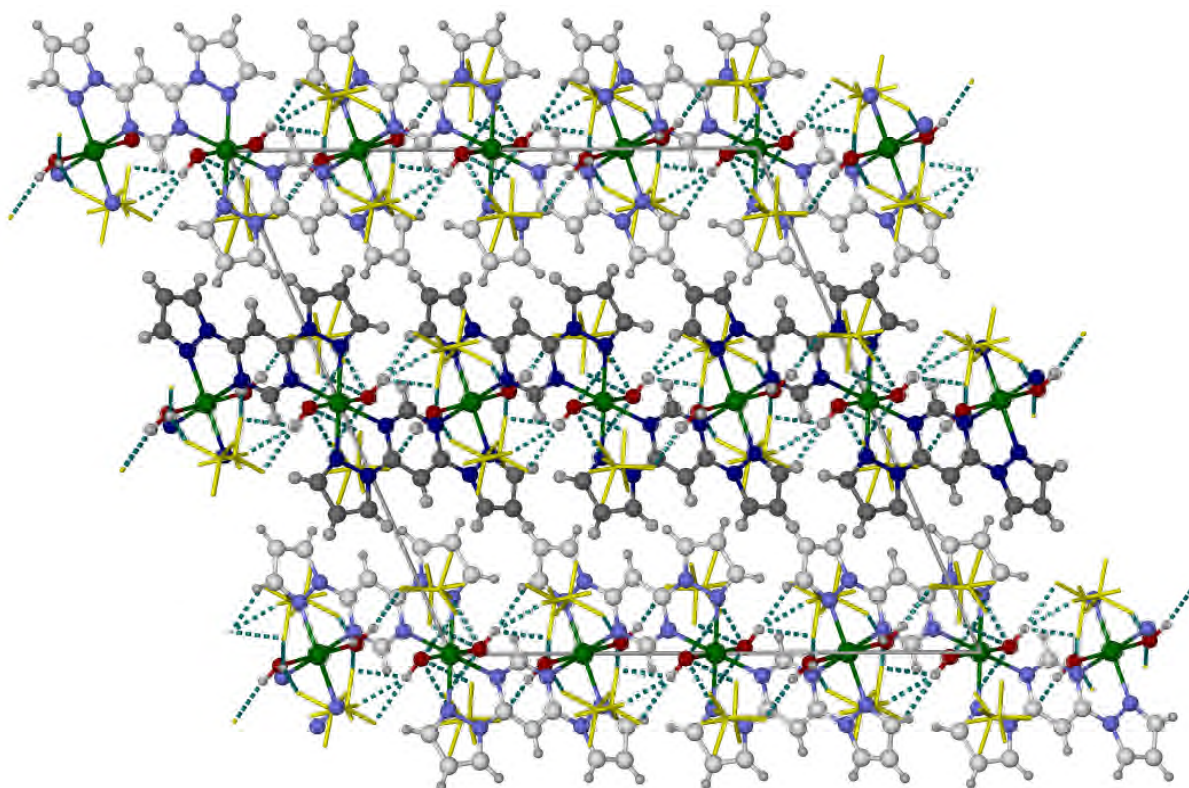


Figure S51 Packing diagram of $[\text{Fe}(\text{OH}_2)_2(\mu\text{-L}^5)][\text{ClO}_4]_2$, showing the association of the polymer chains into sheets *via* intermolecular hydrogen bonding. The view is along the (010) crystal vector, with *c* horizontal. Other details as for Figure S50.

Colour code: C, white or dark grey; H, pale grey; Fe, green; N, pale or dark blue; O, red; ClO_4^- , yellow.

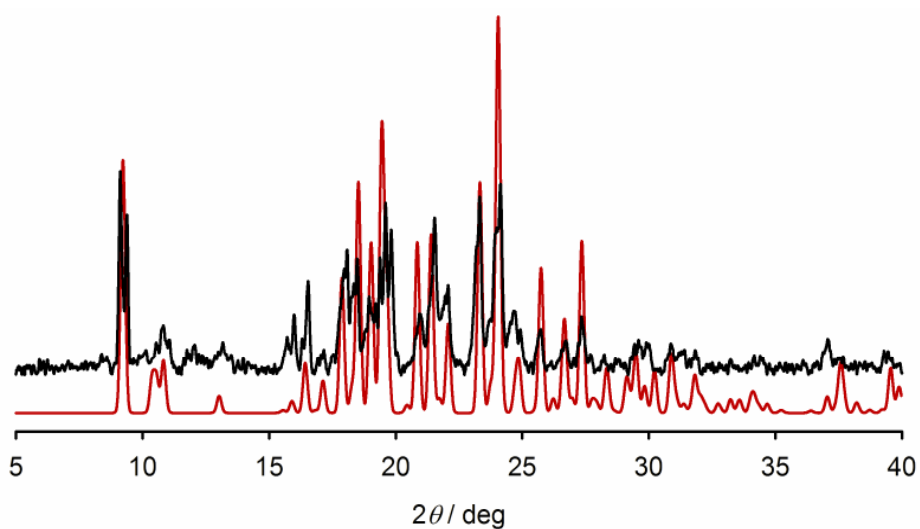


Figure S52 Measured (black) and simulated (red) X-ray powder diffraction data for $[\text{Fe}(\text{OH}_2)_2(\mu\text{-L}^5)][\text{ClO}_4]_2$.

References

- 1 G. M. Sheldrick, *Acta Cryst. Sect. C.: Struct. Chem.*, 2015, **71**, 3.
- 2 L. J. Barbour, *J. Supramol. Chem.*, 2001, **1**, 189.
- 3 O. V. Dolomanov, L. J. Bourhis, R. J. Gildea, J. A. K. Howard and H. Puschmann, *J. Appl. Cryst.*, 2009, **42**, 339.
- 4 H. J. Shepherd, T. Palamarciuc, P. Rosa, P. Guionneau, G. Molnár, J.-F. Létard and A. Bousseksou, *Angew. Chem., Int. Ed.*, 2012, **51**, 3910.
- 5 P. Guionneau, M. Marchivie, G. Bravic, J.-F. Létard and D. Chasseau, *Top. Curr. Chem.*, 2004, **234**, 97.
- 6 J. K. McCusker, A. L. Rheingold and D. N. Hendrickson, *Inorg. Chem.*, 1996, **35**, 2100.
- 7 C. J. O'Connor, *Prog. Inorg. Chem.*, 1982, **29**, 203.
- 8 R. Boča, *Coord. Chem. Rev.*, 2004, **248**, 757.
- 9 I. Dance and M. Scudder, *CrystEngComm*, 2009, **11**, 2233.